

Copyright Warning & Restrictions

The copyright law of the United States (Title 17, United States Code) governs the making of photocopies or other reproductions of copyrighted material.

Under certain conditions specified in the law, libraries and archives are authorized to furnish a photocopy or other reproduction. One of these specified conditions is that the photocopy or reproduction is not to be “used for any purpose other than private study, scholarship, or research.” If a user makes a request for, or later uses, a photocopy or reproduction for purposes in excess of “fair use” that user may be liable for copyright infringement,

This institution reserves the right to refuse to accept a copying order if, in its judgment, fulfillment of the order would involve violation of copyright law.

Please Note: The author retains the copyright while the New Jersey Institute of Technology reserves the right to distribute this thesis or dissertation

Printing note: If you do not wish to print this page, then select “Pages from: first page # to: last page #” on the print dialog screen

The Van Houten library has removed some of the personal information and all signatures from the approval page and biographical sketches of theses and dissertations in order to protect the identity of NJIT graduates and faculty.

ABSTRACT

STUDIES ON PURIFICATION AND FUNCTIONALIZATION OF CARBON NANOTUBES AND THEIR AQUEOUS PHASE BEHAVIOR

**by
Zheqiong Wu**

Carbon nanotubes (CNTs) are known to have unique mechanical, thermal and electrical properties which make them attractive for a wide range of applications ranging from batteries to sensors. CNTs are rolled up graphene sheets where the single-walled CNTs (SWCNTs) and multi-walled CNTs (MWCNTs) are classified according to the number of concentric rings. In this dissertation, the focus is on several different aspects of MWCNTs. These include purification, functionalization and colloidal behavior.

MWCNTs are insoluble in solvents and therefore some degree of functionalization is required prior to their real-world applications. Oxidation debris is generated during carboxylation which is usually the first step in their functionalization. Our group has previously developed microwave induced functionalization of MWCNTs which is a fast process that provides high degree of functionalization. One of the objectives of this research is to study the oxidation debris generated during microwave functionalization.

Oxidation debris affects the dimension of MWCNTs and their surface properties which influence dispersion and stability in chemical and biological environment. Removal of this debris is needed to obtain high purity functionalized MWCNTs. Dilute base-washing is usually used to remove oxidation debris by converting the acidic groups in the debris into their conjugate salts so that they are dissolved and removed. Conventional washing takes a long time and consumes a lot of chemicals. Therefore,

another objective of this research is to study the feasibility of microwave induced base washing as a rapid method for removing oxidation debris.

The degree of functionalization of MWCNTs is an important factor that has not been addressed to date. The effects of the degree of functionalization on physical and chemical properties as well as bioactivity and toxicity are yet to be studied in any detail. The degree of functionalization is altered by varying the treatment time in microwave induced functionalization. Chemical, physical, electrochemical and colloidal behavior of the carboxylated MWCNTs is studied. Variations in chemical, physical, colloidal and electrochemical properties are presented in this dissertation.

Another important aspect of MWCNTs is that they are usually mixtures of different sizes and represent significant variability within the group. The size of MWCNTs affects the physical and chemical properties, biological behaviors and dispersibility. For example, applications in electronics, biological, and optical devices benefit from shorter nanotubes (less than 500 nm), while others like field emission displays require relatively longer tubes (500–2000 nm) due to their more uniform emission. The size dependent behavior of CNTs is also not well understood. Of particular interest to this research is the aqueous dispersibility and colloidal behavior of functionalized MWCNT. In this research, the colloidal behavior of MWCNTs that are functionalized to the same degree but have different length is studied.

**STUDIES ON PURIFICATION AND FUNCTIONALIZATION OF CARBON
NANOTUBES AND THEIR AQUEOUS PHASE BEHAVIOR**

**by
Zheqiong Wu**

**A Dissertation
Submitted to the Faculty of
New Jersey Institute of Technology
in Partial Fulfillment of the Requirements for the Degree of
Doctor of Philosophy in Chemistry**

Department of Chemistry and Environmental Science

May 2016

Copyright © 2016 by Zheqiong Wu

ALL RIGHTS RESERVED

APPROVAL PAGE

**STUDIES ON PURIFICATION AND FUNCTIONALIZATION OF CARBON
NANOTUBES AND THEIR AQUEOUS PHASE BEHAVIOR**

Zheqiong Wu

Dr. Somenath Mitra, Dissertation Advisor Date
Distinguished Professor of Chemistry and Environmental Science, NJIT

Dr. Tamara Gund, Committee Member Date
Professor of Chemistry and Environmental Science, NJIT

Dr. Edgardo Farinas, Committee Member Date
Associate Professor and Chair of Chemistry and Environmental Science, NJIT

Dr. Yong Ick Kim, Committee Member Date
Assistant Professor of Chemistry and Environmental Science, NJIT

Dr. Pradyot Patnaik, Committee Member Date
Consultant, Radiance

BIOGRAPHICAL SKETCH

Author: Zheqiong Wu
Degree: Doctor of Philosophy
Date: May 2016

Undergraduate and Graduate Education:

- Doctor of Philosophy in Chemistry, New Jersey Institute of Technology, Newark, NJ, 2016
- Bachelor of Science in Analysis of Chinese Traditional Medicine, Beijing University of Chinese Medicine, Beijing, P. R. China, 2009

Major: Chemistry

Presentations and Publications:

- Wu, Z. and S. Mitra (2015). "Microwave induced reactive base wash for the removal of oxidation debris from carboxylated carbon nanotubes." *Carbon* 88(0): 233-238.
- Wu, Z. and S. Mitra (2014). "Length reduction of multi-walled carbon nanotubes via high energy ultrasonication and its effect on their dispersibility." *Journal of Nanoparticle Research* 16(8): 1-7
- Wu, Z. and S. Mitra (2014). "Fractionation of carboxylated carbon nanotubes and the corresponding variation in their colloidal behavior." *Environmental Science: Processes & Impacts* 16(10): 2295-2300.
- Wu, Z., R. F. Hamilton Jr, Z. Wang, A. Holian and S. Mitra (2014). "Oxidation debris in microwave functionalized carbon nanotubes: chemical and biological effects." *Carbon* 68(0): 678-686.
- Thakkar, M., Z. Wu, L. Wei and S. Mitra (2015). "Water defluoridation using a nanostructured diatom-ZrO₂ composite synthesized from algal Biomass." *Journal of Colloid and Interface Science* 450: 239-245.
- Wang, Z., Z. Wu, G. Di Benedetto, J. L. Zunino and S. Mitra (2015). "Microwave synthesis of highly oxidized and defective carbon nanotubes for enhancing the performance of supercapacitors." *Carbon* 91: 103-113.

- Silva, R. M., K. Doudrick, L. M. Franzi, C. TeeSy, D. S. Anderson, Z. Wu, S. Mitra, V. Vu, G. Dutrow, J. E. Evans, P. Westerhoff, L. S. Van Winkle, O. G. Raabe and K. E. Pinkerton (2014). "Instillation versus inhalation of multiwalled carbon nanotubes: exposure-related health effects, clearance, and the role of particle characteristics." *ACS Nano* 8(9): 8911-8931.
- Wang, Z., Z. Wu, N. Bramnik and S. Mitra (2014). "Fabrication of high-performance flexible alkaline batteries by implementing multiwalled carbon nanotubes and copolymer separator." *Advanced Materials* 26(6): 970-976.
- Lau, X. C., Z. Wu and S. Mitra (2014). "Enhanced charge-carrier transport through shorter carbon nanotubes in organic photovoltaics." *ACS Applied Materials & Interfaces* 6(3): 1640-1645
- Hamilton, R., Jr., Z. Wu, S. Mitra, P. Shaw and A. Holian (2013). "Effect of MWCNT size, carboxylation, and purification on in vitro and in vivo toxicity, inflammation and lung pathology." *Particle and Fibre Toxicology* 10(1): 1-17.
- Wu, Z. and S. Mitra (March 2014). "Microwave induced functionalization and purification of carbon nanotubes." ACS 247th National Meeting & Exposition, Dallas, TX.
- Wu, Z. and S. Mitra (October 2012). "Aqueous dispersibility as a function of size and aspect ratio of carbon nanotubes." ACS 38th Northeast Regional Meeting, Rochester, NY.



谨以此献给无怨无悔爱我支持我的爸爸, 吴曙光, 妈妈, 李桂华,
老公, 张晗和我的萌娃, Sara.

To my beloved Dad (Shuguang Wu), Mom (Guihua Li), Husband (Han Zhang) and my
cutest baby (Sara). I love you forever.

ACKNOWLEDGMENT

I would like to express my deepest appreciation to Dr. Somenath Mitra, who served as this research advisor, for his guidance, encouragement and support throughout my research. Special thanks are given to Dr. Tamara Gund, Dr. Edgardo Farinas, Dr. Yong Kim and Dr. Pradyot Patnaik for serving as members of my committee. Special thanks are also given to Dr. Xueyan Zhang for her constant support for this research.

Financial support from the National Institute of Health is acknowledged.

I am grateful to my parents (Shuguang Wu and Guihua Li), my husband (Han Zhang) for their support and understanding during the entire course of this research.

TABLE OF CONTENTS

Chapter	Page
1 INTRODUCTION.....	1
1.1 Overview.....	1
1.2 Carbon Nanotube Purification.....	2
1.3 Carbon Nanotube Functionalization.....	3
1.4 Microwave Irradiation Induced Functionalization and Purification of Carbon Nanotubes.....	6
1.5 Physicochemical Characterization of Carbon Nanotube.....	7
1.6 Dispersibility of Carbon Nanotubes.....	10
1.7 Objectives.....	21
2 OXIDATION DEBRIS IN MICROWAVE FUNCTIONALIZED CARBON NANOTUBES: CHEMICAL AND BIOLOGICAL EFFECTS.....	22
2.1 Experimental.....	25
2.1.1 Preparation of the F-MWCNT.....	25
2.1.2 Preparation of Base-washed Samples.....	25
2.1.3 Characterization.....	25
2.1.4 Toxicological Analysis.....	27
2.2 Results and Discussions.....	29
2.2.1 Characterization.....	29
2.2.2 Colloidal Properties of F-MWCNTs and BWF-MWCNTs.....	36
2.2.3 Biological Activity of F-MWCNTs and BWF-MWCNTs.....	38
2.3 Conclusions.....	40

TABLE OF CONTENTS
(Continued)

Chapter	Page
3 MICROWAVE INDUCED REACTIVE BASE WASH FOR THE REMOVAL OF OXIDATION DEBRIS FROM CARBOXYLATED CARBON NANOTUBES	41
3.1 Experimental.....	42
3.1.1 Chemicals.....	42
3.1.2 Preparation of the F-CNTs.....	43
3.1.3 Preparation of Base-washed Samples.....	43
3.1.4 Characterization.....	44
3.2 Results and Discussion.....	45
3.2.1 Sample Preparation.....	45
3.2.2 Characterization.....	46
3.3 Conclusions.....	54
4 LENGTH REDUCTION OF MULTI-WALLED CARBON NANOTUBES VIA HIGH ENERGY ULTRASONICATION AND ITS EFFECT ON THEIR DISPERSIBILITY.....	55
4.1 Experimental.....	56
4.1.1 Chemicals.....	56
4.1.2 Preparation of the f-MWNTs.....	56
4.1.3 Characterization of the f-MWNTs.....	57
4.1.4 Dispersibility Studies.....	58
4.2 Results and Discussion.....	59

TABLE OF CONTENTS
(Continued)

Chapter	Page
4.2.1 Characterization.....	59
4.2.2 Dispersibility as a Function of Length.....	63
4.3 Conclusions.....	68
5 FRACTIONATION OF CARBOXYLATED CARBON NANOTUBES AND THE CORRESPONDING VARIATION IN THEIR COLLOIDAL BEHAVIOR.....	69
5.1 Experimental.....	71
5.1.1 Chemicals.....	71
5.1.2 Preparation of the Carboxylated Multiwall Carbon Nanotubes.....	71
5.1.3 Size Sorting of f-MWCNT-O by Centrifugation.....	71
5.1.4 Characterization.....	72
5.1.5 Dispersibility Studies.....	73
5.2 Results and Discussion.....	74
5.2.1 Characteristics of the Different Fractions.....	74
5.2.2 Dispersibility of the Different Fractions.....	78
5.2.3 Long Term Stability of the Different Fractions.....	82
5.3 Conclusions.....	83
6 VARIATION OF CHEMICAL, ELECTROCHEMICAL AND BIOLOGICAL PROPERTIES OF CARBON NANOTUBES WITH THE DEFREE OF CARBOXYLATION.....	84

TABLE OF CONTENTS
(Continued)

Chapter	Page
6.1 Experimental.....	86
6.1.1 Prepration of the f-CNTs.....	86
6.1.2 Characterizations and Electrochemical Behavior of the f-CNTs.....	86
6.1.3 Dispersibility Studies.....	87
6.1.4 Biological Studies.....	87
6.2 Results and Discussion.....	91
6.2.1 Characterizations.....	91
6.2.2 Electrochemical Behavior of the f-CNTs.....	94
6.2.3 Dispersibility of the f-CNTs.....	98
6.2.4 Biological Effects of f-CNTs.....	101
6.3 Conclusions.....	105
REFERENCES.....	107

LIST OF TABLES

Table	Page
2.1 Elemental Analysis of MWCNT.....	31
2.2 Dimension, Particle Size, Zeta Potential, and Solubility of the F-MWCNT and BWF-MWCNT.....	32
2.3 BET Surface Area of MWCNTs.....	33
2.4 Surface Functional Groups on F-MWCNT and BWF-MWCNT.....	36
3.1 Elemental Analysis of CNT Samples.....	48
3.2 Dimension, Specific Surface Area, Particle Size and Zeta Potential of F-CNT Samples.....	49
3.3 Elemental Analysis of Filtrate.....	53
4.1 Length, Diameter and EDX Result for Materials.....	61
5.1 Length Data for f-MWCNTs.....	76
5.2 Elemental Analysis of f-MWCNTs.....	77
6.1 Diameter, Elemental Analysis, C: COOH Ratio, SSA, ID/IG of CNTs and f-CNTs.....	92
6.2 The Areas Encircled by the CV Curves.....	98

LIST OF FIGURES

Figure	Page
1.1 Zeta potential for a net surface charge particle.....	17
1.2 Schematic diagram of TRDLS for zeta potential measurements.....	19
2.1 SEM images of A) MWCNT-SL, B) F-MWCNT-SL, C) BWF-MWCNT-SL, D) W-MWCNT-SL, E) photograph showing the dispersion of 50 µg/ml of MWCNT-SS; F-MWCNT-SS; BWF-MWCNT-SS; MWCNT-SL; F-MWCNT-SL;BWF-MWCNT-SL;MWCNT-LS;F-MWCNT-LS;BWF-MWCNT-LS(from left to right) in complete RPMI media without phenol red, made from sonication of 5mg/ml stock in 5% infasurf/saline.....	30
2.2 FTIR spectroscopy of A) MWCNT-SL, B) F-MWCNT-SL, C) BWF-MWCNT-SL, D) W-MWCNT-SL.....	34
2.3 Raman spectroscopy of A) MWCNT-SL, B) F-MWCNT-SL, C) BWF-MWCNT-SL, D) W-MWCNT-SL.....	35
2.4 Zeta potential of A) F-MWCNT-SS and BWF-MWCNT-SS, B) F-MWCNT-SL and BWF-MWCNT-SL, C) F- MWCNT-LS and F- MWCNT-LS in different pH.....	38
2.5 24-hr toxicity in the THP-1 model for all MWCNT. Relative dose-dependent toxicity by MTS assay for A) the MWCNT-SS variants, B) the MWCNT-SL variants, C) the MWCNT-LS variants. LDH release for D) the MWCNT-SS variants, E) the MWCNT-SL variants, F) the MWCNT-LS variants. All data expressed as mean ± SEM.....	39
2.6 24-hr IL-1β release in the THP-1 model for all MWCNT. Relative dose-dependent IL-1β release for A) the MWCNT-SS variants, B) the MWCNT-SL variants, C) the MWCNT-LS variants. All data expressed as mean ± SEM. Asterisks indicate *** P < 0.001, ** P < 0.01, or * P < 0.05 compared to no particle (0 µg/ml concentration) control condition. n = 3.....	40
3.1 SEM Images of a)BW-F-CNT _{SS} , b)BW-F-CNT _{SL} , c)BW-F-CNT _{LS} , d)MRW-F-CNT _{SS} , e)MRW-F-CNT _{SL} , f)MRW-F-CNT _{LS} , g)MRW-F-CNT _{SL10} , h) W-CNT _{LS} , i) W-MRW-CNT _{LS}	47
3.2 Raman Spectra of a) F-CNT _{SL} , b) BW-F-CNT _{SL} , c) MRW-F-CNT _{SL}	50

LIST OF FIGURES
(Continued)

Figure	Page
3.3 FTIR Spectra of a) BW-F-CNT _{SL} , b) MRW-F-CNT _{SL} , c) W-BW-CNT _{SL} , and d) W-MRW-CNT _{SL}	51
4.1 SEM Images for a) MWNT, b) f-MWNT-L, c) f-MWNT-S d) Dispersion of f-MWNT-L(left) and f-MWNT-S(right).....	60
4.2 Histograms of size distribution a) MWNT b) f-MWNT-L c) f-MWNT-S.....	61
4.3 FTIR results for a) MWNT, b) f-MWNT-L, c) f-MWNT-S.....	62
4.4 TGA of MWNT, f-MWNT-L and f-MWNT-S.....	63
4.5 (a) Particle size distribution and (b) zeta potential of the f-MWNT-L and f-MWNT-S as a function salt concentration.....	64
4.6 Attachment efficiency of f-MWNTs are shown as a function of Salt concentration. (a) f-MWNT-L and f-MWNT-S in NaCl, (b) f-MWNT-L and f-MWNT-S in MgCl ₂	66
4.7 Long-Term stability measured by UV absorbance at 252nm.....	67
4.8 Double layer in: a) f-MWNT-L, b) f-MWNT-S.....	68
5.1 Schematic diagram of sorting length.....	72
5.2 SEM images of f-MWCNTs.....	74
5.3 Histograms of length distribution.....	75
5.4 FTIR of MWCNTs and f-MWCNT-O.....	77
5.5 (a) Particle size and (b) zeta potential distribution in a 10 mM electrolyte solution NaCl and MgCl ₂	79
5.6 Attachment efficiency of f-MWCNTs in a function of (a) NaCl and (b) MgCl ₂ concentration.....	80

LIST OF FIGURES
(Continued)

Figure	Page
5.7 CCC value of f-MWCNTs in a 10 mM electrolyte solution (a) NaCl and (b) MgCl ₂	81
5.8 Electrostatic double layers in: (a) longer carbon nanotubes, (b) shorter carbon nanotubes.....	81
5.9 Stability of f-MWCNTs in a 10 mM electrolyte solution (a) NaCl and (b) MgCl ₂	82
5.10 Stability index of f-MWCNTs in MilliQ water and a 10 mM electrolyte solution of NaCl and MgCl ₂	82
6.1 SEM images of (a) CNTs (b) f-CNT _{34.8} , (c) f-CNT _{23.8} , (d) f-CNT _{20.6} , (e) f-CNT _{16.2} , (f) f-CNT _{15.7} , (g) f-CNT _{14.9} , (h) f-CNT _{14.7} ; TEM images of (i) f-CNT _{34.8} (j) f-CNT _{14.7}	93
6.2 The cyclic voltammetry of different CNT samples (a) at the scan rate of 0.01V/s in 2 M Na ₂ SO ₄ electrolyte (b) at the scan rate of 0.05V/s in 2 M KOH electrolyte (c) at the scan rate of 0.05V/s in 2 M KOH and Na ₂ SO ₄ electrolyte...	95
6.3 Particle size (a, b, c) and zeta potential (d, e, f) of f-CNTs in MilliQ water and in the present of NaCl and MgCl ₂	99
6.4 Attachment efficiency of f-CNTs in a function of (a) NaCl and (b) MgCl ₂	100
6.5 CCC value of f-CNTs in the present of (a) NaCl and (b) MgCl ₂	101
6.6 Effect of functionalized CNTs on THP-1 macrophage-like cells in an in vitro 24 hr culture. A) Cell toxicity determined by LDH activity in cell media. Data expressed as mean LDH percent ± SEM compared to 100% cell death. B) Cell toxicity determined by MTS assay. Data expressed as mean ± SEM viability relative to control cultures (0 µg/ml). C) IL-1β release expressed as mean ± SEM pg/ml. Asterisks *** indicate P < 0.001, ** P < 0.01, or * P < 0.05 compared to 0 µg/ml concentration.....	103

LIST OF FIGURES
(Continued)

Figure	Page
6.7 Effect of functionalized CNTs on A549 lung epithelial cells in an in vitro 24 hr culture. A) Cell toxicity determined by MTS assay. Data expressed as mean \pm SEM optical density at 490 nm. B) IL-6 release expressed as mean \pm SEM pg/ml. C) IL-33 release expressed as mean \pm SEM pg/ml. D) TNF- α release expressed as mean \pm SEM pg/ml. Asterisks *** indicate $P < 0.001$, ** $P < 0.01$, or * $P < 0.05$ compared to Control (no particle cultures).....	105

CHAPTER 1

INTRODUCTION

1.1 Overview

Carbon nanotubes (CNTs) were discovered as microtubules of graphitic by Sumio Iijima in 1991. These tubules had outer diameters of 4-30nm and a length of up to 1 μm . They are rolled up seamless graphene cylinders. CNTs can be classified into single-walled (SWCNTs), double-walled (DWCNTs) and multi-walled (MWCNTs), depending on the number of concentric rings. The first discovered CNTs were MWCNTs followed by SWCNTs in 1993, with diameters of 0.4-3nm and a length in the micrometer order (Iijima 1991) (Iijima and Ichihashi 1993). The unique structures of CNTs lead their distinctive properties in mechanical, thermal and electrical aspects (Iijima 2002). CNTs attract a wide range of applications based on their unique structures and properties. The thin needle-like structure of CNTs make the possibility of using them as probe tips in atomic force microscopy (Iijima 2002). The nanometer-scale spaces inside and among CNTs allow them used as hydrogen storage(Dillon, Jones et al. 1997). CNTs can also be used as chemical sensors (Kong, Franklin et al. 2000), carriers of Pt particles used as catalyst(Iijima 2002), electron field emission sources (de Heer, Châtelain et al. 1995), electrochemical Actuator (Yun, Shanov et al. 2006), carriers in drug delivery (Bianco, Kostarelos et al. 2005), etc.

CNTs were firstly synthesized by arc discharge technique. Laser ablation and chemical vapor deposition have been used following as the other two main synthesis method. In arc discharge method, two carbon electrodes with or without metal catalysts.

The direct-current arc voltage is applied across two electrodes in an inert gas atmosphere. In laser ablation technique, a high power laser beam is used to ablate the mixture of carbon containing feedstock and metal catalysts in a flow of inert gas. Chemical vapor deposition is the decomposition of hydrocarbons with metal catalysts in the oven at the temperature above 600 °C. The growth mechanisms of CNTs are not exactly known, while tip-growth and root-growth are two most acceptable ones. In the case of tip-growth, hydrocarbon decomposes on the top surface of the metal catalysts, carbon precipitates diffuse through the metal and CNTs form on the bottom of the metal and continuously grow longer and longer. In the root-growth case, CNTs form when the molten metal dissolving carbon is cooled and solidified on the top surface of metal catalysts and extend up to form the graphitic cylinder (Aqel, El-Nour et al. 2012) (Kumar 2011).

1.2 Carbon Nanotube Purification

Metal catalysts are usually involved in all the synthesis technologies. Some metal catalysis residues exist with CNT products as impurities. Some carbonaceous impurities also exist which result from carbon feedstock and byproducts. Carbonaceous impurities usually contains amorphous carbon, fullerenes, graphite sheet and carbon nanoparticles (Hou, Liu et al. 2008) (Aqel, El-Nour et al. 2012). Types of impurities are varied depending on the technology, reaction conditions and which kind of carbon feedstock and metal catalysts involved. These impurities will influence the structures of CNTs as well as their desire properties. Therefore, it is important to remove the impurities to obtain high purity CNTs. Some of the carbonaceous impurities can be easily removed because of the different properties from CNTs. Fullerenes can be removed by dissolving in certain organic solvents while pristine CNTs are difficult to disperse in any ones. Amorphous carbon can be

removed by oxidizing under gentle conditions due to their high degree of defect while CNTs are defect free. Some of the carbonaceous impurities are more difficult to remove due to their similar properties to CNTs, such as polyhedral carbons and graphitic particles. Metal impurities should be removed by dissolving in acid when they are located on the surface of CNTs. Some of the metal impurities are wrapped up by CNT inner layers, which may not be easily removed by acid (Hou, Liu et al. 2008).

Generally, purification methods are classified as chemical and physical ones. The combination of methods within one catalog or from both chemical and physical ones are usually used to obtain high purified CNTs since there is difficult to develop one unified purification methods to remove all impurities. Chemical method is good approaches to remove certain carbonaceous impurities which can be oxidized in mild condition and metal impurities which can expose to the reaction media (Hou, Liu et al. 2008) (Aqel, El-Nour et al. 2012). The disadvantages of this method is during the oxidation of impurities, some tubes may also be oxidized to form defect. Dilute HNO_3 is a common oxidant which can maximize removal of impurities as well as minimize the destruction of CNT structures (Chen and Mitra 2008). Physical method removes impurities due to their different physical properties from CNTs, such as in particle size, gravity, magnetic properties. Purification techniques base on physical properties includes filtration (Bandow, Rao et al. 1997), centrifugation (Yu, Bekyarova et al. 2006), magnetic purification (Thi ên-Nga, Hernadi et al. 2002), ultrasonication (Shelimov, Esenaliev et al. 1998), etc. Comparing with chemical method, the advantages of physical one is protecting CNTs from oxidation.

1.3 Carbon Nanotube Functionalization

Carbon nanotubes are chemical inert due to their mostly defect-free sidewalls, which are also make CNTs difficult to disperse or dissolve in water and organic solvents. This limits CNTs from applications which homogenous mixture of CNTs and other materials such as organic, inorganic and polymeric ones are required. Therefore, some level of functionalization of CNTs are required to increase their dispersibility and solubility in certain solvents prior to introduce them into applications. There are several routes to functionalize CNTs, while covalent functionalization (Chen and Mitra 2008), non-covalent functionalization (Lin, Zhou et al. 2003) are two main ones.

Covalent functionalization is achieved by forming covalent bonds between functional groups and carbon nanotubes, either the ends or the sidewalls. Several covalent functionalization of CNTs have been reported. Carboxylation of CNTs which introducing carboxyl groups on CNTs by oxidation reaction is the most important one(Chen and Mitra 2008), since it is usually the prior step to further functionalization, such as amination (Desai, Addo Ntim et al. 2012), polymerization (Riggs, Guo et al. 2000), amidation and esterification (Sun, Huang et al. 2001). Halogenation of CNTs was also reported by covalent functionalization. fluorinated CNTs were prepared, which had moderate solubility in alcoholic solvents (Mickelson, Chiang et al. 1999). They can also be further modified, such that react with diamines (Stevens, Huang et al. 2003) and diols (Zhang, Kiny et al. 2004). Chlorination or bromination of CNTs has also been done, which the resulting samples can be dissolved in polar solvents (Unger, Graham et al. 2002). Hydrogenation of CNTs was also done by a dissolved metal reduction method in liquid ammonia. Hydrogenation occurred on both outside and inner layers of CNTs (Pekker,

Salvetat et al. 2001). Another route of covalent functionalization is [2+1] cycloadditions. Various functional groups can be linked with CNTs, such as carbene (Hu, Zhao et al. 2003), nitrenes (Holzinger, Abraham et al. 2003), azomethine ylides (Georgakilas, Kordatos et al. 2002) by [2+1] cycloadditions. Sidewall functionalization can also be carried out via radical addition such as diazonium salts (Bahr, Yang et al. 2001). CNTs is under studied for using in drug delivery and other biological applications. Biomolecules can also be attached on CNTs by covalent linkages. DNA was reported attached on amino-CNTs by covalent bond, the resulting DNA-CNT hybrids showed excellent biological selectivity (Lee, Baker et al. 2004). CNT-protein composites were also obtained by diimide-activated amidation reaction (Huang, Taylor et al. 2002).

Non-covalent functionalization is carried out coating CNTs with polymers, surfactants, and biomolecules (Tasis, Tagmatarchis et al. 2006). The combination between functional entities and CNTs is based on various adsorption forces, such as van der Waals forces and π - π stacking. CNT-polymer composites have widely application such as in optoelectronic and space applications (Calvert 1999) due to the outstanding mechanical properties and low density of CNTs. Polymers such as epoxy (Ajayan, Stephan et al. 1994), polystyrene (Watts, Hsu et al. 2001), poly(phenylenevinylene) (PPV) (Ntim, Sae-Khow et al. 2011) were coated on CNTs by non-covalent functionalization. Some of the biomolecules can also be coated on CNTs by non-covalent absorption, such as antibodies (Erlanger, Chen et al. 2001), peptides (Dieckmann, Dalton et al. 2003) and single-chain lipids (Artyukhin, Shestakov et al. 2005). Surfactants are usually used to increase the solubility of CNTs by absorbing them on the surface of CNTs. sodium dodecyl sulfate (SDS), sodium dodecylbenzene sulfonate (NaDDBS) are the common ones, the

latter one was reported to increase the solubility of CNTs in water by the order of 10-100 times (Islam, Rojas et al. 2003).

1.4 Microwave Irradiation Induced Functionalization and Purification of Carbon Nanotubes

Purification and functionalization of CNTs are usually carried out by the conventional techniques, such as regular heating, sonication, refluxing. Those methods usually involve multiple steps, and long-term reaction time from hours to days (Huang, Lin et al. 2002) (Ramanathan, Fisher et al. 2005). Microwave irradiation is an alternative technique for providing faster and more efficient reaction (Park, Banerjee et al. 2006).

Microwave energy was firstly used for Radar devices in World War II and then introduced into home use and industrial applications in the 1950s. Microwave irradiation becomes explore to use as energy source in organic reaction since 1980s (Giguere, Bray et al. 1986) (Caddick 1995) as well as inorganic reactions (Polshettiwar, Nadagouda et al. 2009). Comparing with conventional techniques, reactions under microwave irradiation can be done in minutes with higher yields and purer products (Hayes 2002), the need for solvents also reduces, thus it is eco-friendly. The rapid heat provided by microwave irradiation comparing with conventional heating methods is based on the different heating mechanisms. In conventional chemical reactions, an external heat source is needed and the energy/heat transfer is based on the thermal conductivity of different materials. Since the energy passes from the walls of reaction container to solvents then to reactants, the loss of energy is unavoidable. Therefore, the whole procedure are time consuming. However, microwave can directly transfer energy to the reactants, leading to a rapid increase of temperature which shorten the reaction time. There are two mechanisms to explain how the

energy transfer from microwave to the reactants, dipole rotation and ionic conduction. If the reactants are polar molecules, they will try to align themselves with the rapid electric field changes of microwave, leading to the transfer of energy, which called dipole rotation. If free ions or ionic species are involved in the reaction, ionic conduction will occurred which means the free ions or ionic species align themselves along with the rapid changing field.

The application of microwave irradiation in the synthesis, purification, functionalization of nanomaterials has also attracted much attention. Microwave irradiation is now widely used in the chemistry of nanocarbons. The purification of nanocarbons (Mitra and Iqbal 2008), functionalization of single-wall carbon nanotubes (Mitra and Iqbal 2010), synthesis of metal-carbon nanotubes composites (Mitra and Chen 2009) by microwave irradiation were firstly reported by our research group. Metal-graphene composites such as Pt, Ag (Lin, Baggett et al. 2011); metal oxide-graphene hybrids such as Fe₂O₃, CuO (Zou, Kan et al. 2011) (Lu and Wang 2011); and polymer-graphene like polyethyleneimine (Ponnusamy, Mani et al. 2014), carboxylation of nanodiamond (Desai and Mitra 2013), synthesis of fullerenes from graphite powder and fluorinated graphite (Hetzl, Manning et al. 2012) by microwave irradiation were reported by scientists.

1.5 Physicochemical Characterization of Carbon Nanotubes

In order to understand physicochemical properties of carbon nanotubes, many instruments are used, such as scanning electron microscopy (SEM) and transmission electron microscopy (TEM), energy-dispersive X-ray spectroscopy (EDX), thermogravimetric analysis (TGA), fourier transform infrared spectroscopy (FTIR), raman spectroscopy, BET

surface area analyzer. SEM and TEM are usually used to study morphology of CNTs. Cheng et al. found the more rough surface and different length distribution of CNTs after oxidation by SEM (Cheng, Zhong et al. 2011). Wang et al. reported that high resolution TEM images showed debundling and uneven, disordered sidewall of SWCNTs after acid treatment (Wang, Iqbal et al. 2006). SEM and TEM were used to image SWCNTs and DWCNTs, and high resolution TEM was used to determine diameter of CNTs by Song et al. (Song, Ci et al. 2004). Fu et al. used SEM and TEM to determine the inner diameter and outer diameter of MWCNTs and the length changes of MWCNTs after combine with polymer. The dispersion of tubes in MWCNT/epoxy composites were uniform shown by SEM images (Fu, Chen et al. 2009). Pt, Pd nano particles on CNT surface were shown as bright spots in SEM images to prove the successful attachment of Pt, Pd on CNTs (V. Kumar, Addo Ntim et al. 2012). Chen et al. used SEM to image the minimums surface changes of CNTs after functionalization and purification by microwave irradiation to prove that is a better approach for CNT functionalization and purification with less tube damage (Chen and Mitra 2008).

EDX is equipped with SEM or TEM to analyze the elemental content of CNTs and their derivate. Pristine CNTs usually contain metal residues from metal catalysis during synthesis and other purities, EDX used to determine how the purification works by measuring the elemental percentage (Stobinski, Lesiak et al. 2010). The content of oxygen was measured by EDX to determine the degree of oxidation of CNTs with different reaction time (Wang, Wu et al. 2015). EDX can also be used to confirm the attachment of functional groups or other materials such as Fe (Stercel, Nemes et al. 2001), Pt, Pd (V. Kumar, Addo Ntim et al. 2012).

TGA is usually used to determine the thermal stability of materials and their weight change as the function of increasing temperature. It is carried out either under an air or nitrogen atmosphere at pre-set flow and heating rates. The thermal stability of CNTs is around 680 °C in air and higher than 2600 °C in nitrogen (Somani and Umeno 2009). For pristine CNTs, the weight change in an air flow is typically based on the oxidation of carbon into gaseous carbon dioxide and oxidation of metal impurities into solid oxides. Thus the weight of residues can be used to determine the purity of CNTs. By comparing the weight percentage of residues after purification of CNTs, the degree of purification can be studied. The content of materials which attachment to CNT via functionalization can be analyzed by TGA based on their different behavior under raising temperature. The quantity of metal oxide loading can also be determine by TGA. For example, Addo Nitm et al. reported around 40% of iron was founded in MWCNT-Fe hybrids which preparing by microwave irradiation (Addo Ntim and Mitra 2011). Smaller diameter CNTs have lower thermal stability because of their higher curvature strain, while purer, less defective CNTs are believed to oxidize at higher temperature (Freiman, Hooker et al. 2008).

FTIR is usually involved in the study of functionalized CNTs to confirm the presence of functional groups. C=C stretching around 1580 cm^{-1} shows in all MWCNT spectra which presents in the carbon skeleton of the MWCNTs. The carbonyl stretching frequency (C=O) around 1700 cm^{-1} , stretching vibration (C–O) around 1220 cm^{-1} and vibration (O-H) around 3400 cm^{-1} are provided the evidence of carboxyl groups in carboxylated MWCNTs (Wang, Xia et al. 2010). Desai et al. reported the sharp peaks at 2847 cm^{-1} and 2921 cm^{-1} which were attributed to the stretching vibration of alkyl chain from octadecylamine (ODA), indicated successful functionalization of CNT-ODA

composites (Desai, Addo Ntim et al. 2012). The new peak at 970 cm^{-1} was reported in the Pd-MWCNT spectrum to confirm the presence of Pd in the hybrid (V. Kumar, Addo Ntim et al. 2012).

Raman spectroscopy are usually used as complementary techniques with FTIR. The latter one put emphasis on functional groups and highly polar bonds while the former one is more sensitive to backbone structures and symmetric bonds. There are three characteristic bond in CNT raman spectrum, G-band around 1600 cm^{-1} associated with the in-plane vibration of the C–C bond and D-band around 1300 cm^{-1} assigned to defect and disorder in carbon structures and radial breathing mode(RBM) around 200 cm^{-1} resulting from the vibration of the entire tube (Bokobza and Zhang 2012) (Marulanda 2011). The frequency of RBM can be used to determine diameter of SWCNTs, which is inversely proportional to the reciprocal of the diameter (Marulanda 2011). The ratio of D/G bond can be used to determine the degree of defect of MWCNTs (Wang, Wu et al. 2015).

Large specific surface area (SSA) is a important properties of CNTs. Some potential applications and toxicity of CNTs are based on their SSA, while dimensions, impurities and surface functionalization may affect SSA of CNTs (Birch, Ruda-Eberenz et al. 2013). Thus SSA is a important property needed to be analyze to study characters of CNTs. Brunauer–Emmett–Teller (BET) is a widely used method for determine SSA. Birch et al. reported the SSA of a SWCNT product with a length of $5\text{--}30\text{ }\mu\text{m}$ was $367\text{ m}^2\text{ g}^{-1}$, which is 7% higher than that for a shorter sample from the same company. The SSA of pristine SWCNTs were reported around 4% higher than that of SWCNT-COOH (Birch, Ruda-Eberenz et al. 2013).

1.6 Dispersibility of Carbon Nanotubes

As CNTs find many real world applications, they will be released more and more into the environment by industry and the consumer market. They will be released into environment by wastewater discharge and hydrophobic CNTs tend to settle out of aqueous media into sediments, while water dispersible forms may persist in water resources (Wiesner, Lowry et al. 2006). After being released into environment, CNTs will interact with electrolytes and biological species which may increase the ecological and public health risk. CNTs may either aggregate or disperse in the aqueous media depending on interplay between electrostatic and van der Waals interactions (Thess, Lee et al. 1996). Therefore there is a need to develop a comprehensive understanding of the fate and transport of CNTs in aqueous media. Several reports in literature have addressed this issue (Elimelech, Jia et al. 1998) (Saleh, Pfefferle et al. 2008). The aggregation behavior of CNTs is important to study the fate and transport of CNTs in the environment. Since lots of the applications of CNTs require homogenous dispersions in either aqueous phase or organic solvents, most of the studies were focusing on enhancing the dispersibility of CNTs, by introducing functional groups such as carboxyl groups and amines (Chen and Mitra 2008) (Desai, Addo Ntim et al. 2012), adsorbing of specific polymers on the surface of CNTs (Jung, Koan Ko et al. 2004) or introducing surfactant (Jiang, Gao et al. 2003). Several techniques have been used to investigate the aggregation kinetics of CNTs, such as time-resolved dynamic light scattering (TRDLS), including the hydrodynamic diameter and zeta-potential measurements, UV-Visible spectroscopy (Peng, Jia et al. 2009) (Smith, Wepasnick et al. 2009).

The pristine CNTs tend to entangle and aggregate in solution because they are trying to minimize their surface free energy from strongly attractive van der Waals forces between the hydrophobic graphene layers. Therefore surface modification is required to prepare homogenous dispersion of CNTs. Carboxylation is one of the most important way to enhance the dispersibility of CNTs in water which usually carried out by adding oxidant such as HNO₃ and H₂SO₄. The oxygen-containing functional groups such as carboxyl groups will influence the CNTs' interactions with other dissolved species in solution which may lead to the change of the human and ecological impact of CNTs in aquatic media. TRDLS have been used to investigate the colloidal behavior of nanoparticles including CNTs. TRDLS measures Brownian motion and relates this to the size of particles. The laser illuminate the particles, the light will be scattered in all the direction if the particle is small. The speed of particles that are being moved by Brownian motion is followed the Stokes–Einstein equation. The smaller particles move faster. Speed of movement also lead to the intensity change of scattered light which will be collected and the intensity of the light will be analyzed to calculate hydrodynamic diameter, D_h (MalvernInstrumentsLtd 2004) (Chowdhury and Cui 2011):

$$D_h = k_B T / 6\pi\eta D_t \quad (1.1)$$

where k_B is the Boltzmann constant, T is the absolute temperature, η is the solvent viscosity and D_t is the diffusion coefficient. Aggregation kinetics were measured by monitoring the time-dependent increase in D_h (Smith, Wepasnick et al. 2009).

Critical coagulation concentrations (CCC) are determined by TRDLS under different aquatic conditions via measuring the aggregation rates as the function of

electrolyte concentration (Smith, Wepasnick et al. 2009). The initial rate of change in particle size (R_h) is proportional to kn_0 where k is the initial aggregation rate constant and n_0 is the initial concentration of the CNTs (Schudel, Behrens et al. 1997). The attachment efficiency (α) for suspensions with the same particle concentration was computed as:

$$\alpha = \frac{\left(\frac{dD_h(t)}{dt}\right)_{t \rightarrow 0}}{\left(\frac{dD_h(t)}{dt}\right)_{t \rightarrow 0, \text{ fast}}} \quad (1.2)$$

where $\left(\frac{dD_h(t)}{dt}\right)_{t \rightarrow 0}$ and $\left(\frac{dD_h(t)}{dt}\right)_{t \rightarrow 0, \text{ fast}}$ represent the slow and fast aggregation regimes, respectively (Schudel, Behrens et al. 1997, Elimelech, Jia et al. 1998). Attachment efficiency was determined as the ratio between the hydrodynamic size growth rate at initial aggregation and under the fast aggregation conditions (Zhang, Crittenden et al. 2012). CCC value is the lowest salt concentration when the system reached the fast aggregation regimes. In another word, beyond CCC value, attachment efficiency will no longer dependent on the salt concentration. Literatures showed the precipitation of the carboxylated CNTs in the presence of different salts is dependent on the charge on the cations which generally following Schulze-Hardy, and the well-established Derjaguin–Landau–Verwey–Overbeek (DLVO) theory. Schulze-Hardy rule states that the destabilizing power of the electrolyte is principally due to the valence of its ion that has charge opposite to the colloidal particle surface(counterion), whereas the nature and valence of its ionic species with the same sign(co-ions) have relatively little effect rule (Manivannan, Jeong et al. 2009) (Smith, Wepasnick et al. 2009).

$$CCC \sim \left(\frac{1}{z}\right)^n \quad (1.3)$$

where z is the valence of the electrolyte counterions. Typically, n is 6 in three dimensions and 9 in two dimensions (Sano, Kamino et al. 2000). DLVO theory suggests that the stability of a colloidal system is determined by the sum of these van der Waals attractive (V_A) and electrical double layer repulsive (V_R) forces that exist between particles as they approach each other due to the Brownian motion they are undergoing. This theory proposes that an energy barrier resulting from the repulsive force prevents two particles approaching one another and adhering together. But if the particles collide with sufficient energy to overcome that barrier, the attractive force will pull them into contact where they adhere strongly and irreversibly together. Therefore, if the particles have a sufficiently high repulsion, the dispersion will resist flocculation and the colloidal system will be stable. However, if a repulsion mechanism does not exist then flocculation or coagulation will eventually take place (Derjaguin and Landau 1993) (Verwey and Overbeek 1999). Schulze-Hardy rule results from interplay between van der Waals attraction and electric double-layer repulsion based on DLVO theory (Israelachvili 2011).

Smith et al. were investigate the aggregation behavior of carboxylated CNTs in the presence of electrolytes by TRDLS. Different salts with varied concentration were used: 4 M NaCl, 2 M Na₂SO₄, and 0.04 M MgCl₂ and 0.04 M CaCl₂ CCC values of NaCl, Na₂SO₄, MgCl₂ and CaCl₂ were 93 mM, 98 mM 1.8 mM, and 1.2 mM, respectively, which following Schulze-Hardy rule. The influence of pH on aggregation behavior was also studied in the presence of NaCl. CCC values increased from 26, 46 to 93, 132, and 259 mM

as the pH increased from 3, 4, 6, 8, and 10, respectively, which is a linear correlation (Smith, Wepasnick et al. 2009).

UV-Visible spectroscopy is also used by several research groups to investigate aggregation behavior of CNTs. The shortened, oxidized SWCNTs were studied by Sano et al. for colloidal behavior in the presence of chloride salts: Na^+ , K^+ , Mg^{2+} , Ca^{2+} , La^{3+} , and Ce^{3+} . UV absorbance of SWCNTs in the electrolyte solution were measured for obtaining CCC values, which were 37 mM, 26 mM, 0.31 mM, 0.20 mM, 0.050 mM, 0.052 mM, respectively for Na^+ , K^+ , Mg^{2+} , Ca^{2+} , La^{3+} , and Ce^{3+} . The results showed the CCC value is inversely proportional to counterion, and n was demonstrated to be 6 in this case. Therefore it is clearly proved that the aggregation behavior of SWCNT dispersions in the presence of electrolytes followed the Schulze-Hardy rule (Sano, Okamura et al. 2001). Peng et al. studied the precipitation behavior of oxidized CNTs by UV-Visible spectroscopy. The absorbance was taken at 252nm in the presence of NaCl, KCl, MgCl_2 , CaCl_2 , FeCl_3 and AlCl_3 and the precipitation value were obtained to be 185, 125, 1.05, 0.55, 0.15 and 0.036 mmol/L, respectively. This result also followed the Schulze-Hardy rule. The effect on aggregation kinetics of electrolytes with same z and different anions were also studied. For univalent and bivalent cations, precipitation value of cations with the same charge seems to be inversely proportional to cation radius. While, for trivalent cations Fe^{3+} and Al^{3+} , precipitation value does show relationship with cation radius. No significant change was found on the stability of CNTs by different anions (Peng, Jia et al. 2009). Long-term stability of CNTs were also studied by UV-Visible spectroscopy. Jiang et al. were one of the first groups to study the colloidal stability of the dispersions by UV-Visible spectrophotometric measurements. The stability of CNTs with and without sodium dodecyl

sulfate (SDS) over 500h. The concentration of supernatant CNT supernatant without SDS dropped 50%, and 15% for that SDS FOR 500h. CNT dispersion was still tend to precipitate after 500h, while after 150 h, no more precipitation was found for CNT dispersions with SDS (Jiang, Gao et al. 2003). The time dependent stability for 24h of oxidized CNT with and without electrolytes were investigated using UV-Visible spectroscopy by Ntim et al. It was found that the dispersion was stable in deionized water over 24 h. Stability of oxidized CNTs was better in the presence of the Na⁺ than Mg²⁺, which was consistent with the Schulze-Hardy rule (Ntim, Sae-Khow et al. 2011).

In general, there are three principles for dispersing fine particles in water: the repulsion between the particles with their zeta potentials, the steric hindrance of the adsorption layer, and the reduction of hydrophobic linkages among dispersed particles (Jiang, Gao et al. 2003). Therefore, zeta potential measurement is also important to investigate dispersibility of CNTs. A net charge at the particle surface affects the distribution of ions in the surrounding interfacial region, leading to an increased concentration of counter ions close to the surface. Therefore an electrical double layer exists around each particle. The liquid layer surrounding the particle exists as two parts; an inner layer, called the Stern layer, where the ions are strongly bound and an outer, diffuse, layer where they are less firmly attached. Within the outer layer, there is a notional boundary inside which the ions and particles form a stable entity. When a particle moves, ions within the boundary move with it, while any ions beyond the boundary do not move with the particle. This boundary is called the surface of hydrodynamic shear or slipping plane. The potential that exists at slipping plane is known as the Zeta potential (Figure 1.1). If all the particles in suspension have a large absolute value of zeta potential then they will

tend to repel each other but not aggregate. However, if the particles have low absolute zeta potential values then there is no force to prevent the particles coming together and aggregating. The general dividing line between stable and unstable suspensions is generally taken at either +30mV or -30mV. Particles with zeta potentials more positive than +30mV or more negative than -30mV are normally considered stable (MalvernInstrumentsLtd 2004).

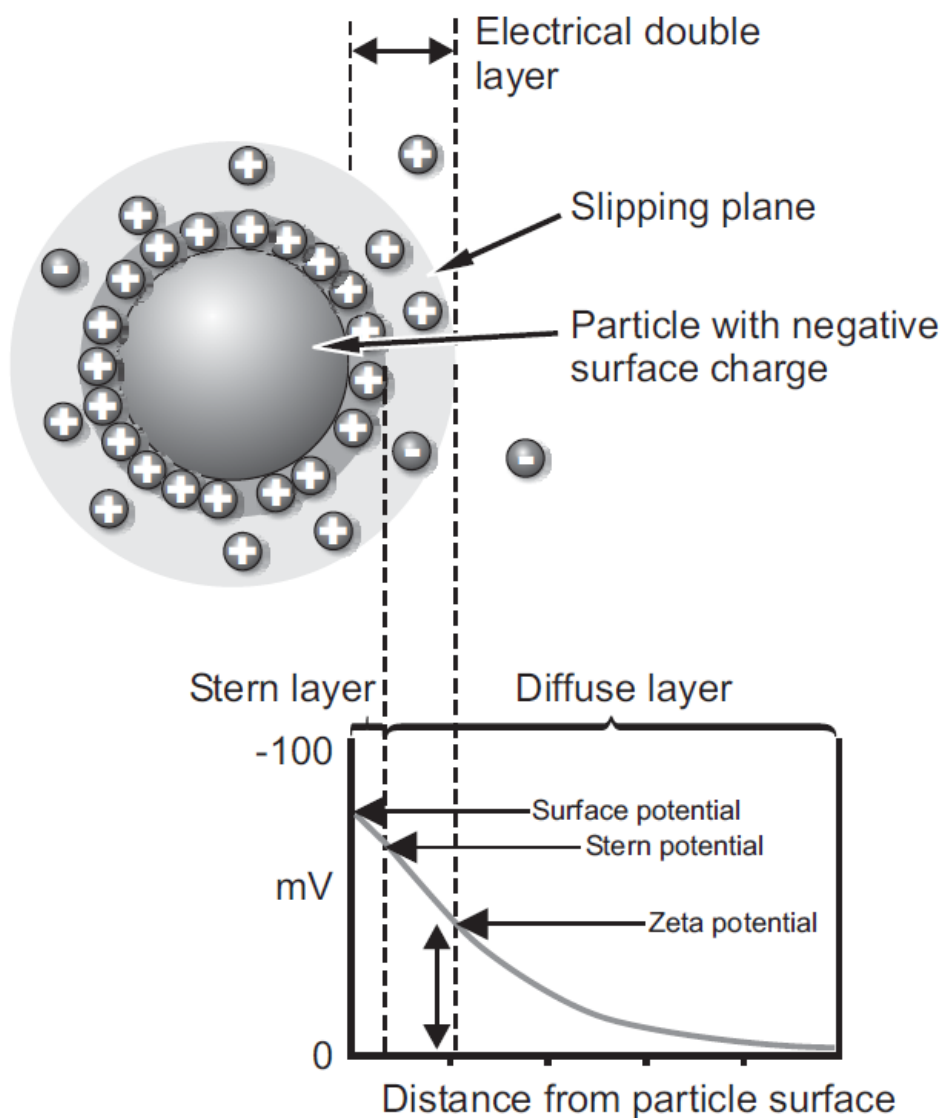


Figure 1.1 Zeta potential for a net surface charge particle.

Source: Zetasizer nano series user manual, 2004.

When an electric field is applied across an electrolyte, charged particles suspended in the electrolyte are tended to move towards the opposite charged electrode. This phenomenon is called electrophoresis. Viscous forces applying on the particles tend to oppose this movement. The particles will move at a constant velocity when these two opposing forces reach equilibrium. The velocity of a particle in an electric field is usually mentioned as its electrophoretic mobility, which is dependents on several factors, listed as strength of electric field or voltage gradient, the dielectric constant of the medium, the viscosity of the medium and zeta potential. When zeta potential measurement is carried out by TRDLS, an electric field is applied to the cell, any particles moving through the measurement volume will result in the intensity of light, which will be detected to fluctuate with a frequency proportional to the particle speed (Figure 1.2) (MalvernInstrumentsLtd 2004). Then the zeta potential will be calculated by using Henry equation:

$$U_E = 2\varepsilon z f(ka)/3\eta \quad (1.4)$$

where U_E is electrophoretic mobility, ε is dielectric constant, z is zeta potential, η is viscosity and $f(Ka)$ is Henry's function. Henry's function is determined either 1.5 or 1 depending on several factors such as size of particles, dielectric constant of media, concentration of electrolytes etc.

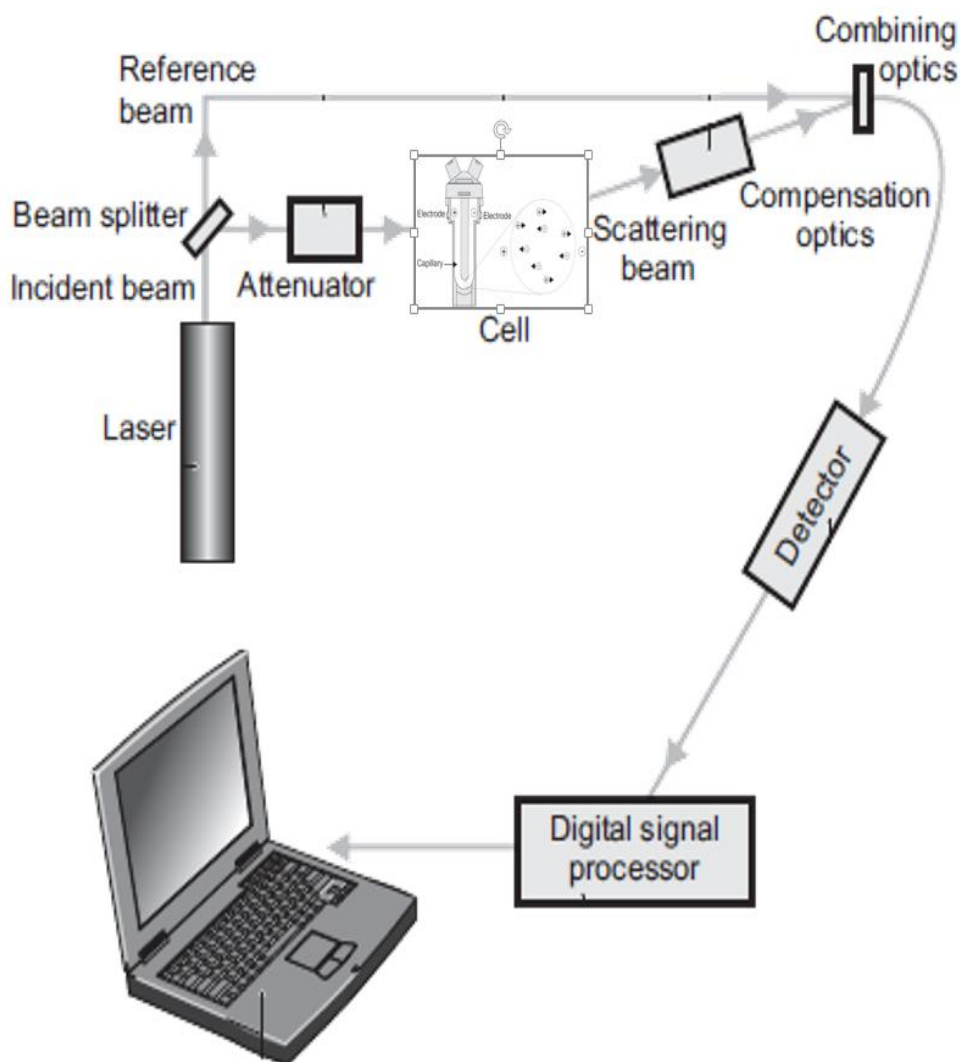


Figure 1.2 Schematic diagram of TRDLS for zeta potential measurements .
 Source: *Zetasizer nano series user manual, 2004.*

Jiang et al, reported the relationship between zeta potentials of the CNT dispersions with and without SDS and pH. The result showed that CNTs are negatively charged. In addition, zeta potential value of CNT dispersion with SDS was lower than the one without SDS from pH 2 to pH 12, expect around pH 11. This means that some acidic sites on CNTs were formed during purification by acid treatment which can be dissociated in the alkaline solutions. The maximum zeta potential value of CNT dispersion with SDS was measured as -40 mV, comparing with -30 mV for the CNT suspension without SDS, which means

that SDS can adsorb onto the CNTs to enhance the stability of CNTs. The effect of SDS is because of the electrostatic repulsion which can stabilize the CNTs against van der Waals attraction (Jiang, Gao et al. 2003). Zeta potential of the oxidized CNT dispersion in the presence of different salts with various concentrations were studied by Peng et al. Zeta potential increases with the precipitation of CNTs with NaCl, CaCl₂ and AlCl₃. Zeta potential measurements showed that the oxidized CNTs were negatively charged in aqueous phase, which is due to oxygen-containing groups such as carboxyl groups. These oxygen-containing groups attract metal cations, leading to neutralize of the negative surface charge. In the presence of salts, the electrolyte neutralized the negative surface charge on the oxidized CNTs, compressed the electrical double layer and thus decreased the electrostatic repulsive forces between dispersed CNTs particles which lead to aggregation (Weiser and Sons 1949) (Peng, Jia et al. 2009). Heister et al. reported the zeta potential of oxidized CNTs with and without oxidation debris as the function of pH. The results showed that the zeta potential reached maximum value at pH 2 in both cases. It became more negative with increasing pH from 2 to 10, and then slightly increased from pH 10 to 12. It is because that at acidic pH more carboxylic groups become deprotonated with increase of pH. While, the increase of zeta potential at basic pH is due to increased negative charge in the medium. There were significant different of zeta potential between CNTs with and without oxidation debris. This is probable because that oxidation debris contains a major part of the samples functionalities (Hu, Yu et al. 2005) (Wang, Shirley et al. 2009) and hence contributes to the total zeta potential, as long as it is attached to the CNT surface (Heister, Lamprecht et al. 2010).

1.7 Objectives

The objectives of this research are;

1. Investigating oxidation debris of microwave induced carboxylated CNTs.
2. Removal of oxidation debris by a reactive microwave process
3. Size reduction and size sorting of carboxylated carbon nanotubes to generate CNTs of different size and study their colloidal stability in aqueous environment.

CHAPTER 2

OXIDATION DEBRIS IN MICROWAVE FUNCTIONALIZED CARBON NANOTUBES: CHEMICAL AND BIOLOGICAL EFFECTS

Dilute base-washing has been shown to remove oxidation debris by converting the acidic groups to their dissolvable conjugate salts. In this chapter we present for the first time the effect of base-washing of microwave induced carboxylated carbon nanotubes (CNTs). Three multiwalled carbon nanotubes (MWCNTs) with different dimensions were studied, and the biological/toxicological properties were evaluated with human THP-1 cells. The carbon to oxygen ratio, the BET surface area, the ratio of D–G bands based on Raman measurements as well as the solubility changed with base wash. Most dramatic was in increase in carboxylic groups on the surface and a corresponding decrease in phenolic and lactonic groups. However, zeta potential, particle size and colloidal stability at different pH showed no significant alterations with the wash. The analysis of the wash showed the presence of graphitic carbon but the absence of small CNT fragments. Toxicity measurements and IL-1b release from the THP-1 cells in the presence of MWCNTs also showed no alteration with base wash. These results demonstrated that the oxidation under microwave conditions generated relatively less debris and fragmentation, and this is a good approach to acid functionalization of CNTs.

Since their first discovery, carbon nanotubes (CNTs) have attracted much attention due to their unique structural and electronic properties (Iijima 1991, Anand, Addo Ntim et al. 2011, Nair, Qin et al. 2012). Several processes for large-scale synthesis/manufacture of CNTs have been developed by various research groups, and almost all of them use transition metal catalysts. CNT formation occurs along with other non-tubular carbon

(NTC) species such as amorphous carbon, fullerenes and graphite (Iijima 1991, Thess, Lee et al. 1996, Cheng, Li et al. 1998). These impurities along with residual metal catalysts are not well characterized or controlled, and typically buried in the powdery support material (Hou, Liu et al. 2008, Aqel, El-Nour et al. 2012). The conventional approach to purification of raw CNTs is via some form of acid treatment, and these methods often lead to over-functionalization of CNTs forming unwanted oxidation products (Hou, Liu et al. 2008, Heister, Lamprecht et al. 2010). In addition, several different methods have been used to functionalize CNTs rendering them soluble in aqueous and non-aqueous media. A majority of the methods use acid treatment as a first step to introduce covalently bonded carboxylic functional groups on CNTs (Goyanes, Rubiolo et al. 2007, Salzmann, Llewellyn et al. 2007). This then can be further functionalized to amine, ester, amide, polymeric, or other groups (Lin, Rao et al. 2002, Coleman, Bailey et al. 2003, Goyanes, Rubiolo et al. 2007, Rogel-Hernández, Alonso-Nuñez et al. 2011). In short, acid treatment is an important step in both purification and functionalization of CNTs.

It has been reported that during conventional acid treatment, oxidation debris is generated and attach to the CNT surface by π -stacking, which are not easily removed by conventional water washing (Fogden, Verdejo et al. 2008, Heister, Lamprecht et al. 2010). Oxidation debris is known to affect the dimension of CNTs and their surface properties, which influence dispersion and stability in chemical and biological environments (Heister, Lamprecht et al. 2010). Dilute base-washing has been proposed as a method to remove oxidation debris by converting the acidic groups in the debris into their conjugate salts so that they are dissolved and removed. The resulting product is finally washed by a dilute

acid to remove the sodium ions from the samples (Verdejo, Lamoriniere et al. 2007, Fogden, Verdejo et al. 2008). Base-washing has been shown to significantly alter the CNT properties as it has altered the length, and particle size distribution in aqueous environments. Zeta potential and colloidal stability have also showed significant difference before and after base-washing (Heister, Lamprecht et al. 2010), while Raman analysis has shown peaks for disordered graphitic carbon in the filtrate and a decrease in the intensity of D to G band ratio in the CNTs (Fogden, Verdejo et al. 2008, Heister, Lamprecht et al. 2010).

Most efforts in CNT functionalization have involved the use of conventional chemical techniques, such as refluxing and sonication (Huang, Lin et al. 2002, Sun, Fu et al. 2002). Many of these reactions are carried out over long periods of time and sonication involves a high shear force environment which induces tube damage such as shortening of length (Datsyuk, Kalyva et al. 2008, Heister, Lamprecht et al. 2010). Another approach developed for both purification and functionalization of CNTs is the use of microwave energy, which has been found to be fast and provides a high degree of functionalization (Chen and Mitra 2008). However, CNT chemistry under microwave radiation is known to be somewhat different resulting in dramatically lower activation energy (Perreux and Loupy 2001, Chen and Mitra 2008). Therefore, it is important to evaluate the oxidation debris generated during microwave functionalization. This chapter presents the effect of base-washing on microwave functionalized carbon nanotubes. In addition, the effects on the biological activity/toxicity of the modified CNTs were determined using THP-1 cells.

2.1 Experimental

2.1.1 Preparation of the F-MWCNTs

The synthesis of the carboxylated multiwall carbon nanotubes (F-MWCNT-SS, F-MWCNT-SL, and F-MWCNT-LS) were carried out under the microwave accelerated reaction system by dispersing pre-weighed MWCNTs into a mixture of concentrated H₂SO₄ and HNO₃. The reaction vessels were subject to microwave radiation at a preset temperature of 140 °C for 20 minutes. After cooling down to room temperature, the product was vacuum filtered and washed using Milli Q water through pore size 10 µm until a neutral pH. F-MWCNT samples were then dried in a vacuum oven at 70 °C until a constant weight was achieved.

2.1.2 Preparation of Base-washed Samples

F-MWCNT samples were washed with 0.01M NaOH until the filtrate turned colorless (from brown tint). The resulting products were washed with Milli Q water until a neutral pH was obtained. Finally, the products were washed by 0.01M HCl, and then washed with Milli Q water to neutral pH again. The base-washed samples and filtrates were referred to as BWF-MWCNT-SS, BWF-MWCNT-SL, BWF-MWCNT-LS and W-MWCNT-SS, W-MWCNT-SL; W-MWCNT-LS.

2.1.3 Characterization

A scanning electron microscope (SEM, LEO 1530 VP, Carl Zeiss SMT Inc., Peabody, MA) equipped with an energy-dispersive X-ray analyzer (EDX, Oxford Instruments, Concord, MA) was used for microscopic, dimensional and elemental analysis of the

samples. Specific surface areas of the samples were measured using Quantachrome NOVA 3000 series (Model N32-11) High Speed Gas Sorption Analyzer at 77.40 K (Boynton Beach, FL). Before each experiment, the samples were heated at 300 °C in a vacuum oven and degassed for three hours. The samples were mixed with purified KBr and pressed into pellets. Fourier transform infrared spectroscopy (FTIR) analysis was carried out using a Perkin-Elmer instrument (Waltham, MA) coupled with Raman spectroscopy using a DXR Raman microscope (Thermo Fisher Scientific Inc., Madison, WI). The solubility was measured as follows. Solutions of F-MWCNT and BWF-MWCNT were prepared at different concentrations from 0.5 to 5 mg/ml at 0.5mg/l interval. The solution was then sonicated for 30mins, allowed to settle for 24 hour to precipitate. This provided a rough estimate of the solubility range. Then a super saturated solution was prepared and allowed to settle for 24 hours. The saturated solution was decanted and dried until constant weight to estimate solubility.

The Boehm titration was carried out for determining the functional groups on the surface of the functionalized CNTs using a procedure published before (Goertzen, Thériault et al. 2010). Pre weighed amount of F-MWCNT and BWF-MWCNT was added to 50ml of 0.05M of the three bases, namely NaHCO_3 , Na_2CO_3 and NaOH . The samples were shaken for 24 hours and filtered. Ten milliliter of the filtrate was taken for titration. This was acidified by the addition of 30ml 0.5M HCl . The samples were then titrated with 0.05 M NaOH . The samples were degassed to remove CO_2 for 2 hours. Phenolphthalein was used as the indicator to determine the endpoint (Goertzen, Thériault et al. 2010). Particle size and zeta-potential were measured at 25 °C by Zetasizer nano ZS90 (Malvern Instruments Ltd., Worcestershire, UK) at a 90 ° detector angle.

2.1.4 Toxicological Analysis

MWCNT suspensions were prepared as follows. The MWCNTs were weighed and suspended in 5% Infasurf (calfactant, ONY, Inc. Amherst, NY) diluted in sterile saline. Nanotube suspensions were sonicated for 2 min at half max power in a Masonix cup horn sonicator (XL2020, Farmingdale, NY) attached to a Forma circulating water-bath at 550 watts and 20 Hz (8000 Joules) at a stock concentration of 5 mg/ml.

Human THP-1 cell line culturing was carried out as follows. THP-1 cells, a human monocytic cell line obtained from ATCC (Manassas, VA), were suspended in RPMI media (MediaTech, Manassas, VA) supplemented with 10% fetal bovine serum, 50 μ M beta-mercapto ethanol, 1 mM sodium pyruvate, 250 ng/ml amphotericin B, and 100 U/ml penicillin and streptomycin (all supplements Media Tech, Manassas, VA) in 75 cm³ flasks at 37 °C. The cells in suspension were differentiated into a macrophage-like cell by adding 150 nM Vitamin D3 for 24 hr. The adherent cells were scrapped with a rubber policeman (Corning, Corning, NY). The cells were then centrifuged at 400 x g for 5 min, the resulting cell pellet was re-suspended in 1 ml of complete media, and a 40 μ l sample was then counted on a Z2 Coulter Counter (Beckman Coulter, Miami, FL). The cells were suspended at 1 x 10⁶ cells/ml and a small amount of phorbol 12-myristate 13-acetate (5 nM PMA, Sigma) and lipopolysacharride (10 ng/ml LPS, Sigma) was added. PMA co-stimulation was necessary to stimulate phagocytosis of the MWCNTs. LPS co-stimulation was necessary to induce NF- κ B translocation leading to pro-IL-1 β synthesis for the NLRP3 inflammasome to cleave for IL-1 β release in the transformed THP-1 model (Dostert et al., 2008; Palomaki et al., 2011). Cells, at a volume of 350 μ l, were then pipetted in to 1.5 ml microfuge tubes. The MWCNT conditions were added from 5 mg/ml

concentrated stock suspensions to the cells at a final concentration of 25 $\mu\text{g/ml}$. The MWCNT variants used a range of concentrations (0, 6.25, 12.5, 25, and 50 $\mu\text{g/ml}$). The resulting cell/particle suspension was mixed by pipette action. The cells were then transferred to 96-well tissue culture plates at 100 μl per well in triplicate (100 x 103 cells/well), and cultured for an additional 24 hr. All cultures were maintained in 37 $^{\circ}\text{C}$ water-jacketed CO₂ incubators (ThermoForma, Houston, TX). Viability and IL-1 β levels were determined as described below.

2.1.4.1 Toxicity Assays. MTS assay -Cell viability was determined by MTS reagent using the CellTiter96 assay (Promega, Madison, WI) according to the manufacturer's protocol with the exception below. This assay used a colorimetric dye read by a colorimetric plate reader (Molecular Devices, Sunnyvale, CA). In order to avoid artifacts in the optical density values steps were taken to remove the MTS reagent (transferring it into another plate) from the cell/particle mixture adhered to the plate bottom. The formation of bubbles was avoided and the plate was read at 490 nm.

LDH assay – Lactate dehydrogenase was assayed with 50 μl of culture supernatant isolated from 24 hr cultures by CytoTox-96 Homogeneous Membrane Integrity Assay (Promega, Madison, WI) according to the manufacturer's protocol with the following exception. The LDH substrate/culture media reaction was allowed to progress for only 10 min before the stop solution was added. The plates were read at 490nm on a colorimetric plate reader (SpectraMax 190 from Molecular Devices, Sunnyvale, CA). All data was normalized to 100% cell lysis that was conducted 30 min before the 24 hr culture ended (10

µl Promega lysis buffer added) in specially designated control wells with the same number of cells.

2.1.4.2 Cytokine Assays. Human IL-1 β DuoSets were obtained from R&D Systems (Minneapolis, MN) and ELISA assays performed according to the manufacturer's protocol. Plates were read at 450 nm and data expressed as mean \pm SEM pg/ml in culture supernatant.

2.2 Results and Discussion

2.2.1 Characterization

SEM images of MWCNT-SL samples are presented in Figure 2.1. The other MWCNT samples are not presented here for brevity. After acid treatment, the CNTs remained intact with minimal visible tube defect. The elemental analysis (Table 2.1) was carried out by EDX. The main metal impurities in the raw samples were Fe and Ni, which were totally removed after functionalization. The percentages of oxygen in F-MWCNT samples were much higher than in the original MWCNTs due to the generation of carboxylic groups. The oxygen content decreased by 33, 50, 46% following the base wash for MWCNT-SS, MWCNT-SL, and MWCNT-LS, respectively. The carbon to oxygen ratio for the MWCNT base-washed samples increased from 13, 8, and 9 to 21, 18, and 18, respectively indicating the removal of oxygen containing moieties during the base wash.

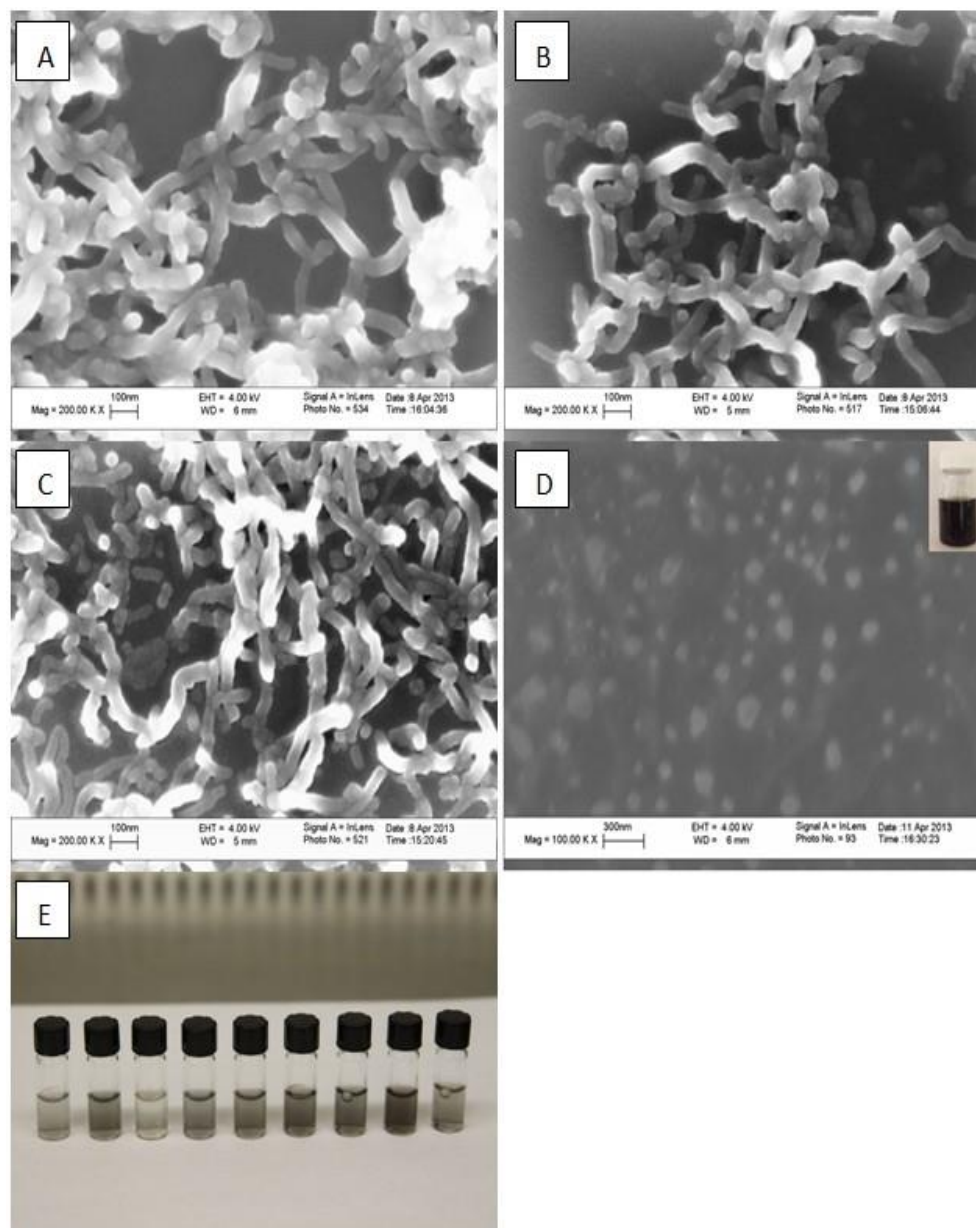


Figure 2.1 SEM images of A) MWCNT-SL, B) F-MWCNT-SL, C) BWF-MWCNT-SL, D) W-MWCNT-SL, E) Photograph showing the dispersion of 50 µg/ml of MWCNT-SS; F-MWCNT-SS; BWF-MWCNT-SS; MWCNT-SL; F-MWCNT-SL; BWF-MWCNT-SL; MWCNT-LS; F-MWCNT-LS; BWF-MWCNT-LS (from left to right) in complete RPMI media without phenol red, made from sonication of 5mg/ml stock in 5% infasurf/saline.

Table 2.1 Elemental Analysis of MWCNTs

	Elemental analysis (% weight)				Carbon to Oxygen ratio
	C	O	Ni	Fe	
MWCNT-SS	96	2	1	1	64
F-MWCNT-SS	91	9	-	-	13
BWF-MWCNT-SS	94	6	-	-	21
W-MWCNT-SS	57	43	-	-	1.8
MWCNT-SL	95	3	1	1	42
F-MWCNT-SL	86	14	-	-	8
BWF-MWCNT-SL	93	7	-	-	18
W-MWCNT-SL	65	35	-	-	2.5
MWCNT-LS	98	1	1	-	131
F-MWCNT-LS	87	13	-	-	9
BWF-MWCNT-LS	93	7	-	-	18
W-MWCNT-LS	59	41	-	-	1.9

The dimensions of the MWCNTs, before and after the base-wash, are presented in Table 2.2. The length and diameter did not show any statistically significant differences during base wash, which confirmed that the microwave process did not fragment the MWCNTs, nor cause excessive external tube damage. The previous studies using reflux and ultrasonication reported change in length after base wash, which was attributed to the generation of small fragments during functionalization (Heister, Lamprecht et al. 2010). The SEM of the oxidation debris did not show the presence of any nanotubes or tube

fragments, which also implied that the microwave treatment did not cause much fragmentation, and the debris comprised mainly of nontubular carbons.

Table 2.2 Dimension, Particle Size, Zeta Potential, and Solubility of the F-MWCNT and BWF-MWCNT

	Length (nm)	Diameter (nm)	Particle size (nm)	Zeta potential (mV)	Solubility (mg/ml)
F-MWCNT-SS	897.7±430.5	24.5±6.4	104	-43	1.91
BWF-MWCNT-SS	805.9±396.2	23.6±5.3	113	-40	1.85
F-MWCNT-SL	760.9±518.9	32.5±9.0	92	-44	1.49
BWF-MWCNT-SL	730.6±450.6	32.1±4.6	82	-46	2.23
F-MWCNT-LS	-	22.5±5.6	100	-44	1.32
BWF-MWCNT-LS	-	22.7±4.3	95	-44	1.65

The Brunauer, Emmett, and Teller (BET) surface area of all samples are shown in Table 2.3. All MWCNTs had large surface area. For all three sizes, the specific surface areas of carboxylated carbon nanotubes were higher than those of pristine ones and lower than those of samples after base wash. It implies that during acid treatment the specific surface area increased, resulting from more defects on the surface. The increasing of surface area after base wash was due to the removal of oxidation debris which led more surface being exposed.

Table 2.3 BET Surface Area of MWCNTs

	MWCNT -SS	F-M WC NT-S S	BWF- MWC NT-S S	MWCN T-SL	F-M WCN T-SL	BWF- MWC NT-S L	MWC NT-L S	F-M WCN T-LS	BWF -MW CNT- LS
BET surface area (m ² /g)	140.6	156.0	168.9	204.9	233.7	264.7	217.3	240.4	264.0

FTIR spectroscopy (Figure 2.2) was used to qualitatively analyze functional groups on the surface of materials. The carbonyl stretching frequency (C=O) around 1716 cm⁻¹ and stretching vibration (C-O) around 1223 cm⁻¹, provided the evidence of carboxyl groups in all F-MWCNT and BWF-MWCNT samples, which was absent in raw MWCNT. C=C stretching around 1580 cm⁻¹, which was present in the carbon skeleton of the MWCNTs, was seen in all materials. The FTIR analysis showed the same peaks after base-wash, which meant the base wash did not affect the attachment of carboxylic groups on the surface of MWCNTs.

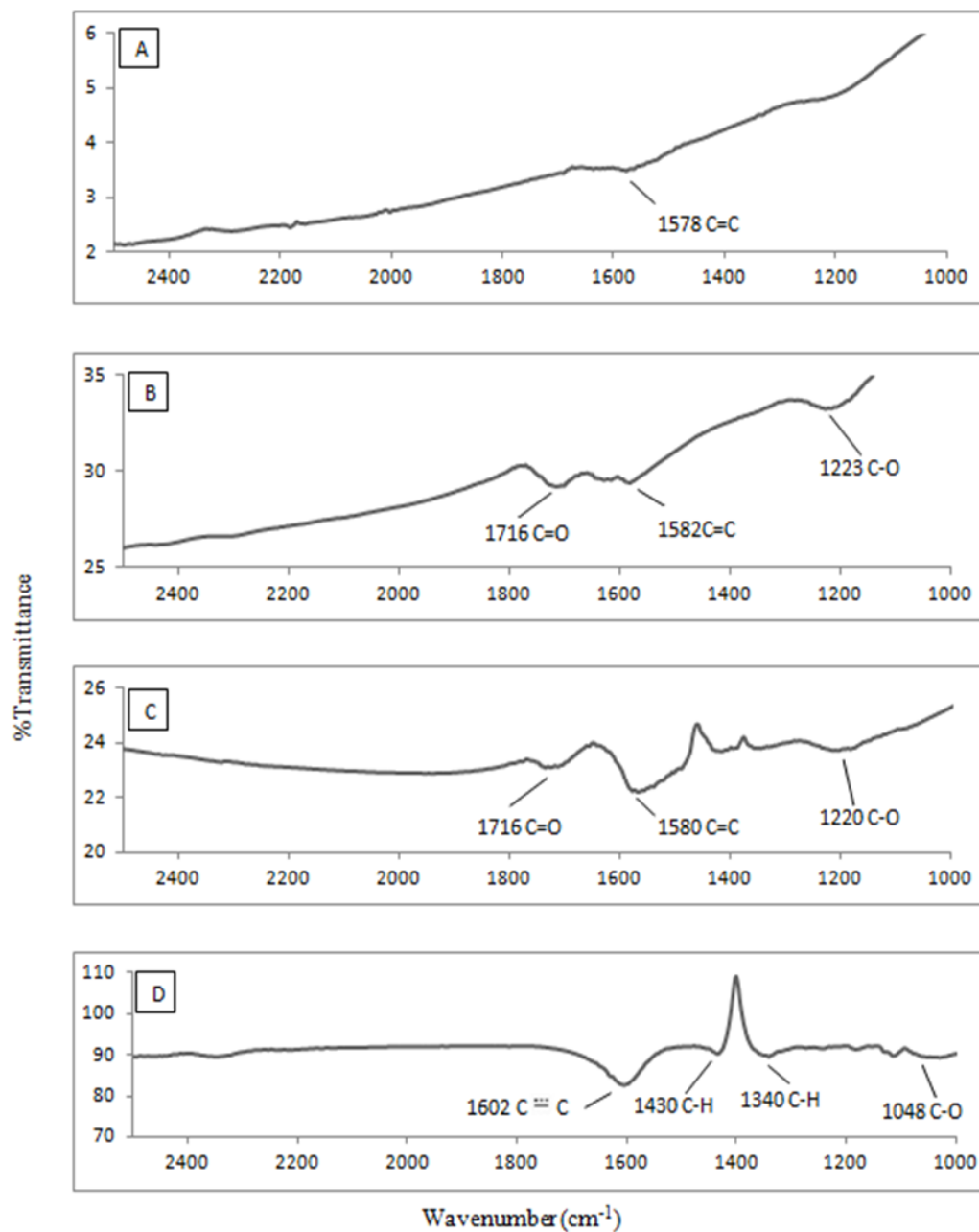


Figure 2.2 FTIR spectroscopy of A) MWCNT-SL, B) F-MWCNT-SL, C) BWF-MWCNT-SL, D) W-MWCNT-SL.

Figure 2.3 shows the Raman spectra of the different MWCNT samples. The ratio of intensity between D band (defect band) and G band (graphite band) increased by 12.9% from raw MWCNT-SL to F-MWCNT-SL, and decreased by 26.4% with base washing,

indicating defect generation during acid treatment and removal of defective debris during the base-wash. This implied that the base-wash was effective in removing some debris.

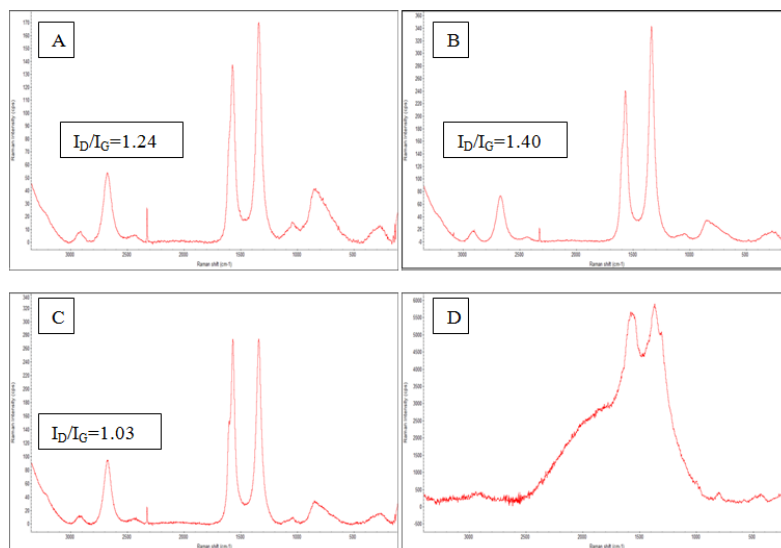


Figure 2.3 Raman spectroscopy of A) MWCNT-SL, B) F-MWCNT-SL, C) BWF-MWCNT-SL, D) W-MWCNT-SL.

Wash residue did not show any carbonyl peaks. It did show the presence of benzene ring stretching at 1602 cm^{-1} , and C–H vibration at 1340 cm^{-1} and 1430 cm^{-1} . In addition, C–O stretching (1048 cm^{-1}) was observed proving the removal of oxidation debris, which were attributed to polyaromatic fragments (Verdejo, Lamoriniere et al. 2007) (Stěfani, Paula et al. 2011). Raman spectroscopy of the filtrate did not show any characteristic peaks for carbon nanotubes, but resembled peaks of graphite, implying that the oxidation debris contained disordered graphitic carbon but not small fragments of the nanotubes. By removing impurities from the surface, the base-wash exposed much of the carboxylated groups in the MWCNTs and resulted in an increase in aqueous solubility. This was especially true for MWCNT-SL, which showed an increase in solubility from 1.49 to 2.23 mg/ml.

Three different bases were used to determine different surface groups (phenols, lactonic and carboxyl groups). NaOH reacted with all surface groups while Na₂CO₃ reacted with carboxyl and lactonic groups, and NaHCO₃ only reacted with carboxyl groups. The amount of functional groups which reacted with each was calculated using a procedure published before (Goertzen, Thériault et al. 2010). Table 2.4 showed the functional group concentration on the surface of F-MWCNT and BWF-MWCNT. The concentration of carboxyl group increased after base wash while the amount of other functional groups like phenols and lactonic groups decreased; C/O ratio changed due to the removal of the acidic groups. More carboxyl groups were exposed after the base wash due to the removal of the oxidation debris.

Table 2.4 Surface Functional Groups on F-MWNCT and BWF-MWCNT

	Carboxyl groups ($\mu\text{mol/g}$)	Lactonic groups ($\mu\text{mol/g}$)	Phenolic groups ($\mu\text{mol/g}$)
F-MWCNT-SS	1014 \pm 6	1304 \pm 208	1352 \pm 231
BWF-MWCNT-SS	1404 \pm 5	861 \pm 127	633 \pm 33
F-MWCNT-SL	626 \pm 5	798 \pm 5	2021 \pm 288
BWF-MWCNT-SL	1151 \pm 262	526 \pm 99	1183 \pm 185
F-MWCNT-LS	846 \pm 136	774 \pm 46	800 \pm 144
BWF-MWCNT-LS	1544 \pm 215	674 \pm 46	387 \pm 53

2.2.2 Colloidal Properties of F-MWCNTs and BWF-MWCNTs

The difference in colloidal behavior of F-MWCNTs and BWF-MWCNTs was studied using dynamic light scattering as described above. Particle size distribution and

zeta-potential of the MWCNT samples are presented in (Table 2.2). Raw MWCNTs showed poor solubility in water and settled out of the suspension. Both F-MWCNTs and BWF-MWCNTs were more stable in water. As can be seen from Table 2.2, there was not much different between F-MWCNTs and corresponding BWF-MWCNTs. The presence of the oxidation debris did not affect the stability or dispersibility of carbon nanotubes.

Zeta-potential of samples after acid treatment and base-wash in different pH was also measured (Figure 2.4). For all the samples, zeta-potential became more negative with increasing pH because more carboxylic groups were deprotonated in an acidic environment. While zeta-potential became less negative with increasing pH from 7-14, resulting from increased negative charge in the medium. Once again, the base-wash did not significantly alter the zeta-potential values. This was different from the previous report using other methods of functionalization where base-washed samples showed very different colloidal behavior with less negative zeta-potentials and the average difference between functionalized and base washed MWCNTs were nearly nineteen (Heister, Lamprecht et al. 2010).

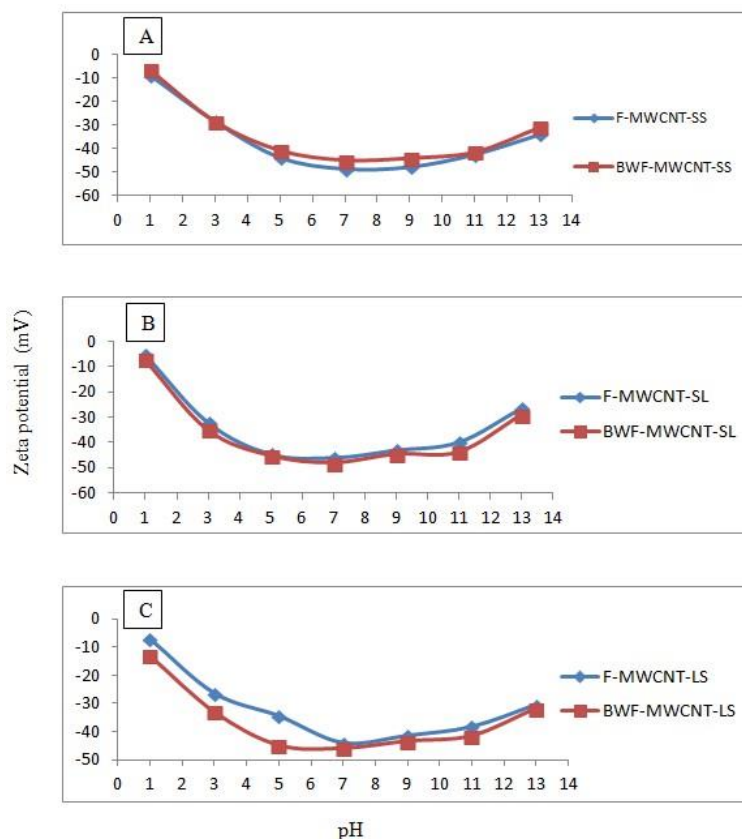


Figure 2.4 Zeta potential of A) F-MWCNT-SS and BWF-MWCNT-SS, B) F-MWCNT-SL and BWF-MWCNT-SL, C) F-MWCNT-LS and BWF-MWCNT-LS in different pH.

2.2.3 Biological Activity of F-MWCNTs and BWF-MWCNTs

The biological activities of the different MWCNTs were assessed by a standard MTS/LDH viability assays (Figure 2.5) and by the LPS-stimulated release of IL-1 β (Figure 2.6), which requires activation of the NLRP3 inflammasome (Hamilton Jr, Buford et al. 2012). Figure 2.1(E) shows the dispersion of the MWCNTs in the cell culture medium. The validation and reliability of these two assays using differentiated THP-1 cells (a human macrophage-like cell model) have been recently described (Xia, Hamilton et al. 2013). The two assays were conducted after 24 hr treatments with the particles. All of the MWCNTs caused significant toxicity by MTS assay, which was dose-dependent for all of the

particles. In contrast, there was no significant increase in LDH caused by the particles. The MTS assay has been a more sensitive indicator of MWCNT toxicity. Regardless of the assay employed, there was no significant difference in toxicity as a result of functionalization or base wash. The original MWCNTs for all sizes caused significant increase in IL-1 β release. Functionalization of MWCNTs with carboxyl groups decreased the ability of the MWCNTs to activate IL-1 β release from the macrophage-like cell line. Although base-wash changed the surface properties of the functionalized MWCNTs, there was no increase or decrease in the ability to stimulate IL-1 β release regardless of size. In general, the base wash did not appear to alter biological activity with regards to this cell line.

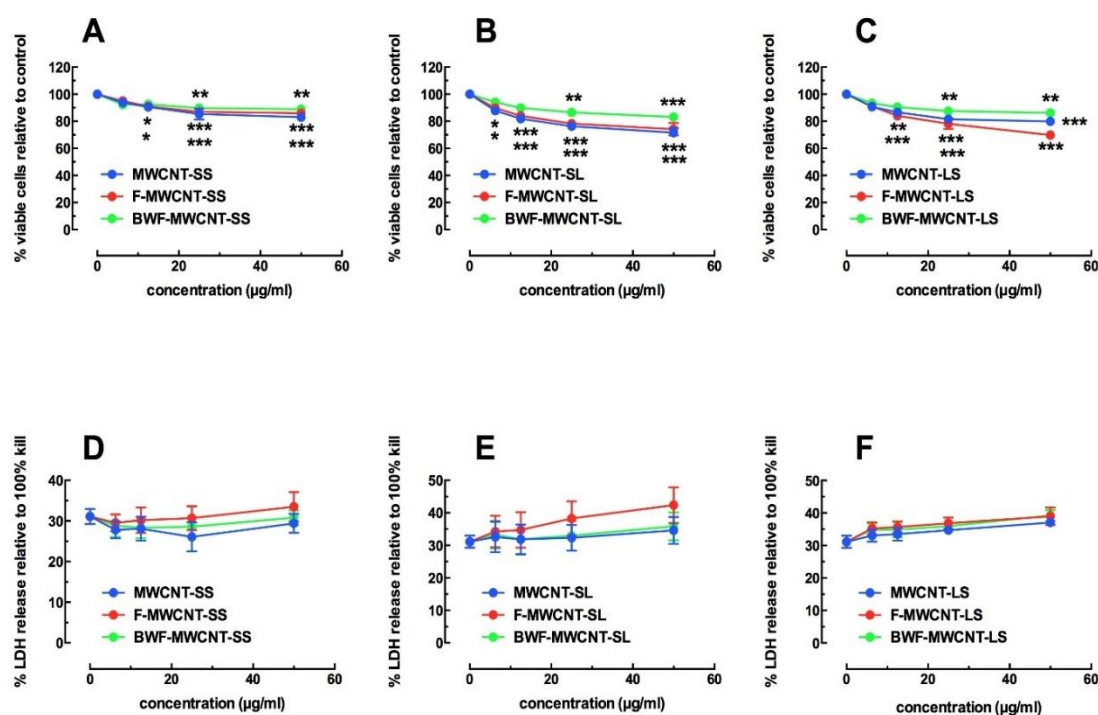


Figure 2.5 24-hr toxicity in the THP-1 model for all MWCNT. Relative dose-dependent toxicity by MTS assay for A) the MWCNT-SS variants, B) the MWCNT-SL variants, C) the MWCNT-LS variants. LDH release for D) the MWCNT-SS variants, E) the MWCNT-SL variants, F) the MWCNT-LS variants. All data expressed as mean \pm SEM. Asterisks indicate *** P < 0.001, ** P < 0.01, or * P < 0.05 compared to no particle (0 μ g/ml concentration) control condition. n = 3.

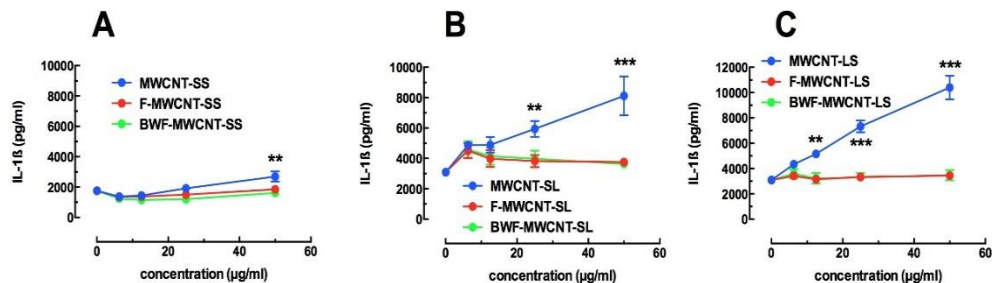


Figure 2.6 24-hr IL-1 β release in the THP-1 model for all MWCNT. Relative dose-dependent IL-1 β release for A) the MWCNT-SS variants, B) the MWCNT-SL variants, C) the MWCNT-LS variants. All data expressed as mean \pm SEM. Asterisks indicate *** $P < 0.001$, ** $P < 0.01$, or * $P < 0.05$ compared to no particle (0 μ g/ml concentration) control condition. $n = 3$.

2.3 Conclusions

MWCNTs of three different dimensions were used for studying the effects of base-washing of microwave carboxylated MWCNTs. Chemical, structural and biological/toxicological alterations were studied before and after base wash. While there were chemical changes along with solubility, there was no alternation in size, colloidal stability or dispersibility. There was a significant increase (as much as 83.9%) in carboxylic groups on the surface and a corresponding decrease in phenolic and lactonic groups. The wash did not show the presence of MWCNT fragments either. Based on standard MTS viability assay and the stimulated release of IL-1 β , toxicological properties did not change with base wash. The minimum alteration of many of the chemical and biological properties were attributed to minimum tube damage and debris formation during microwave processing and the study showed that microwave reaction is a good way to introduce carboxyl groups on MWCNTs.

CHAPTER 3

MICROWAVE INDUCED REACTIVE BASE WASH FOR THE REMOVAL OF OXIDATION DEBRIS FROM CARBOXYLATED CARBON NANOTUBES

Removal of oxidation debris for generating high purity functionalized carbon nanotubes (CNTs) has been a challenge, where base washing has been found to be an effective purification treatment. In this chapter we report microwave induced reactive base wash (MRW) as a fast, green alternate to conventional filtrate washing. Carboxylated CNTs of three different dimensions were subjected to MRW and the results were compared to conventional base-wash. The results showed that MRW was an effective method for the removal of oxidation debris which reduced the reaction time from 4 h to 20 min and alkali consumption by 75%. The CNTs from MRW were similar to those from conventional base wash in terms of dimensions, elemental composition, BET surface area and colloidal stability in aqueous media.

Many applications such as photovoltaics and drug delivery require high purity CNTs (Campidelli, Klumpp et al. 2006) and much effort has gone into purification of raw CNTs. It has been reported that oxidation debris are generated during carboxylation via acid treatments. The debris comprises of partially oxidized polyaromatic fragments that attach to the CNT surface by π -stacking, and are not easily removed by washing with water (Fogden, Verdejo et al. 2008, Heister, Lamprecht et al. 2010). These impurities adversely affect physical and chemical properties such as dimensions, surface properties, dispersibility and stability in chemical and biological environments (Heister, Lamprecht et al. 2010). Dilute base-washing has been used to remove the debris (Heister, Lamprecht et al. 2010) where the acidic groups are converted into their conjugate salts and washed out.

Chemical, physical and structural properties of carboxylated CNTs are known to improve after the base wash because it eliminates the impurities from the surface (Heister, Lamprecht et al. 2010, Wu, Hamilton Jr et al. 2014).

The conventional approach to debris removal is to wash the oxidized CNTs with dilute base followed by water. Finally, a dilute acid wash is used to reinstate the surface carboxylic groups (Verdejo, Lamoriniere et al. 2007, Fogden, Verdejo et al. 2008, Wu, Hamilton Jr et al. 2014). The first step usually needs a large amount of base and it takes several hours (or days) to wash the debris out and also generates much waste. Moreover, during long filtrations some CNTs are lost. Therefore, it is important to develop efficient base wash techniques that require less time and chemicals.

CNTs are known to be microwave active and the latter has been used for purification and functionalization (Chen and Mitra 2008). These processes have been carried out with less reagents and in significantly shorter time. This chapter presents microwave induced reactive base wash (MRW) of carboxylated CNTs as a fast, green method for the removal of oxidation debris.

3.1 Experimental

3.1.1 Chemicals

Three types of multi-walled carbon nanotubes were purchased from Cheap Tubes Inc (Brattleboro, VT). Purity of each was higher than 95%. The CNTs were categorized based on size. Those which had relatively shorter length and diameter (0.5-2 μ m long and 10-20 nm OD) were referred to as CNTSS; shorter length and relative larger diameter (0.5-2 μ m long and 30-50 nm OD) were referred to as CNTSL, and longer length and smaller

diameter (10-30 μm long and 10-20 nm OD) were referred to as CNTLS. All other chemicals were purchased from Sigma Aldrich (St Louis, MO) with purity higher than 95%.

3.1.2 Preparation of the F-CNTs

The preparation of the functionalized multiwall carbon nanotubes (F-CNT_{SS}, F-CNT_{SL}, and F-CNT_{LS}) were carried out in a microwave accelerated reaction system (CEM Corp. Mars System). Pre-weighed amounts of CNTs were treated with a mixture of concentrated H₂SO₄ and HNO₃ under microwave radiation at 140 °C for 20 minutes. After cooling down to room temperature, the products were vacuum filtered and washed by Milli Q water through 10 μm filter paper until a neutral pH was obtained. The F-CNTs were then dried under vacuum oven at 70 °C until a constant weight was achieved.

3.1.3 Preparation of Base-washed Samples

F-CNT samples were washed by dilute base via conventional washing through filtration as well as by MRW. For conventional washing, F-CNT samples were filtered through a 10 μm filter paper and washed with 0.01M NaOH until the filtrate turned from brown to colorless. This method has been reported before (Verdejo, Lamoriniere et al. 2007, Wu, Hamilton Jr et al. 2014). The wash was continued with Milli Q water until a filtrate of neutral pH was obtained. Finally, the F-CNTs were washed by 0.01M HCl, and then washed with Milli Q water to obtain a neutral pH. These filter-washed samples and filtrates were referred to as BW-F-CNT_{SS}, BW-F-CNT_{SL}, BW-F-CNT_{LS} and W-CNT_{SS}, W-CNT_{SL}; W-CNT_{LS}

For MRW, the F-CNT samples were treated with different volumes 0.01M NaOH under microwave irradiation at 100 °C for different periods of time. The resulting solids

were filtered and washed using additional 5 ml of 0.01M NaOH to determine if the oxidation debris had been completely removed. Then the resulting products were washed with Milli Q water until a neutral pH was obtained. Once again the products were washed with 0.01M HCl and then washed with Milli Q water to obtain a neutral pH. These microwave-washed samples and filtrates were referred to as MRW-F-CNT_{SS}, MRW-F-CNT_{SL}, MRW-F-CNT_{LS} and W-MRW-CNT_{SS}, W-MRW-CNT_{SL}, W-MRW-CNT_{LS}.

3.1.4 Characterization

Scanning electron microscopy (SEM) and energy-dispersive X-ray analyzer (EDX) were carried out using a LEO 1530 VP, (Carl Zeiss SMT Inc., Peabody, MA) equipped with EDX (Oxford Instruments, Concord, MA). For FTIR analysis, the samples were mixed with purified KBr and pressed into pellets, and then the analysis was carried out using a Perkin-Elmer instrument (Waltham, MA) instrument. Raman spectra were obtained using a DXR Raman microscope (Thermo Fisher Scientific Inc., Madison, WI). Specific surface areas of the samples was carried out using a Quantachrome NOVA 3000 series (Model N32-11) High Speed Gas Sorption Analyzer at 77.40 K (Boynton Beach, FL). Before each experiment, the samples were heated and degassed at 300 °C in a vacuum oven for three hours. Particle size and zeta-potential were measured at 25 °C by Zetasizer nano ZS90 (Malvern Instruments Ltd., Worcestershire, UK) at a 90 ° detector angle.

3.2 Results and Discussion

3.2.1 Sample Preparation

MRW was tested under different conditions. Based on previous studies (Heister, Lamprecht et al. 2010, Wu, Hamilton Jr et al. 2014), the turning of filtrate color from brown to colorless was used as an indicator for complete removal of the debris. In initial screening reactions, 50 ml 0.01M NaOH was used to treat 0.2 g F-CNTs by MRW for reactions times of 5, 10, 15 and 20 min. For 5 min reaction time, the filtrate showed a light yellow color which was attributed to incomplete reaction. For reactions times of 10, 15 and 20 min, the filtrates showed brown color. An additional wash using 5ml NaOH still showed brown solution which implied that the oxidation debris remained in the sample. The ratio of the base to F-CNTs was doubled to complete the reaction within a shorter time period. Now 50 ml of 0.01M NaOH was used to treat 0.1g F-CNTs for 15 and 20 min. The filtrate of these two batches showed brown color. A wash with an additional 5ml NaOH was clear for the 20 min MRW while the one from 15 min still showed light brown color. Therefore, 50ml of 0.01 M NaOH and 20 min reaction time was considered to be the optimum condition for removing oxidation debris from 0.1g F-CNT by MRW.

To determine the amount of solvent needed in an equivalent conventional base wash, 0.1g F-CNT was dispersed in 50ml NaOH, put on a shaker and shaken for 20 min, after which the sample was filtered. If the filtrate was brown, the F-CNT was redispersed in another 50ml NaOH, and the shaking/filtration was repeated till a clear filtrate was obtained. It was found that four rounds of 20 min shaking batch with a total 200 ml NaOH was needed to complete the base wash. In another experiment, the CNT solution was

shaken overnight and filtered, with a NaOH consumption of 150 ml. The process of filtration took one hour per round, so the whole process required an additional 3 to 4 hours.

It is quite evident that the MRW required shorter reaction times and significant less amounts of base. The faster reaction in MRW was due to the molecular heating in microwave irradiation which directly heated the reactive species. In the absence of microwave radiation, the reaction was slower and this led to higher base requirement. In general, faster reaction time and less reagent usage make MRW a more environmental friendly approach to remove the oxidation debris.

3.2.2 Characterization

The characteristics of the BW-F-CNT and MRW-F-CNT samples were studied and compared. The MRW-F-CNT prepared from the 10 min reaction and 0.2g F-CNT_{SL} and 50 ml of the base was used as the benchmark where the oxidation debris had not been removed completely (referred as MRW-F-CNT_{SL10}). SEM images of BW-F-CNT and MRW-F-CNT samples are presented in Figure 3.1. All CNTs remained intact with minimal visible tube defect. The elemental analysis of CNTs (Table 3.1) was carried out by EDX. The oxygen content decreased after base wash due to the removal of oxidation debris, which is in line with what has been reported before (Wu, Hamilton Jr et al. 2014). The percentage of oxygen decreased by 38, 53, and 47% in BW-F-CNT_{SS}, BW-F-CNT_{SL}, BW-F-CNT_{LS} respectively, and 44, 53, and 33% for the corresponding MRW-F-CNT samples. The C/O ratio were 22, 20, 18 for BW-F-CNT_{SS}, BW-F-CNT_{SL}, BW-F-CNT_{LS} and 24, 20, 14 for the corresponding MRW-F-CNT samples. This showed that the final product from MRW was similar to conventional base wash. On the other hand, the C/O ratio of MRW-F-CNT_{SL10} (which was 10) was closer with that of F-CNT_{SL} (8.3). This was

attributed to the incomplete removal of oxidation debris. This implied that optimal process conditions were necessary for successful MRW.

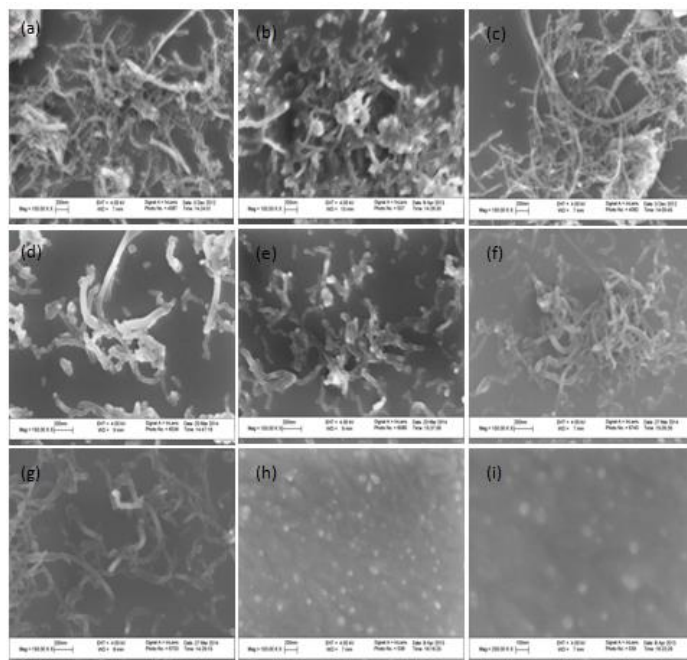


Figure 3.1 SEM images of a)BW-F-CNT_{SS}, b)BW-F-CNT_{SL}, c)BW-F-CNT_{LS}, d)MRW-F-CNT_{SS}, e)MRW-F-CNT_{SL}, f)MRW-F-CNT_{LS}, g)MRW-F-CNT_{SL10}, h) W-CNT_{LS}, i) W-MRW-CNT_{LS}.

Table 3.1 Elemental Analysis of CNT Samples

	C (%)	O (%)	C/O ratio
CNT _{SS} (0.5-2 μ m long and 10-20 nm OD)			
F-CNT _{SS}	90.7	9.3	13
BW-F-CNT _{SS}	94.2	5.8	22
MRW-F-CNT _{SS}	94.8	5.2	24
CNT _{SL} (0.5-2 μ m long and 30-50 nm OD)			
F-CNT _{SL}	86.1	13.9	8.3
BW-F-CNT _{SL}	93.5	6.5	20
MRW-F-CNT _{SL}	93.5	6.5	20
MRW-F-CNT _{SL10}	87.7	12.3	10
CNT _{LS} (10-30 μ m long and 10-20 nm OD)			
F-CNT _{LS}	87.1	12.9	11
BW-F-CNT _{LS}	93.2	6.8	18
MRW-F-CNT _{LS}	91.3	8.7	14

The dimensions of the F-CNT, BW-F-CNT and MRW-F-CNT samples are presented in Table 3.2. The length and diameter showed minor differences before and after MRW, which confirmed that the MRW did neither fragment nor cause excessive tube damage. Also the dimension of BW-F-CNTs and their corresponding MRW-F-CNT samples showed similar results. The length of BW-F-CNT_{SS}, BW-F-CNT_{SL}, were shortened by 10 and 4% while 12 and 4% for the corresponding MRW-F-CNT samples. At the same time MRW-F-CNT_{SL10} showed only 1% decrease of length compare with F-CNT_{SL}. Figure 3.2 shows the Raman spectra of the different CNT samples. The intensity ratio of D (defect band) and G band (graphite band) (I_D/I_G) is shown in Table 3.2. I_D/I_G decreased by 16, 15, 28% with base washing for BW-F-CNT_{SS}, BW-F-CNT_{SL},

BW-F-CNT_{LS} respectively and 16, 14, 28% for the corresponding MRW-F-CNT samples.

This shows that the two methods produced similar results.

Table 3.2 Dimension, Specific Surface Area, Particle Size and Zeta Potential of F-CNT Samples

	Length (nm)	Diameter (nm)	Surface area (m ² /g)	I _D /I _G	Particle size(nm)	Zeta potenti al(mV)
CNT _{SS} (0.5-2μm long and 10-20 nm OD)						
F-CNT _{SS}	898 ±431	25 ±6	156	1.02 ±0.01	104.4	-43.4
BW-F-CNT _{SS}	806 ±396	24 ±5	169	0.86 ±0.02	113.3	-40.5
MRW-F-CNT _{SS}	792 ±307	24 ±3	166	0.84 ±0.03	113.3	-40.1
CNT _{SL} (0.5-2 μm long and 30-50 nm OD)						
F-CNT _{SL}	761 ±519	33 ±9	234	1.37 ±0.01	92.3	-43.5
BW-F-CNT _{SL}	731 ±451	32 ±5	265	1.16 ±0.05	82.1	-46.3
MRW-F-CNT _{SL}	734 ±309	32 ±3	264	1.18 ±0.01	81.9	-46.2
MRW-F-CNT _{SL10}	750 ±248	33 ±4	240	1.34 ±0.04	89.6	-45.0
CNT _{LS} (10-30 μm long and 10-20 nm OD)						
F-CNT _{LS}	-	23 ±6	240	1.41 ±0.01	99.9	-43.7
BW-F-CNT _{LS}	-	23 ±4	264	1.01 ±0.04	95.2	-44.3
MRW-F-CNT _{LS}	-	23 ±4	266	1.01 ±0.05	95.9	-44.1

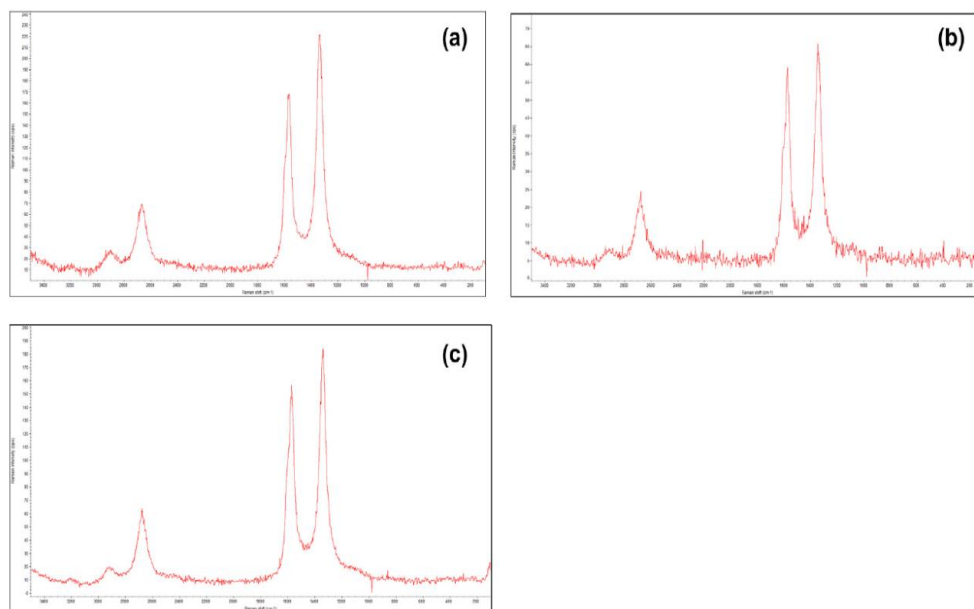


Figure 3.2 Raman spectra of a) F-CNT_{SL}, b) BW-F-CNT_{SL}, c) MRW-F-CNT_{SL}.

FTIR spectroscopy (Figure 3.3) was used to qualitatively analyze functional groups on the functionalized and base washed CNTs. The presence of C=C stretching around 1583 cm^{-1} which was present in the original carbon skeleton of the CNTs, the carbonyl stretching frequency (C=O) around 1726 cm^{-1} , stretching vibration (C-O) around 1220 cm^{-1} and (O-H) around 3473 cm^{-1} provided the evidence of carboxyl groups in all the F-CNTs. The FTIR analysis showed the same peaks by both conventional and MRW (including MRW-F-CNT_{SL10}). This implied that the base-wash did not affect the attachment of carboxylic groups on the surface of CNTs. Figure 3.3 (a) and (b) shows the FTIR spectra of BW-F-CNT_{SL} and MRW-F-CNT_{SL}. Other F-CNTs, BW-F-CNTs and MRW-F-CNT samples showed similar spectra and are not shown here for brevity.

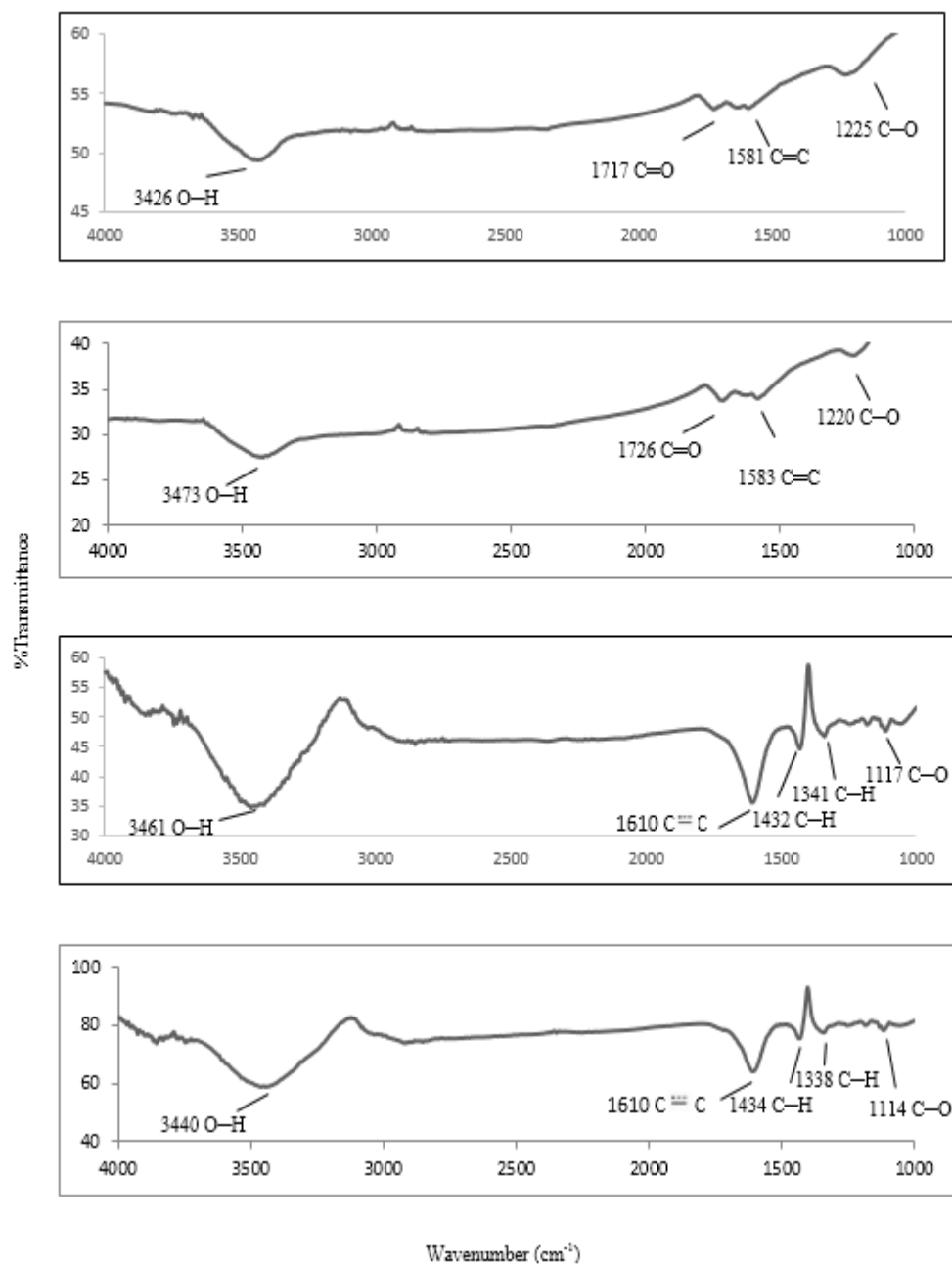


Figure 3.3 FTIR spectra of a) BW-F-CNT_{SL}, b) MRW-F-CNT_{SL}, c) W-BW-CNT_{SL}, and d) W-MRW-CNT_{SL}.

The Brunauer, Emmett, and Teller (BET) surface area of all samples are shown in Table 3.2. All CNTs had large surface area. For all three sizes, the specific surface areas (SSA) of carboxylated carbon nanotubes were lower than those of samples after base wash,

which was in line with what has been reported before (Wu, Hamilton Jr et al. 2014). The SSA increased after base wash by 8, 13, 10% for BW-F-CNT_{SS}, BW-F-CNT_{SL}, BW-F-CNT_{LS} and 6, 13, and 11% for the corresponding MRW-F-CNT samples. It implies that during MRW as well as conventional base wash, the SSA increased due to the removal of oxidation debris. Once again, the SSA from the two base wash approaches were quite similar, which implied that MRW was as effective as the conventional method. The SSA of MRW-F-CNT_{SL10} also increased somewhat compared to F-CNT_{SL} but not as much as those from MRW or conventional base wash, where the removal of oxidation debris was complete.

The colloidal behavior of BW-F-CNTs and MRW-F-CNTs was studied using dynamic light scattering. Particle size and zeta-potential of the CNT samples are presented in (Table 3.2). Both BW-F-CNTs and MRW-F-CNTs were stable in water. The difference of zeta potential was 7, 6, and 1% for BW-F-CNT_{SS}, BW-F-CNT_{SL}, BW-F-CNT_{LS} and 8, 6, 1% for MRW-F-CNT_{SS}, MRW-F-CNT_{SL}, MRW-F-CNT_{LS} for the corresponding F-CNT samples. Once again it can be seen from Table 3.F2 that the MRW and conventional base washed samples showed similar agglomerate size. The difference of particle size was 9, 11, and 5% for BW-F-CNT_{SS}, BW-F-CNT_{SL}, BW-F-CNT_{LS} and 9, 11, and 4% for MRW-F-CNT_{SS}, MRW-F-CNT_{SL}, MRW-F-CNT_{LS} for the corresponding F-CNT samples. This again showed that the difference between F-CNTs and corresponding BW-F-CNTs and MRW-F-CNTs was insignificant. The presence of the oxidation debris did not affect the stability or dispersibility of carbon nanotubes. MRW-F-CNT_{SL10} also showed similar colloidal properties compared to F-CNT_{SL}.

The SEM images of the oxidation debris W-CNT_{LS} and W-MRW-CNT_{LS} presented in Figure 3.1 (h, i). Images of debris for other two sizes are not presented here for brevity. The oxidation debris from both methods (including W-MRW-CNT_{SL10}) showed similar morphology, but no tube fragments. The elemental analysis of the wash is presented in Table 3.3. The results showed low C/O ratios in the range of 1.8 to 3.0. This implied that over-functionalized fragments were present in the wash. The results from MRW and conventional wash were somewhat similar, which was further evidence that the two methods were comparable. The FTIR analysis of the wash residues from the two methods showed the presence of conjugated C-C with C=O stretching at 1610 cm⁻¹, C-H bending vibrations at 1338 cm⁻¹ and 1434 cm⁻¹. In addition, C-O stretching (1114cm⁻¹) and O-H stretching (3440 cm⁻¹) were observed, which implied the removal of oxidation debris, which was attributed to partially oxidized polyaromatic fragments. O-H (3440 cm⁻¹) vibration may due to the extra NaOH from washing procedure.

Table 3.3 Elemental Analysis of Filtrate

	C (%)	O (%)	C/O ratio
CNT _{SS} (0.5-2µm long and 10-20 nm OD)			
W-CNT _{SS}	57.6	42.4	1.8
W-MRW-CNT _{SS}	58.5	41.5	1.9
CNT _{SL} (0.5-2 µm long and 30-50 nm OD)			
W-CNT _{SL}	65.8	34.2	2.6
W-MRW-CNT _{SL}	69.1	30.9	3.0
W-MRW-CNT _{SL10}	67.1	32.9	2.7
CNT _{LS} (10-30 µm long and 10-20 nm OD)			
W-CNT _{LS}	59.9	40.1	2.0
W-MRW-CNT _{LS}	60.6	39.4	2.1

3.3 Conclusions

MRW was developed for removing the oxidation debris generated during CNTs functionalization. CNTs of different dimensions were tested where the decreases of oxygen content in F-CNTs after MRW were between 33 to 53%, reduction in length was between 4 and 12%, and specific surface area increased by 6 to 13%. The zeta potential of MRW samples were between -40 and -45 mV, which was similar to the original F-CNTs. The dimensions, elemental composition, surface area and colloidal properties of MRW and base-washed samples by conventional method were similar. The chemical properties of the debris from the two methods were also similar. In summary, MRW is an effective method for the removal of oxidation debris that is much faster and consumes less reagents than the conventional approach.

CHAPTER 4

LENGTH REDUCTION OF MULTI-WALLED CARBON NANOTUBES VIA HIGH ENERGY ULTRASONICATION AND ITS EFFECT ON THEIR DISPERSIBILITY

In Chapter 4, length dependent dispersibility of carboxylated multiwalled carbon nanotubes is presented using a novel approach that ensures the same diameter and the degree of functionalization. The longer multiwalled nanotubes were reduced in length by ultrasonication and then their dispersibility was studied in comparison to the original tubes. Colloidal studies showed dependence on the length where the shorter tubes showed higher aggregation in terms of larger particle size, zeta potential and lower critical coagulation concentrations (CCC) in the presence of electrolytes. It is hypothesized that the longer tubes entangled more leading to a more complex electrostatic double layer that increased their stability.

Carbon nanotubes (CNTs) possess some highly desirable properties suited for diverse applications and its demand is expected to increase significantly over the next decade. More recently there has been much interest in the effect of size on the physical and chemical properties of CNTs (Lau, Wu et al. 2014, Wu, Hamilton Jr et al. 2014). There also exist different physical and chemical methods to synthesize CNT of different lengths and diameter and also alter their length (Su, Zhang et al. 2012, Ren, Kanaan et al. 2014). Chemical treatments such as acid treatment is known to shorten the CNTs (Chen and Mitra 2008), while sonication (Yudasaka, Zhang et al. 2000), electron beam cutting, lithography and milling have been used as physical means to reduce length (Chowdhury and Cui 2011).

It is important to realize that CNTs represent a diverse group of nanotubes that vary in size, shape and chirality. Toxicity (Si, Wang et al. 2011) and dispersibility (Krause,

Villmow et al. 2011) are also known to be functions of length, and therefore there is a need to study the fate and transport of CNTs as a function of length. The size dependent behavior of CNTs is yet to be studied in details. Of particular interest in the area of aqueous dispersibility is the colloidal behavior of functionalized hydrophilic nanotubes such as the carboxylated analogs (Ntim, Sae-Khow et al. 2011). Previous studies have reported the dispersibility of CNTs of different sizes (length and diameter) from different sources (Ntim, Sae-Khow et al. 2012). However, carboxylation of different batches does not ensure the same degree of carboxylation, and the wide variations in length and diameter introduces uncertainty. This chapter presents the length dependent dispersibility of CNTs. A novel approach that ensures the same diameter and the degree of functionalization for the different carboxylated CNTs is proposed where the longer carboxylated MWNTs are reduced in length and then their dispersibility is studied on a comparative basis.

4.1 Experimental

4.1.1 Chemicals

Multiwall carbon nanotubes (MWNT) (OD <8nm, length 0.5-2 μ m, purity >95%) were purchased from Cheap Tubes Inc., and all other chemicals were purchased from Sigma Aldrich with purity higher than 95%.

4.1.2 Preparation of the f-MWNTs

The synthesis of the carboxylated multiwall carbon nanotubes (f-MWNT) were carried out using a Microwave Accelerated Reaction System. Pre-weighted amounts of MWNT were dispersed into a mixture of concentrated H₂SO₄ and HNO₃ and placed in the reaction

chamber. The reaction vessels were subject to microwave radiation at a preset temperature of 140 °C for 20 min. After cooling down to room temperature, the product was vacuum filtered using MilliQ water with pore size 10 µm until the filtration reached a neutral pH. The original f-MWNT (referred to as f-MWNT-L) was then dried in a vacuum oven at 70 °C until constant weight (Chen, Iqbal et al. 2007, Chen and Mitra 2008). The f-MWNT-L were dispersed in MilliQ water at a concentration of 50 mg l⁻¹ and the 100ml solution were ultrasonicated by sonic ruptor 250 from OMNI International the homogenizer company at 100 watts, 20 kHz for 7 hours under 25 °C water bath to reduce the length of the CNTs and make the tubes shorter (f-MWNT-S).

4.1.3 Characterization of the f-MWNTs

Scanning electron microscope (SEM) data for all samples was collected on a LEO 1530 VP scanning electron microscope under 4kv extra high voltage. Small amount of sample was stuck on the carbon tape to get normal SEM image. No carbon coating needed. Around 40 tubes of each sample were measured independently to obtain the length distribution by SEM. Sample was dispersed in water in a dilute suspension via low power sonication (2watts 5 mins). The suspension was dropped on the silica chip which was stuck on the carbon tape and air dried. The sample was analyzed by SEM to obtain the length data. Elemental analysis was carried out by energy-dispersive X-ray analyzer (EDX) which was attached to the SEM. Approximately 0.1mg MWNT and f-MWNT were mixed with 350mg KBr and pressed into pellets for obtaining the Fourier Transform Infrared spectroscopy (FTIR) data by a Perkin-Elmer instrument while 350 mg KBr was used as the blank. TGA was performed using a Pyris 1 TGA from Perkin-Elmer Inc from 30 °C to 900 °C under a flow of air at 10 ml min⁻¹, at a heating rate of 10 °C per min. Oversaturated

solutions were prepared and allowed to settle for 24 hours for obtaining water solubility of f-MWNT-L and f-MWNT-S.

4.1.4 Dispersibility Studies

50 mg/l stock solution of f-MWNT-L and f-MWNT-S were prepared by sonicating pre-weighted amounts f-MWNT in MilliQ water. 400mM stock solutions of sodium chloride and magnesium chloride were prepared by dissolving pre-weighed amount of salt in MilliQ water. Different concentrations of f-MWNT and salts solutions were diluted by stock solutions on an as needed basis.

Particle size distribution was measured with a 1mg/l f-MWNT dispersions and Zeta potential was measured at 5 mg/l as a function of salt concentration, which was varied from 10 to 200 mM. These measurements were made at 25 °C using a Malvern Instrument (Zetasizer nano ZS90) and the detector angle was set at 90° for particle size measurements. The aggregation behavior were measured using 1mg/l f-MWNT dispersions in the presence of salt solutions which concentrations ranged from 0.5 mM to 250 mM, and the measurements were made for a time period ranging from 180s to 3h. Long-term stability was measured at a concentration of 6 mg/l f-MWNT dispersions in the presence of 10mM salts solutions using UV absorbance at 252nm. The data were collected at 0, 1, 2, 4, 6 and 24 hours.

4.2 Results and Discussion

4.2.1 Characterization

SEM images of MWNT, f-MWNT-L, f-MWNT-S, are shown in Figure 4.1. Length and diameter of CNTs are shown in Table 4.1. The size distribution of each fraction is further illustrated in the histograms in Figure 4.2. It clearly showed that the f-MWNT-L, f-MWNT-S were significantly different in terms of their length. Based on the student's t-test, the length of the different CNTs were significantly different at 95% confidence interval. The length of the CNTs decreased on carboxylation, and the ultrasonication further shortened the CNTs. The diameter after acid functionalization increased slightly but no significant difference in diameter was observed between MWNT, f-MWNT-L and f-MWNT-S. The slight increase in diameter after acid functionalization was due to the introduction of functional groups, and ultrasonication did not affect the diameter of tubes. The solubility in pure water increased from 0.99 to 2.16 mg/ml after length reduction via ultrasonication, which implied that the two f-MWNTs behaved differently in aqueous medium. The water dispersions of two f-MWNTs are shown in Figure 4.1(d).

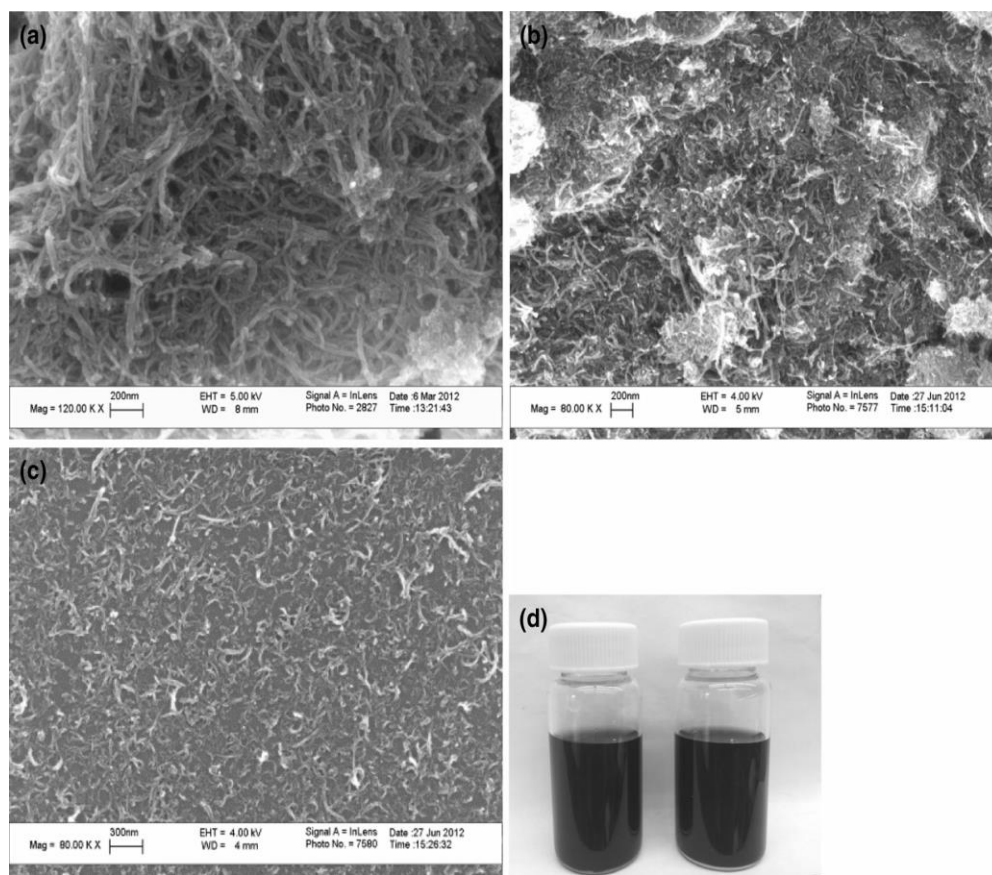
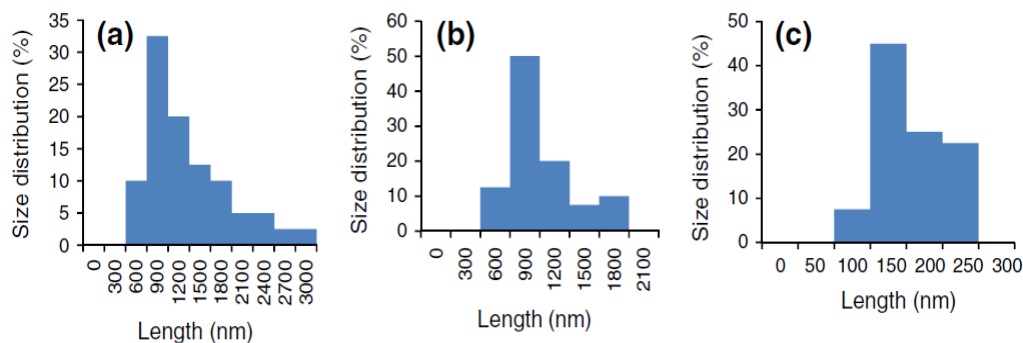


Figure 4.1 SEM images for a) MWNT, b) f-MWNT-L, c) f-MWNT-S d) dispersion of f-MWNT-L(left) and f-MWNT-S(right).

Table 4.1 Length, Diameter and EDX Result for Materials

	Length		Diameter		Weight percentage (%)	
	Mean (nm)	t-Test(p)	Mean (nm)	t-Test(p)	C	O
MWNT (A)	1167±58 6	n/a	6.4 ±1.5	n/a	97.5±0.3	2.5±0.3
f-MWNT-L(B)	902±311	P(A,B)=0.014	6.9 ±1.7	P(A,B)=0.19	94.1±0.4	5.9±0.4
f-MWNT-T-S (C)	158±47	P(B,C)=3.907E-18	6.9 ±1.8	P(B,C)=0.90	93.7±0.02	6.3±0.0 2

**Figure 4.2** Histograms of size distribution a) MWNT b) f-MWNT-L c) f-MWNT-S.

The carboxylic stretching frequency (C=O) at 1716 cm^{-1} and stretching vibration (C-O) at 1227 cm^{-1} was seen in both carboxylated CNTs and the shortened CNTs after ultrasonication. This was absent in raw MWNT and provided evidence of the presence of carboxylic group. C=C stretching at 1576 cm^{-1} , which exists in the carbon skeleton was seen in all materials (Figure 4.3). EDX data (Table 4.1) also showed significant increase in oxygen concentration after carboxylation. No significant difference

was seen between f-MWNT-L and f-MWNT-S, which implied that ultrasonication did not affect the surface functional groups

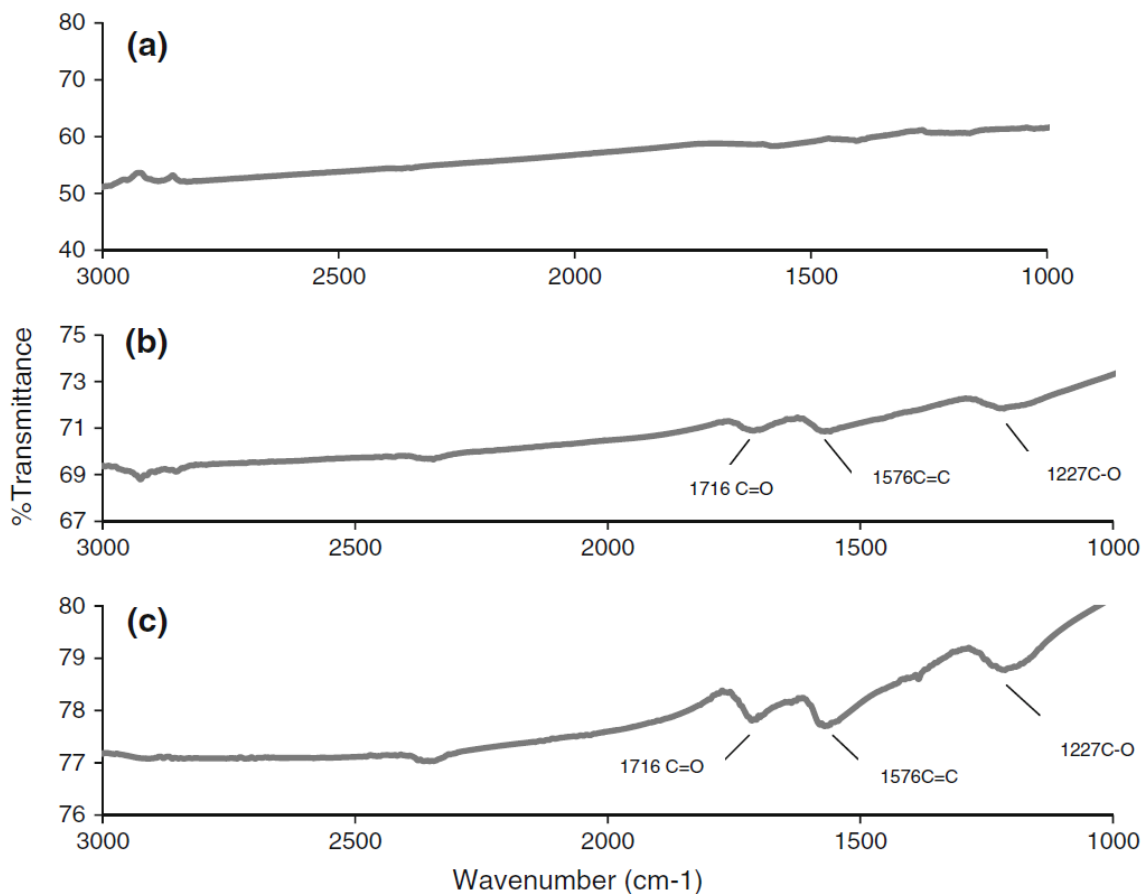


Figure 4.3 FTIR results for a) MWNT, b) f-MWNT-L, c) f-MWNT-S.

The TGA of all the samples are presented in Figure 4.4. It showed that there was no weight loss till 450 °C for the original MWNTs but the decomposition of the carboxylic group lead to weight loss in both f-MWNT-L and f-MWNT-S. However, f-MWNT-L and f-MWNT-S showed identical TGA profiles which were consistent with EDX data. This showed the surface functional groups remained unchanged after ultrasonication.

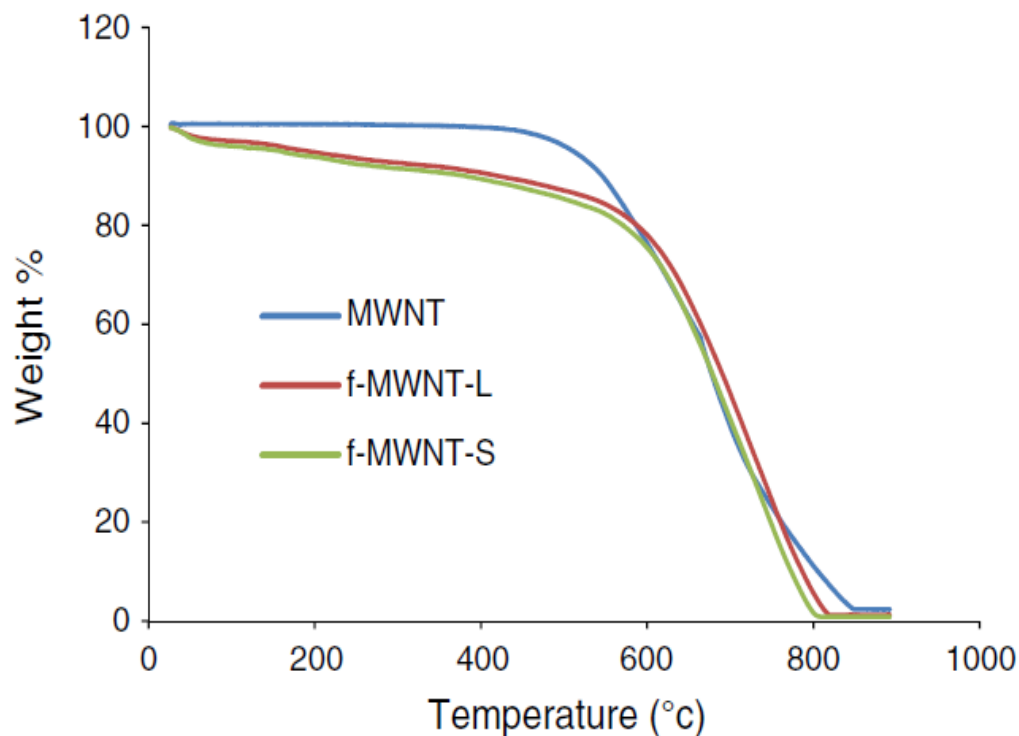


Figure 4.4 TGA of MWNT, f-MWNT-L and f-MWNT-S.

4.2.2 Dispersibility as a Function of Length

Figure 4.5a and 4.5b shows the particle size distribution and zeta potential of f-MWNT-L and f-MWNT-S in water as a function of salt concentration. The dispersibility of the carboxylated MWNT in aqueous phase were due to the electrostatic repulsive forces between negative surface charges of the oxygen-containing groups. In the presence of salt, the positively charged metal ions (Na^+ , Mg^{2+}) neutralized the negative surface charges and compressed the double layer of the dispersed nanotubes. This led to their aggregation. The f-MWNT-S showed significantly more aggregation than the f-MWNT-L in the presence of salts. The zeta potential values were consisted with the particle size aggregation. The zeta potential increased with salt concentration as stability decreased. It was observed that the f-MWNT-S had lower absolute zeta potential than the f-MWNT-L, implying that the shorter tubes were more prone to aggregation.

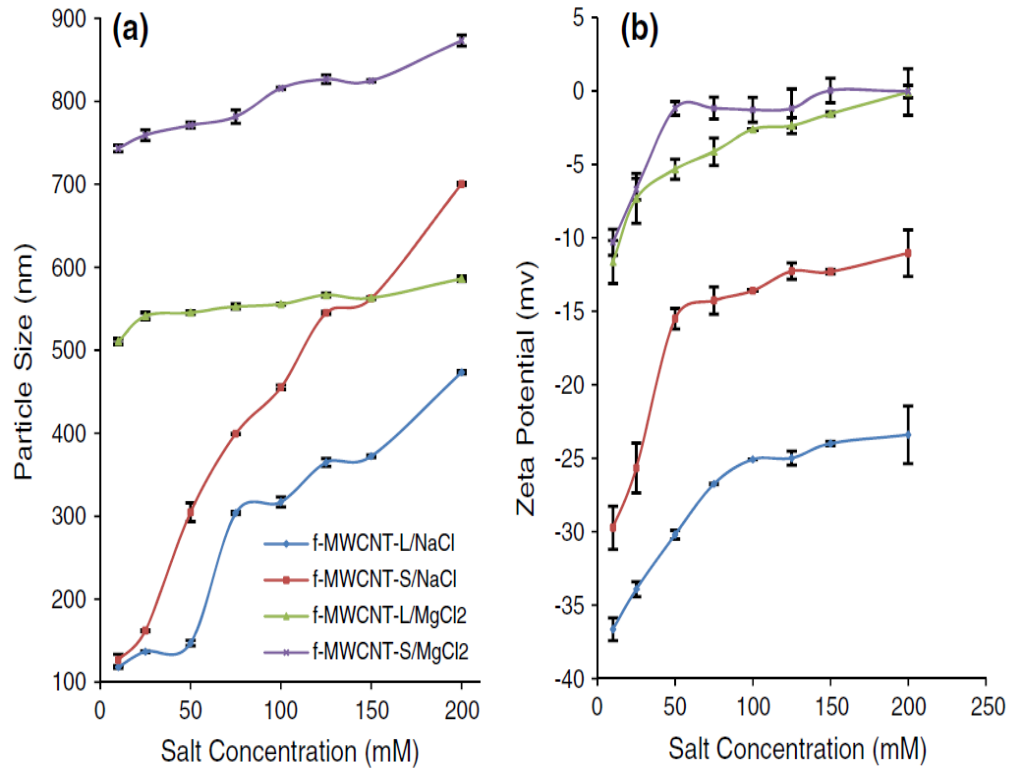


Figure 4.5 (a) Particle size distribution and (b) zeta potential of the f-MWNT-L and f-MWNT-S as a function salt concentration.

The aggregation kinetics of the f-MWNTs was studied by time resolved dynamic light scattering. The initial rate of change in particle size (R_h) is proportional to kn_0 where k is the initial aggregation rate constant and n_0 is the initial concentration of the f-MWCNTs (Schudel, Behrens et al. 1997). The attachment efficiency (α) for suspensions with the same particle concentration was computed as:

$$\alpha = \frac{\left(\frac{dD_h(t)}{dt}\right)_{t \rightarrow 0}}{\left(\frac{dD_h(t)}{dt}\right)_{t \rightarrow 0, \text{fast}}} \quad (4.1)$$

$\left(\frac{dD_h(t)}{dt}\right)_{t \rightarrow 0}$ and $\left(\frac{dD_h(t)}{dt}\right)_{t \rightarrow 0, \text{fast}}$ represent the slow and fast aggregation regimes respectively (Schudel, Behrens et al. 1997, Elimelech, Jia et al. 1998). Attachment

efficiency was determined as the ratio between the hydrodynamic size growth rate at initial aggregation and under the fast aggregation conditions (Zhang, Crittenden et al. 2012). Figure 4.6 shows the attachment efficiencies of the f-MWNTs in NaCl and MgCl₂ as a function of salt concentration. It was observed that at low ionic strengths attachment efficiency increased with salt concentration. At high ionic strengths, attachment efficiency was independent of salt concentration. The critical coagulation concentration (CCC) was obtained from the intersection of the slopes in slow and fast regimes (Ntim, Sae-Khow et al. 2011). f-MWNT-S showed lower CCC in both NaCl and MgCl₂(Figure 4.6). The CCC values were the points when the system reached the fast aggregation regimes, so a lower value implied a faster aggregation. The CCC values were 81.5 and 196 mM respectively for f-MWNT-S and f-MWNT-L in NaCl, and the corresponding values in MgCl₂ were 1.65 and 5.90 mM. This implied that the shortened f-MWNT reached favorable regime at a lower concentration. In general, all the f-MWNTs had higher CCC values in NaCl than in MgCl₂. This was consistent with Schulze-Hardy Rule that states that the CCC depends upon the counterion valence, which implies that the destabilizing power of the electrolyte is principally due to the valence of the counter ion, and an ionic specie of the same valence as the functional group has relatively less effect.

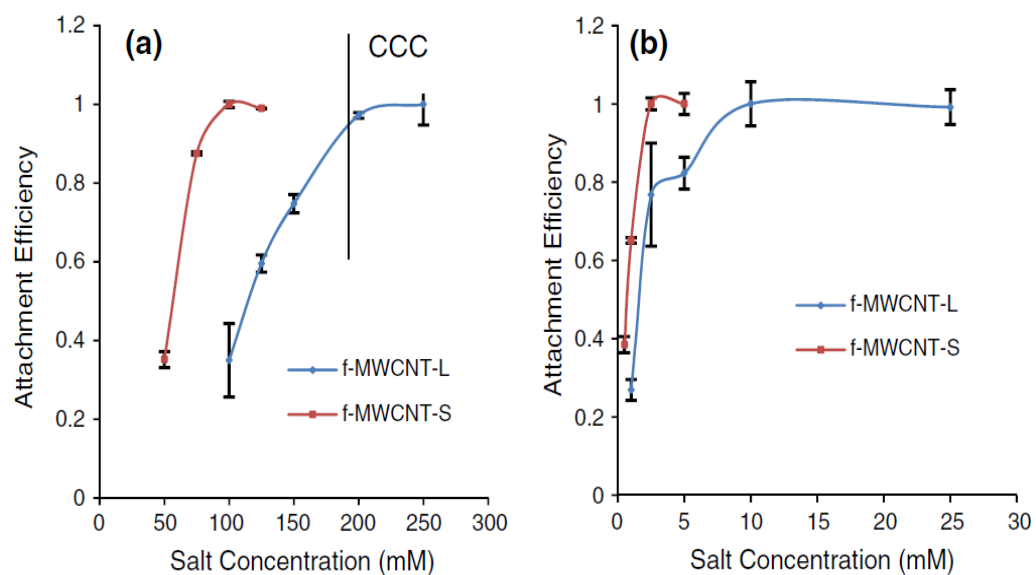


Figure 4.6 Attachment efficiency of f-MWNTs are shown as a function of salt concentration. (a) f-MWNT-L and f-MWNT-S in NaCl, (b) f-MWNT-L and f-MWNT-S in MgCl₂.

Long-term colloidal stability of f-MWNTs as a function of time measured by UV absorbance at 252nm was shown in Figure 6.7. f-MWNT-L and f-MWNT-S were both stable in MiliQ water over 24hours. f-MWNT-S showed marginally lower stability in the electrolytic environment compared to f-MWNT-L.

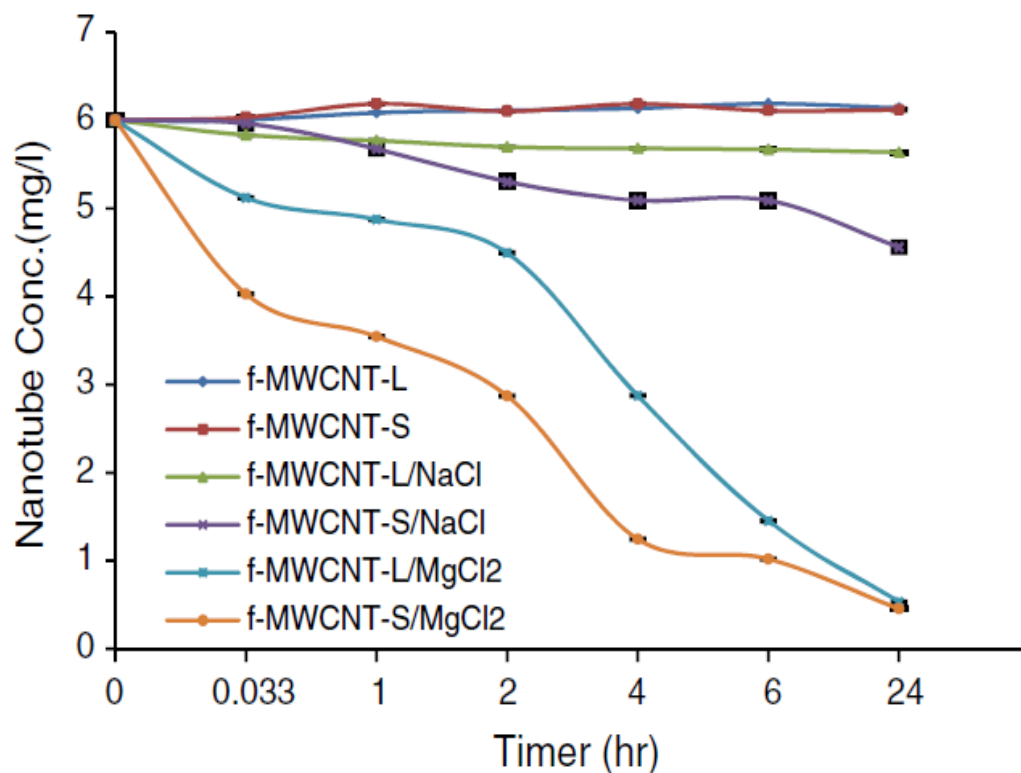


Figure 4.7 Long-term stability measured by UV absorbance at 252nm.

Under normal circumstances, one would expect the longer MWNTs to form larger aggregates and agglomerate more easily and show lower CCC values. However, in the small diameter MWNT studied here, the longer nanotubes tended to entangle themselves generating a more complex and stable electric double layer, while the shorter ones were less entangled leading to a simpler but less stable electrostatic double layer. This is schematically shown in Figure 4.8.

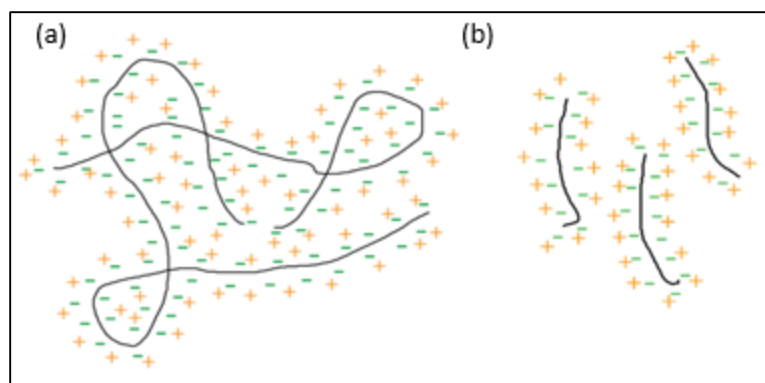


Figure 4.8 Double layer in: a) f-MWNT-L, b) f-MWNT-S.

4.3 Conclusions

High energy ultrasonication was an effective method for reducing length without altering chemical properties and diameter. The ultrasonication led to an 82% reduction in length from 902 to 158 nanometers. Overall, water solubility of the shorter nanotubes after ultrasonication was higher than the original materials. The aggregation rate of f-MWNT-S was higher compared to the f-MWNT-L. The decrease in CCC values was quite dramatic from 196 to 81.5 for NaCl and from 5.90 to 1.65 for MgCl₂. It is hypothesized that entanglement lead to different double layer formation which altered stability. It is hypothesized that the stability of CNTs will depend upon entanglement patterns which can be function of other factors which have not been addressed in this chapter, these include such as diameter and rigidity.

CHAPTER 5

FRACTIONATION OF CARBOXYLATED CARBON NANOTUBES AND THE CORRESPONDING VARIATION IN THEIR COLLOIDAL BEHAVIOR

In Chapter 5, length dependent dispersibility of carboxylated multiwalled carbon nanotubes is presented using a novel approach where a batch of carboxylated nanotubes were size sorted via ultracentrifugation into different fractions with lengths ranging from 150 to 950nm. The different fractions had the same tube diameter and degree of oxidation. The dispersibility of the nanotube fractions showed dependence on the length where the longer tubes showed more aggregation in terms of larger particle size, zeta potential and lower critical coagulation concentrations (CCC) in the presence of electrolytes. It is hypothesized that the longer tubes formed a more complex electrostatic double layer that increased their entanglement and aggregation.

Carbon nanotubes (CNTs) possess some highly desirable properties that make them attractive to many applications ranging from materials to electronics. There also exist different physical and chemical methods to synthesize CNTs of different dimensions (Su, Zhang et al. 2012, Ren, Kanaan et al. 2014). Typical CNT synthesis uses high energy methods such as laser ablation, chemical vapor deposition and electric arc, and the products are mixtures of different sizes and represent significant variability within the group. More recently there has been much interest in the effect of size on the physical and chemical properties of CNTs (Lau, Wu et al. 2014, Wu, Hamilton Jr et al. 2014). For example some applications in electronic, biological, and optical devices benefit from shorter nanotubes (less than 500nm), while others like field emission displays require

relatively longer tubes (500-2000 nm) due to their more uniform emission (Lee, Jeong et al. 2006).

It is important to realize that CNTs represent a diverse group of nanotubes that vary in size, shape and chirality. Biological behavior (Si, Wang et al. 2011) and dispersibility (Krause, Villmow et al. 2011) are also known to be functions of length, and therefore there is a need to study their fate and transport as a function of length. The size dependent behavior of CNTs is yet to be studied in details. Of particular interest in the area of aqueous dispersibility is the colloidal behavior of functionalized, hydrophilic CNTs such as the carboxylated analogs (Ntim, Sae-Khow et al. 2011). Different groups have reported the dispersibility of CNTs of different sizes (length and diameter) from different sources (Jang and Sakka 2010, Krause, Mende et al. 2010, Ntim, Sae-Khow et al. 2012). However, there are several uncontrolled variables such as degree of carboxylation and physical/chemical variabilities that arise out of different manufacturing processes. Therefore much of the data are not directly comparable (Krause, Mende et al. 2010). Moreover, as already mentioned, each manufactured batch of CNTs typically represents a wide range of tubes and it is important to study the variability within the group. This chapter presents the length dependent dispersibility of CNTs within a manufactured batch. A novel approach that ensures the same origin of the tubes as well as the degree of functionalization is proposed where the different sizes are generated from the same functionalized group and their dispersibility is studied on a comparative basis.

5.1 Experimental

5.1.1 Chemicals

Multiwall carbon nanotubes (MWCNTs) (OD 30-50nm, length 0.5-2 μ m, purity >95%) were purchased from Cheap Tubes Inc., and all other chemicals were purchased from Sigma Aldrich with purity higher than 95%.

5.1.2 Preparation of the Carboxylated Multiwall Carbon Nanotubes

The synthesis of the carboxylated multiwall carbon nanotubes(f-MWCNT-O) was carried out in a Microwave Accelerated Reaction System (Chen and Mitra 2008). Pre-weighted amounts of MWCNTs were added to reaction chamber together with a mixture of concentrated H₂SO₄ and HNO₃. The reaction vessels were subject to microwave radiation at a preset temperature of 140 °C for 20 min. After cooling to room temperature, the product was vacuum filtered using MilliQ water with pore size 10 μ m until the filtration reached a neutral pH. f-MWCNT-O was then dried in a vacuum oven at 70 °C until constant weight.

5.1.3 Size Sorting of f-MWCNT-O by Centrifugation

Size sorting via centrifugation was carried out using a procedure reported before (Feng, Xie et al. 2007). f-MWCNT-O were dispersed in MilliQ water at 0.5mg/ml by low power sonication for half an hour prior to high-speed centrifugation. The different size nanotubes were obtained from the same sample, thus eliminating the possibility of batch to batch variation. The original mixture was size sorted as shown in Figure 5.1. The highly dispersible f-MWCNT-O was sonicated at low power to disperse in water and then centrifuged at 10,000 rpm for 1 h. The sediment and residual solution were collected

separately. The sediment was redispersed in water and centrifuged at 10,000 rpm for 1 h again. The following sediment and residual solution were collected as fractions 1-1 and 1-2 respectively. These steps were repeated where each fraction of the sediment was redispersed in water and further centrifuged at 12000, 14000 and 16000 RPM to obtain sediments 2-1, 3-1, 4-1, and residual solution 2-2, 3-2, 4-2, 5.

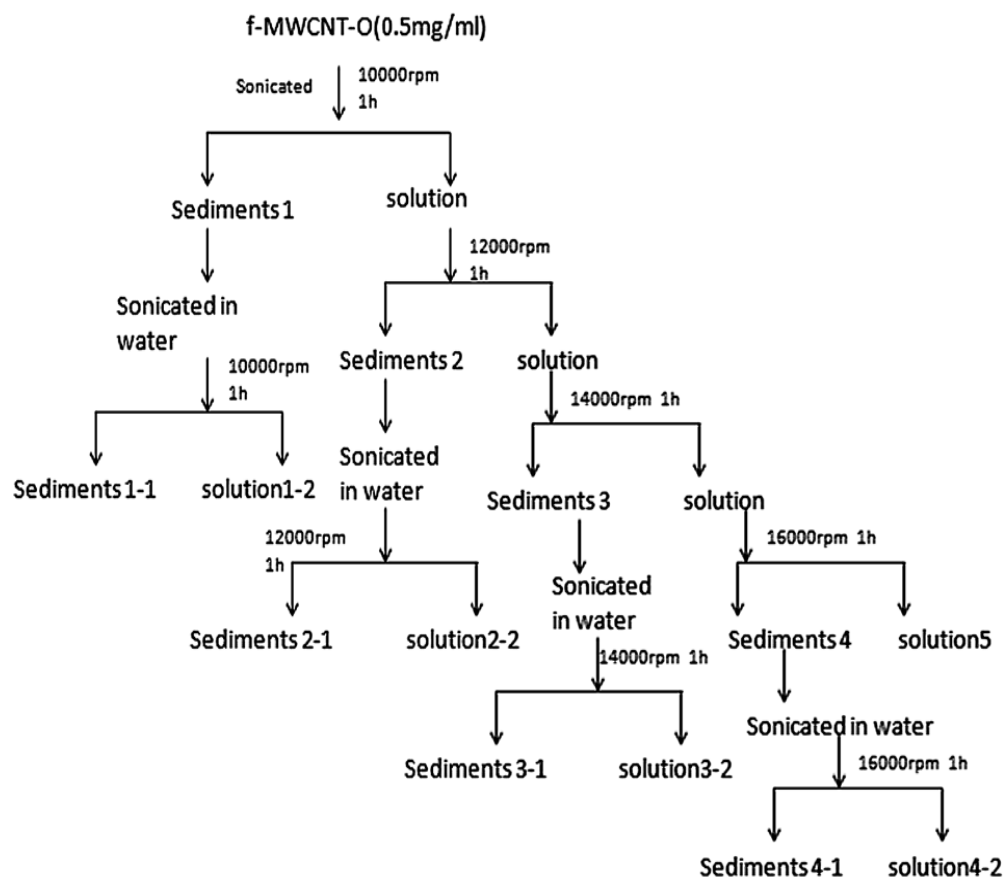


Figure 5.1 Schematic diagram of sorting length.

5.1.4 Characterization

Five f-MWCNTs Solutions (1-2, 2-2, 3-2, 4-2 and 5) referred as f-MWCNT₉₃₈, f-MWCNT₆₂₉, f-MWCNT₄₂₇, f-MWCNT₂₄₃, and f-MWCNT₁₅₃ based on their mean length (Table 5.1) were collected for dispersibility study. Scanning electron microscope (SEM) data for samples was collected on a LEO 1530 VP scanning electron microscope. Around

40 tubes of each sample were measured independently to obtain the length distribution by SEM. Elemental analysis was done by an energy-dispersive X-ray analyzer and Fourier transform infrared spectroscopy (FTIR) analysis was carried out using a Perkin-Elmer instrument.

5.1.5 Dispersibility Studies

The concentration of each fraction was determined by UV absorbance at 252 nm. 400mM stock solutions of sodium chloride and magnesium chloride were prepared by dissolving weighted amount of salt in MilliQ water. Different concentrations of f-MWCNTs and salts solutions were diluted according to need.

Particle size distribution of 1mg/l f-MWCNTs dispersions and Zeta potential of 5mg/l f-MWCNTs dispersions were measured as a function of salt concentration. Salt concentrations were varied from 10 to 200 mM. Particle size and zeta potential were measured at 25 °C using dynamic light scattering ((DLS), Malvern Instrument Model Zetasizer nano ZS90) at a 90 ° scatter angle. The aggregation behaviors were measured using 1mg/l f-MWCNTs dispersion in the presence of salt solutions where the concentration ranged from 0.5 to 250mM, and for a period anywhere between 160s to 1.5h. Long-term stability was measured using UV absorbance at 252 nm for 6mg/l f-MWCNTs dispersions with 10mM salts solutions. The data were collected at 0, 1, 2, 4, 6 and 24 hours.

5.2 Results and Discussion

5.2.1 Characteristics of the Different Fractions

SEM images of f-MWCNTs are shown in Figure 5.2. It was evident that the length decreased with increase in the speed of centrifugation. The length of carbon nanotubes are shown in Table 5.1 and the histogram of length distribution are shown in Figure 5.3. Based on the student's t-test, the length of the different centrifuged fractions were significantly different at 95% confidence interval.

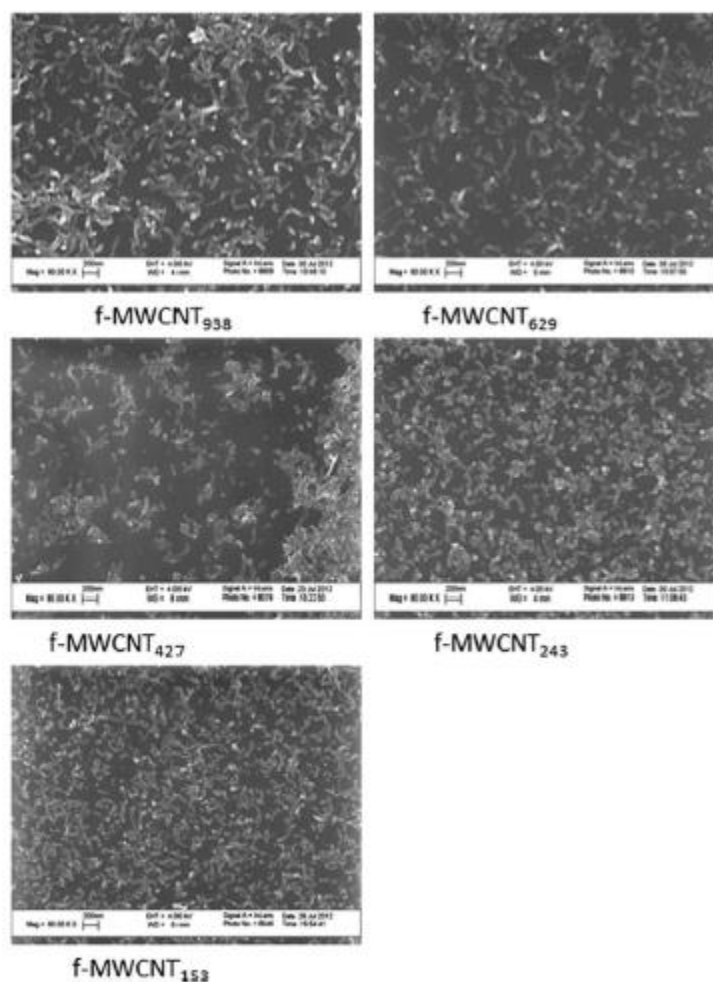


Figure 5.2 SEM images of f-MWCNTs.

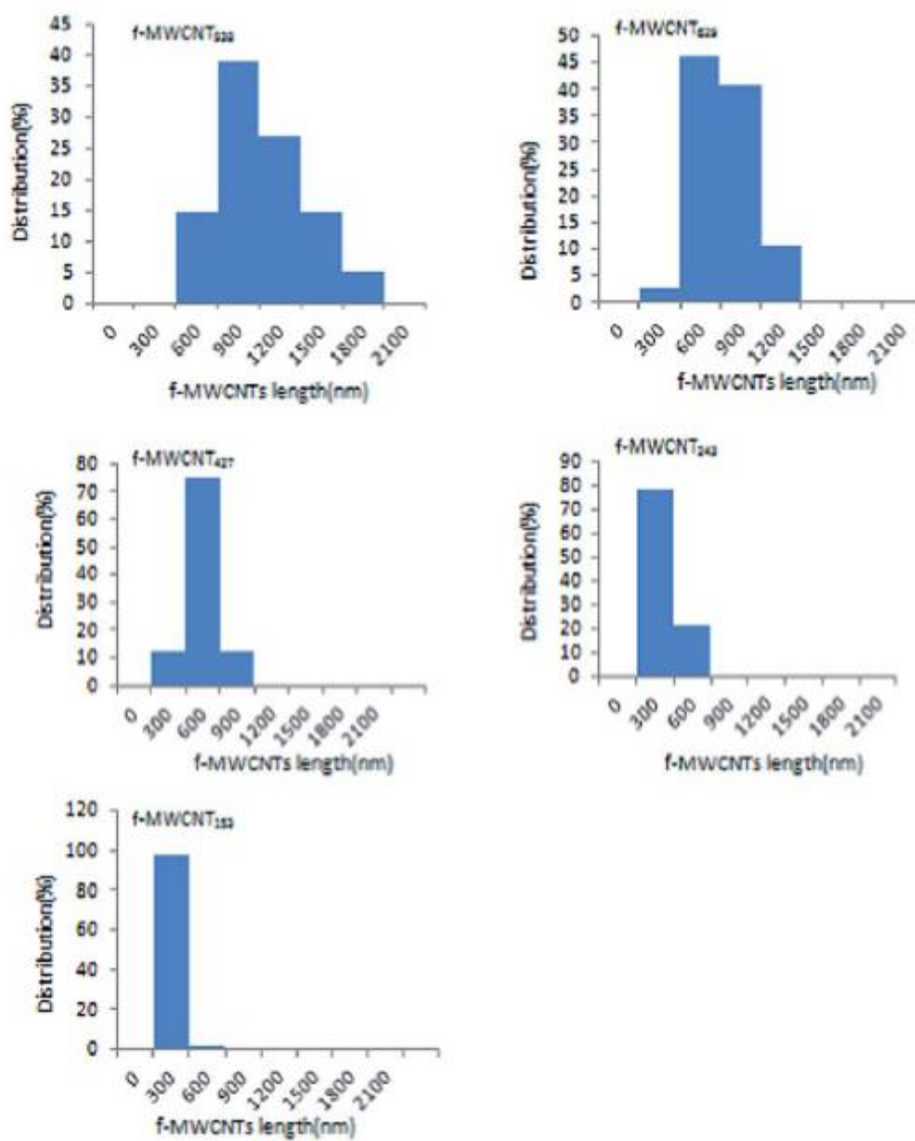


Figure 5.3 Histograms of length distribution.

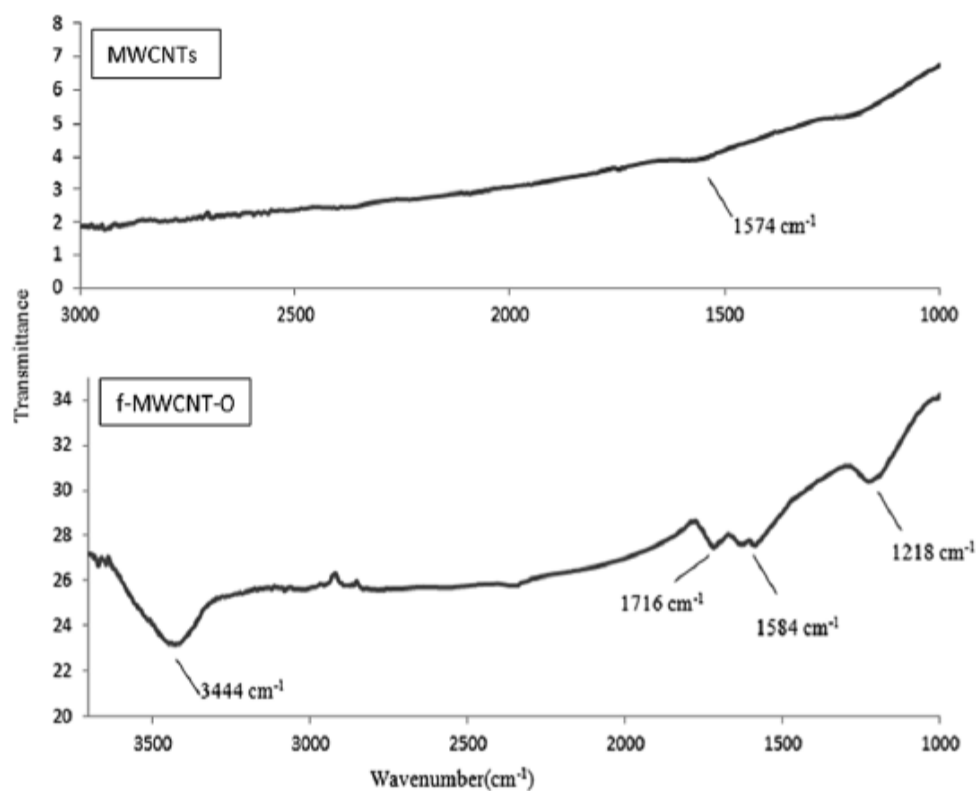
Table 5.1 Length Data for f-MWCNTs

Samples	Length (nm)	t-TEST (P)
f-MWCNT938	938 \pm 276	N/A
f-MWCNT629	629 \pm 222	P(1-2 and 2-2)=5.75E-7
f-MWCNT427	427 \pm 134	P(2-2 and 3-2)=5.09E-6
f-MWCNT243	243 \pm 57	P(3-2 and 4-2)=1.91E-12
f-MWCNT153	153 \pm 55	P(4-2 and 5)=3.97E-10

The elemental analysis including residual metals such as Fe and Ni were tested by EDX and the data is presented in Table 5.2. The increase of oxygen content after functionalization was due to the formation of carboxylic groups. FTIR (Figure 5.4) also showed the presence of carboxylic groups after functionalization as evidenced by the carboxylic stretching frequency (C=O) around 1716 cm^{-1} , stretching vibration (C-O) around 1218 cm^{-1} and stretching (O-H) vibration around 3444 cm^{-1} . All these were absent in raw MWCNT. C=C stretching around 1580 cm^{-1} was present in the carbon skeleton of all samples. All the samples after centrifugation showed the same spectra as the original functionalized nanotubes. No significant difference in the percentage of oxygen was detected in the different fractions after centrifugation. This implied that the degree of carboxylation was same in all the fractions and was not a function of length.

Table 5.2 Elemental Analysis of f-MWCNTs

	C(% by weight)	O(% by weight)	Fe(% by weight)	Ni(% by weight)
MWCNTs	96.71	2.91	0.02	0.36
f-MWCNT-O	90.34	9.66	0	0
f-MWCNT ₉₃₈	90.22	9.78	0	0
f-MWCNT ₆₂₉	90.70	9.30	0	0
f-MWCNT ₄₂₇	90.39	9.61	0	0
f-MWCNT ₂₄₃	90.77	9.23	0	0
f-MWCNT ₁₅₃	90.60	9.40	0	0

**Figure 5.4** FTIR of MWCNTs and f-MWCNT-O.

5.2.2 Dispersibility of the Different Fractions

DLS employs (Chowdhury and Cui 2011, Ntim, Sae-Khow et al. 2011)(Chowdhury and Cui 2011, Ntim, Sae-Khow et al. 2011) the Stokes-Einstein equation to calculate the hydrodynamic diameter (Chowdhury and Cui 2011, Ntim, Sae-Khow et al. 2011), D_h :

$$D_h = k_B T / 6\pi\eta D_t \quad (5.1)$$

where k_B is the Boltzmann constant, T is the absolute temperature, η is the solvent viscosity and D_t is the diffusion coefficient. DLS has also been extensively used to measure the agglomeration behavior as well as zeta potential of anisotropic particles such as CNTs (Peng, Jia et al. 2009, Heister, Lamprecht et al. 2010, Wu, Hamilton Jr et al. 2014). The particle size distribution of the f-MWCNTs in the presence of a salt is presented in Fig. 5a. The water dispersibility of f-MWCNTs was due to the negatively charged oxygen-containing groups on the surface of the tubes. In the presence of salt solutions, positively charged metal ions compressed the double layer, which led to aggregation of tubes. The longer CNTs formed larger aggregates than the shorter CNTs in the presence of electrolyte (Figure 5.5a). This was attributed to the ‘‘stout’’ nature of the (30-50 nm OD) shorter tubes. This made them less prone to aggregation compared to the longer tubes

which showed more inter tube interactions that led to the formation of larger agglomerates. This observation was in agreement previous report for CNTs of this diameter (Ntim, Sae-Khow et al. 2012).

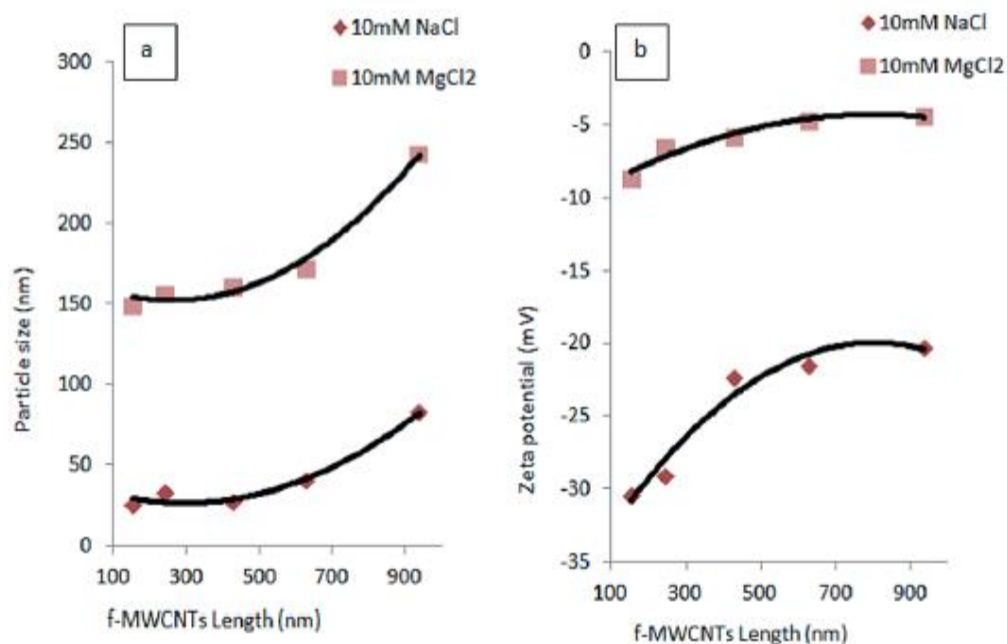


Figure 5.5 (a) Particle size and (b) zeta potential distribution in a 10 mM electrolyte solution NaCl and MgCl₂.

Figure 5.5b shows the zeta potential of the f-MWCNTs in electrolytic media. It was observed that the shorter tubes had more negative zeta potential than the longer tubes, which implied that the longer CNTs were less stable which made them more prone to aggregation. This was consistent with particle size (Figure 5.5a). The divalent Mg salt caused a relative larger value in the zeta potential for all the f-MWCNTs compared to the monovalent Na salt. This was in agreement with the fact that the larger particle sizes were observed with the Mg salt (Figure 5.5a). This observation is in line with Schulze–Hardy rule (Elimelech, Jia et al. 1998), which states that it is the valence of the counter ions that has the principal effect on the stability of the colloid.

Attachment efficiency (α) was obtained from the ratio between the hydrodynamic size growth rates during initial aggregation to that under the fast aggregation conditions (Elimelech, Jia et al. 1998, Ntim, Sae-Khow et al. 2012). Figure 5.6 shows attachment efficiency for all five f-MWCNTs in the presence of NaCl and MgCl₂ respectively. At low ionic strengths, α increased with salt concentration while at high ionic strengths, α was independent of salt concentrations. The critical coagulation concentration (CCC) is the point when α became independent of salt concentration.

Figure 5.7 shows the CCC value of f-MWCNTs in the presence of salt. CCC value increased with the decrease of length of tubes. This again implied that the shorter f-MWCNTs were more stable than the longer tubes. All the f-MWCNTs had higher CCC values in NaCl than in MgCl₂. The CCC values increased from 101.35 to 208.39 mM with decrease in length in the presence of NaCl, and the corresponding increase was from 0.55 to 2.52 mM in the presence of MgCl₂. The relatively lower CCC values observed in the longer tubes were attributed to van der Waals forces and π - π interactions between tubes which led to more self-entanglement and aggregation in comparison to the shorter ones. This is schematically shown in Figure 5.8. This was consistent with particle size and zeta potential measurements presented above.

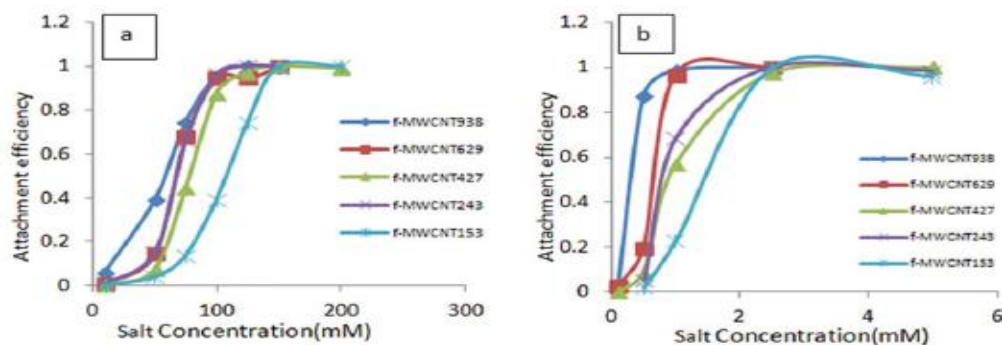


Figure 5.6 Attachment efficiency of f-MWCNTs in a function of (a) NaCl and (b) MgCl₂ concentration.

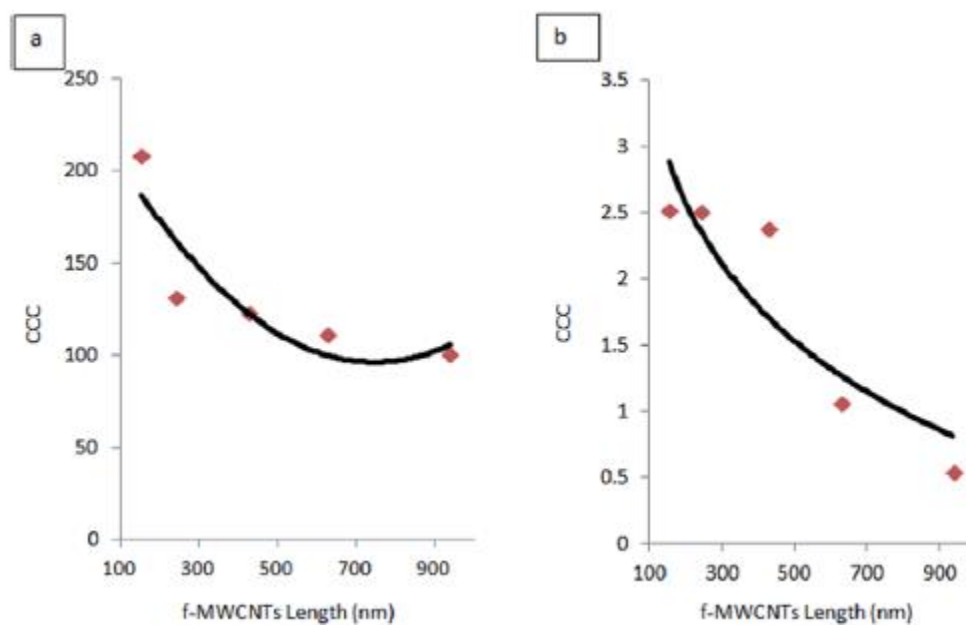


Figure 5.7 CCC value of f-MWCNTs in a 10 mM electrolyte solution (a) NaCl and (b) MgCl₂.

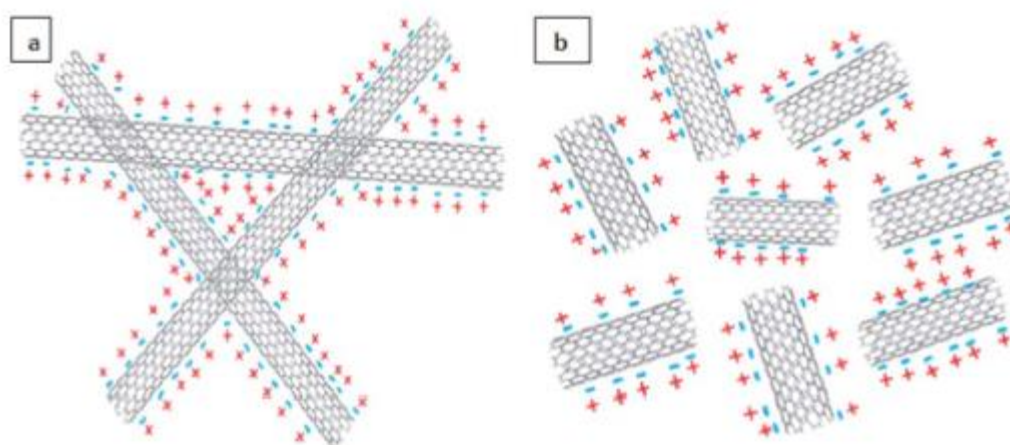


Figure 5.8 Electrostatic double layers in: (a) longer carbon nanotubes, (b) shorter carbon nanotubes.

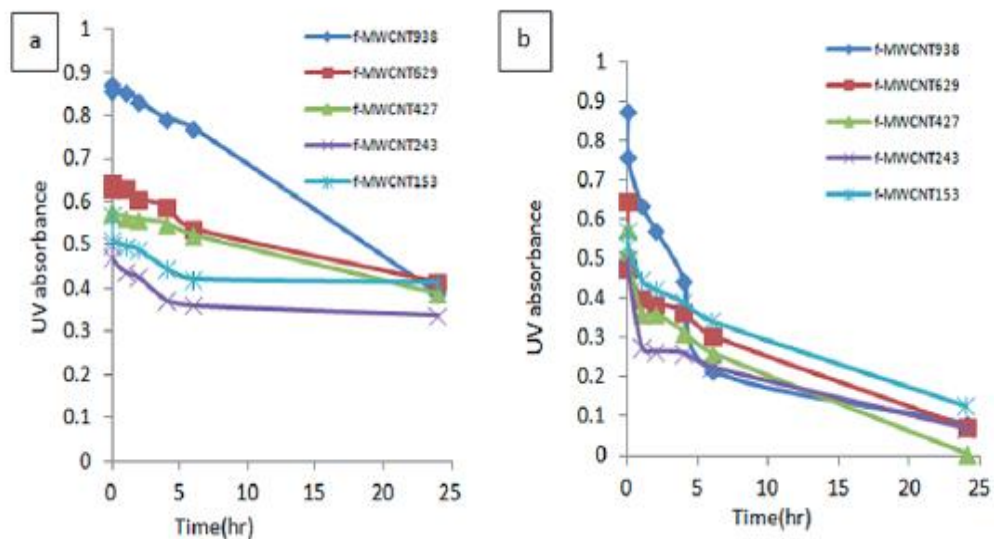


Figure 5.9 Stability of f-MWCNTs in a 10 mM electrolyte solution (a) NaCl and (b) MgCl₂.

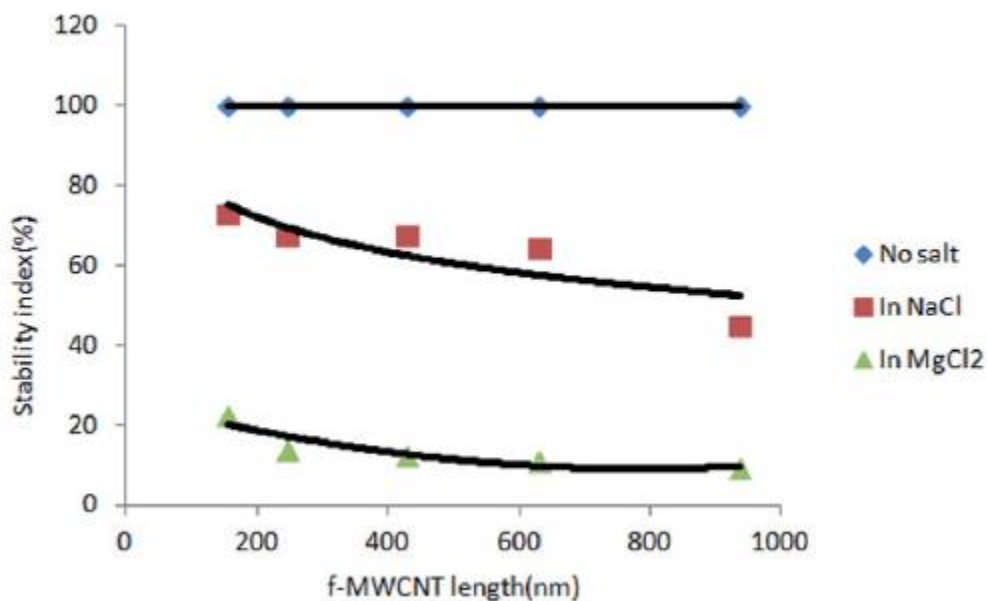


Figure 5.10 Stability index of f-MWCNTs in MilliQ water and a 10 mM electrolyte solution of NaCl and MgCl₂.

5.2.3 Long Term Stability of the Different Fractions

All f-MWCNTs were stable in MilliQ water over a 24 hour period where their UV absorption did not change with time. However, they aggregated in the presence of salts and

precipitated which led to a decrease in concentration in the colloidal phase. Colloidal stability of f-MWCNTs as a function of time was measured by UV absorbance at 252 nm and is shown in Figure 5.9. The stability index was defined as the ratio of the UV absorbance at a point in time to that of the initial value (Figure 5.10). A larger value implied a higher stability. Shorter tubes were more stable compared to the longer ones in both Mg and Na salts. In the case of NaCl, the stability index dropped from 72 to 45% as the length increased from 153 to 938 nm, while in case of MgCl₂ the corresponding drop was 22 to 9%.

5.3 Conclusions

MWCNTs of different lengths were separated out of the same batch via ultracentrifugation. Based on particle size, zeta potential, CCC values and long term stability in NaCl and MgCl₂, the colloidal behaviors of f-MWCNTs of different length were found to be quite different. Shorter nanotubes showed smaller particle size, more negative zeta potential values, higher CCC values and were more stable in a 24 hour period. The variation in colloidal stability as a function of length was attributed to different entanglement patterns which led to the formation of complex electric double layers. It is emphasized that the results are for CNTs of 30-50 nm diameter. Smaller diameter CNTs may be expected to be more flexible and larger diameter more rigid thus leading to different entanglement profiles. These factors can further alter their length dependent colloidal stability. These factors are important for the study of the fate of CNTs in water resources such as lakes, rivers and ground water where significant amounts of ions may be encountered.

CHAPTER 6

VARIATION OF CHEMICAL, ELECTROCHEMICAL AND BIOLOGICAL PROPERTIES OF CARBON NANOTUBES WITH THE DEGREE OF CARBOXYLATION

In Chapter 6, multiwalled carbon nanotubes (CNTs) were carboxylated via microwave irradiation where the treatment time was varied to alter the degree of functionalization, and as many as one in fifteen carbons in the CNT could be oxidized. Chemical, physical, electrochemical and colloidal behavior of the carboxylated CNTs was studied. All properties changed with the degree of functionalization to a point beyond which they appeared to remain constant. The surface area increased from 173.9 to 270.9 m²/g while the critical coagulation concentration (CCC) values increased from 142.14 to 168.69 mM in the presence of NaCl, and the corresponding increase was from 0.97 to 5.32 mM in the presence of MgCl₂. As seen from cyclic voltammetry curves, the functionalized CNTs showed mainly non-Faradic interactions with Na₂SO₄, but showed Faradic behaviors in alkaline KOH. The effects of functionalization on bioactivity and toxicity were also tested and showed that the functionalization affected toxicity and inflammatory responses. However the attenuated toxicity and bioactivity were mainly independent of the degree of functionalization with the exception being IL-33 release from A549 cells which showed an increase with the level of functionalization.

The most common approaches to CNT functionalization include covalent attachment of functional groups and noncovalent interactions with polymers including DNA (Lin, Rao et al. 2002, 2010). Introducing carboxylic groups on CNTs is usually the first step in covalent functionalization which also renders the CNTs dispersible in water (Chen and Mitra 2008). Carboxylated CNTs are usually prepared by refluxing, sonication

or microwave treatment with strong acids (Huang, Lin et al. 2002, Sun, Fu et al. 2002, Chen and Mitra 2008). Other methods such as ozonation, hydrogen peroxide, and ammonium hydroxide have also been used (Datsyuk, Kalyva et al. 2008, Naeimi, Mohajeri et al. 2009, Mart ın, Gutierrez et al. 2013, Morales-Lara, P erez-Mendoza et al. 2013). The strength of the reagents and the treatment time determines the degree of functionalization in terms of the number of carboxylated groups generated on the CNT structure. While most of the oxidation methods are effective, microwave irradiation has been reported to be faster than conventional methods such as refluxing (Chen and Mitra 2008). Since it is an intense short term treatment, it is estimated that the degree of functionalization can be controlled by relatively smaller variations in treatment time.

While there has been much work on functionalization of CNTs, there is very little understanding of the degree of functionalization in terms of the ratio of carbon atoms to the functional groups attached to the tube structure. The effects of the degree of functionalization on physical and chemical properties are yet to be studied in any details. Another important consideration is the effects of such functionalization on bioactivity and toxicity of CNTs. Typically these have been attributed to the tube dimensions (Palom ăki, V ăim ăki et al. 2011, Fenoglio, Aldieri et al. 2012), presence of contaminants (Hamilton Jr, Buford et al. 2012), and release of reactive oxygen species (Nel, Xia et al. 2006) and the degree of functionalization has not been taken into consideration. Therefore, it is also important to study how the level of functionalization affects the biological and toxic properties of CNTs. The objective of this study is to investigate how the degree of carboxylation affects physical, chemical, colloidal, electrochemical as well as biological and toxicological properties of CNTs.

6.1 Experimental

6.1.1 Preparation of the f-CNTs

Multiwall carbon nanotubes (CNTs) (OD 20-30 nm, length 10-30 μm , purity >95%) were purchased from Cheap Tubes Inc., and all other chemicals were purchased from Sigma Aldrich with purity higher than 95%. The synthesis of the functionalized CNTs (referred to as f-CNTs) was carried out in a Microwave Accelerated Reaction System (Chen and Mitra 2008). Pre-weighed amounts of CNTs with a mixture of concentrated H_2SO_4 and HNO_3 were added to reaction chambers. The reaction vessels were subject to microwave radiation at a preset temperature of 140 $^\circ\text{C}$. The time of treatment was varied from 5 to 120 min. After cooling to room temperature, the products were vacuum filtered using Milli Q water with 10 μm filter papers until the filtration reached a neutral pH. The f-CNTs were then dried in a vacuum oven at 70 $^\circ\text{C}$ until constant weight.

6.1.2 Characterizations and Electrochemical Behavior of the f-CNTs

Scanning electron microscope (SEM) images and elemental analysis data for samples were collected on a LEO 1530 VP scanning electron microscope equipped with an energy-dispersive X-ray analyzer. Around 40 nanotubes from each sample were measured independently to obtain the diameter distribution by SEM. TEM measurements were carried out using Hitachi H-7500 instrument by dispersing the samples in Milli Q water and adding to 200-mesh TEM grids prior to drying. The specific surface areas (SSA) of the samples were measured using a Quantachrome NOVA 3000 series (Model N32-11) High Speed Gas Sorption Analyzer at 77.40 K. The samples were heated and degassed at 300 $^\circ\text{C}$

in a vacuum oven for three hours before the measurements. Defects on the CNT structure were studied by Raman spectroscopy with a DXR Raman instrument.

Electrochemical behavior of different CNT samples were measured by cyclic voltammetry using an electrochemical analyzer (Model: 320C, Homiangz LLC) at a scan rate of 0.01V/s in 2 M Na₂SO₄ and 0.05V/s in 2 M KOH where the working electrode(3mg) comprised of 15% polyvinylidene fluoride (PVDF), 10% carbon black, and 75% CNTs.

6.1.3 Dispersibility Studies

50 mg/l stock solutions of f-CNTs were prepared by sonicating pre-weighted amounts f-CNTs in Milli Q water. 400 mM stock solutions of sodium chloride and magnesium chloride were prepared by dissolving pre-weighted amounts of salts in Milli Q water. Different concentrations of f-CNTs and salt solutions were prepared by diluting the stock solutions.

Particle size of 1 mg/l f-CNTs dispersions and Zeta potential of 5 mg/ f-CNTs dispersions were measured in Milli Q water and in the presence of 10 mM salt. Particle size and zeta potential were measured at 25°C using a Malvern Instrument (Zetasizer nano ZS90) at a 90° scatter angle. The aggregation distributions were measured using 1 mg/l f-CNTs dispersion in the presence of salt solutions where the concentration ranged from 0.5 to 300 mM, and the measurement period was between 160 s to 1.5 hr.

6.1.4 Biological Studies

All CNTs samples were tested for Endotoxin contamination. This was determined by washing/sonicating 1 mg/ml CNT in endotoxin-free water for 30 min followed by centrifugation at 16,000 x g for 15 min prior to assay. The assay (ToxinSensor) was

performed on the isolated supernatant according to the manufacturer's protocol (GenScript, Piscataway, NJ). The endotoxin contamination was found to be less than 0.66 ng per microgram of CNTs in each sample and these levels were not expected to adversely impact the studies with either THP-1 or A549 cells.

All nanotubes were weighed and suspended in dispersion media (DM), which consisted of mouse serum albumin (Sigma, St. Louis, MO; 1 mg/ml) and 1,2 dipalmitoyl-sn-glycero-3-phosphocholine (DSPC, Sigma, 1 µg/ml) diluted in phosphate-buffered saline (PBS). Nanotube suspensions were sonicated for 2 min at half max power in a Masonix cup-horn sonicator (XL2020, Farmingdale, NY) attached to a Forma circulating water-bath at 550 watts and 20 Hz (8000 Joules) at a stock concentration of 5 mg/ml.

6.1.4.1 Human THP-1 Cell Line Culturing. THP-1 cells, a human monocytic cell line obtained from ATCC, were suspended in RPMI media (MediaTech, Manassas, VA) supplemented with 10% fetal bovine serum, 50 µM beta-mercapto ethanol, 1 mM sodium pyruvate, 250 ng/ml amphotericin B, and 100 U/ml penicillin and streptomycin (all supplements Media Tech, Manassas, VA) in 75 cm² flasks at 37 °C. The cells in suspension were differentiated into a macrophage-like cell by adding 150 nM Vitamin D3 (1 α , 25-dihydroxy, EMD Millipore, Darmstadt, Germany) for 24 hr. The semi-adherent cells were scrapped with a rubber policeman in the existing media (Corning, Corning, NY). The cells were then centrifuged at 400 x g for 5 min, the resulting cell pellet was re-suspended in 1 ml of complete media, and a 40 µl sample was then counted on a Z2 Coulter Counter (Beckman Coulter, Miami, FL). The cells were suspended at 1 x 10⁶ cells/ml and a small amount of phorbol 12-myristate 13-acetate (5 nM PMA, Sigma) and lipopolysacharride

(10 ng/ml LPS, Sigma) was added. PMA co-stimulation is necessary to stimulate phagocytosis of the CNT. LPS co-stimulation is necessary to induce NF- κ B translocation leading to pro-IL-1 β synthesis for the NLRP3 inflammasome to cleave for IL-1 β release in the transformed THP-1 model (Xia, Hamilton et al. 2013). Cells, at a volume of 350 μ l, were then pipetted into 1.5 ml microfuge tubes. The MWCNT conditions were added from 5 mg/ml concentrated stock suspensions to the cells at a final concentration of 25 μ g/ml. The MWCNT variants used a range of concentrations (0, 6.25, 12.5, 25, and 50 μ g/ml). The resulting cell/particle suspension was mixed by pipette action. The cells were then transferred to 96-well tissue culture plates at 100 μ l per well in triplicate (100 x 10³ cells/well), and cultured for an additional 24 hr. All cultures were maintained in 37 $^{\circ}$ C water-jacketed CO₂ incubators (ThermoForma, Houston, TX). Viability and IL-1 β levels were determined as described below. Three experimental replicates were done for each experiment.

6.1.4.2 Human A549 Cell Line Culturing. A549 cells, a human lung epithelial cell line obtained from ATCC, were suspended in modified F-12 media (MediaTech, Manassas, VA) supplemented with 10% fetal bovine serum, 250 ng/ml amphotericin B, and 100 U/ml penicillin and streptomycin (all supplements Media Tech, Manassas, VA) in 75 cm² flasks at 37 $^{\circ}$ C. This cell line is adherent, so trypsin/EDTA was used to dislodge the cells for passing and/or experimental particle exposures. Suspended cells were centrifuged at 400 x g for 4 min, prior to counting as described above. The A549 cells were seeded in 96-well plates at 15 x 10³ cells/well for 24 hr prior to CNT exposure. At 24 hr the supernatants were removed and replaced with new media containing 50 μ g/ml of a specific CNT in triplicate wells. The culture proceeded for an additional 24 hr before viability (MTS only)

and cytokine levels were determined as described below. Three experimental replicates were done for each experiment.

6.1.4.3 Toxicity Assays. Cell viability was determined by MTS assay using the CellTiter96 assay (Promega, Madison, WI) according to the manufacturer's protocol with a modification as described below. This assay used a colorimetric dye read by a colorimetric plate reader (Molecular Devices, Sunnyvale, CA). In order to avoid artifacts in the optical density values steps were taken to remove the MTS reagent (transferring it into another plate) from the cell/particle mixture adhered to the plate bottom. The formation of bubbles was avoided and the plate was read at 490 nm. Data were expressed as % viable cells relative to control cultures without particle (0 $\mu\text{g}/\text{ml}$). In addition, lactate dehydrogenase (LDH) was determined in 24 hr culture supernatants by using CellTox96 assay (Promega, Madison, WI) according to the manufacturer's protocol. Data were expressed as % LDH relative to 100% cell death (obtained from lysed cells just prior to assay).

6.1.4.4 Cytokine Assays. Human IL-1 α , IL-1 β , IL-6, IL-33 and TNF- α DuoSets were obtained from R&D Systems (Minneapolis, MN) and ELISA assays performed according to the manufacturer's protocol. Plates were read at 450 nm and data expressed as pg/ml.

6.1.4.5 Statistical Analyses. Statistical analyses involved comparison of means using a one or two-way ANOVA followed by Dunnett's test or Bonferroni's test to compensate for increased type I error. All probabilities were two-tailed unless otherwise stated. Statistical power was greater than 0.8. Statistical significance was defined as a probability of type I error occurring at less than 5% ($P < 0.05$). The minimum number of experimental replications was 3. Graphics and analyses were performed on PRISM 5.0.

6.2 Results and Discussion

6.2.1 Characterizations

The elemental analysis of CNTs and f-CNTs were measured by EDX and the data is presented in Table 6.1. The oxygen content increased with the treatment time from 5 to 40 min but did not change significantly beyond that. Raw CNTs also had residual Ni catalysts, which decreased from raw CNTs to the functionalized CNTs for treatment times of 5 and 10 min and there was no Ni detected beyond 20 min. The IR data showed the absence of carboxylic groups in the raw CNTs, therefore the source of the oxygen here was assumed to be from metal oxides. Assuming all oxygen in f-CNTs were from the COOH groups, the number of carboxylic per carbon (C: COOH) was calculated based on EDX data. The ratio decreased from 34.8 to 16.2 with treatment time 5 to 40 min with relatively less significant change (up to 14.7) beyond that. The functionalized CNTs with different treatment times were referred as f-CNT_{34.8}, f-CNT_{23.8}, f-CNT_{20.6}, f-CNT_{16.2}, f-CNT_{15.7}, f-CNT_{14.9}, f-CNT_{14.7} based on the C: COOH ratio. The specific surface area (SSA) of samples are shown in Table 1. This increased from 173.9 to 266 m²/g with treatment time from raw CNTs to 40 min. There was no further increase in SSA beyond 40 min.

The intensity ratio of the D (defect band) and G band (graphite band) from Raman spectroscopy increased from raw CNT to f-CNT_{16.2}. The higher I_D/I_G ratio typically implies higher levels of defects associated with functionalization. It is evident that the degree of functionalization based on I_D/I_G ratio did not change much beyond 40min. Based on all these results, 40 min appears to be the treatment time where the degree of functionalization reached its maximum.

The morphologies of f-CNTs are shown in SEM and TEM images (Figure 6.1). The diameters of carbon nanotubes are presented in Table 6.1. It has been reported that the diameter of CNTs increase on functionalization (Wu and Mitra 2014), and that is what was observed here. Based on the Student's t-test, there were significant differences between raw CNT and f-CNT_{34.8}, f-CNT_{23.8}, and f-CNT_{20.6}. However, there was no significant change in diameters from f-CNT_{20.6} to f-CNT_{14.7}. The TEM images of the CNT_{34.8} and CNT_{14.7} are shown in Figure 6.1, the latter showed many smaller fragments, which implied that some tubes may have been shortened when treated for long periods. It could be seen that when the CNTs were treated for longer periods CNTs dispersed better and tended to aggregate less in water.

Table 6.1 Diameter, Elemental Analysis, C: COOH Ratio, SSA, ID/IG of CNTs and f-CNTs

Sample name	Treatment time(min)	Diameter (nm)	% by Weight			C:COOH	SSA (m ² /g)	ID/IG
			C	O	Ni			
CNTs	0	20±5	93.5	4.90	1.60	N/A	173.9	0.89
f-CNT _{34.8}	5	23±4	91.9	6.84	1.26	34.8	220.3	1.10
f-CNT _{23.8}	10	33±7	89.9	9.65	0.45	23.8	246.8	1.29
f-CNT _{20.6}	20	36±8	89.0	11.0	-	20.6	245.7	1.36
f-CNT _{16.2}	40	38±9	86.6	13.4	-	16.2	266.0	1.61
f-CNT _{15.7}	60	38±9	86.2	13.8	-	15.7	263.2	1.60
f-CNT _{14.9}	90	38±8	85.6	14.4	-	14.9	250.6	1.62
f-CNT _{14.7}	120	38±9	85.5	14.5	-	14.7	270.9	1.59

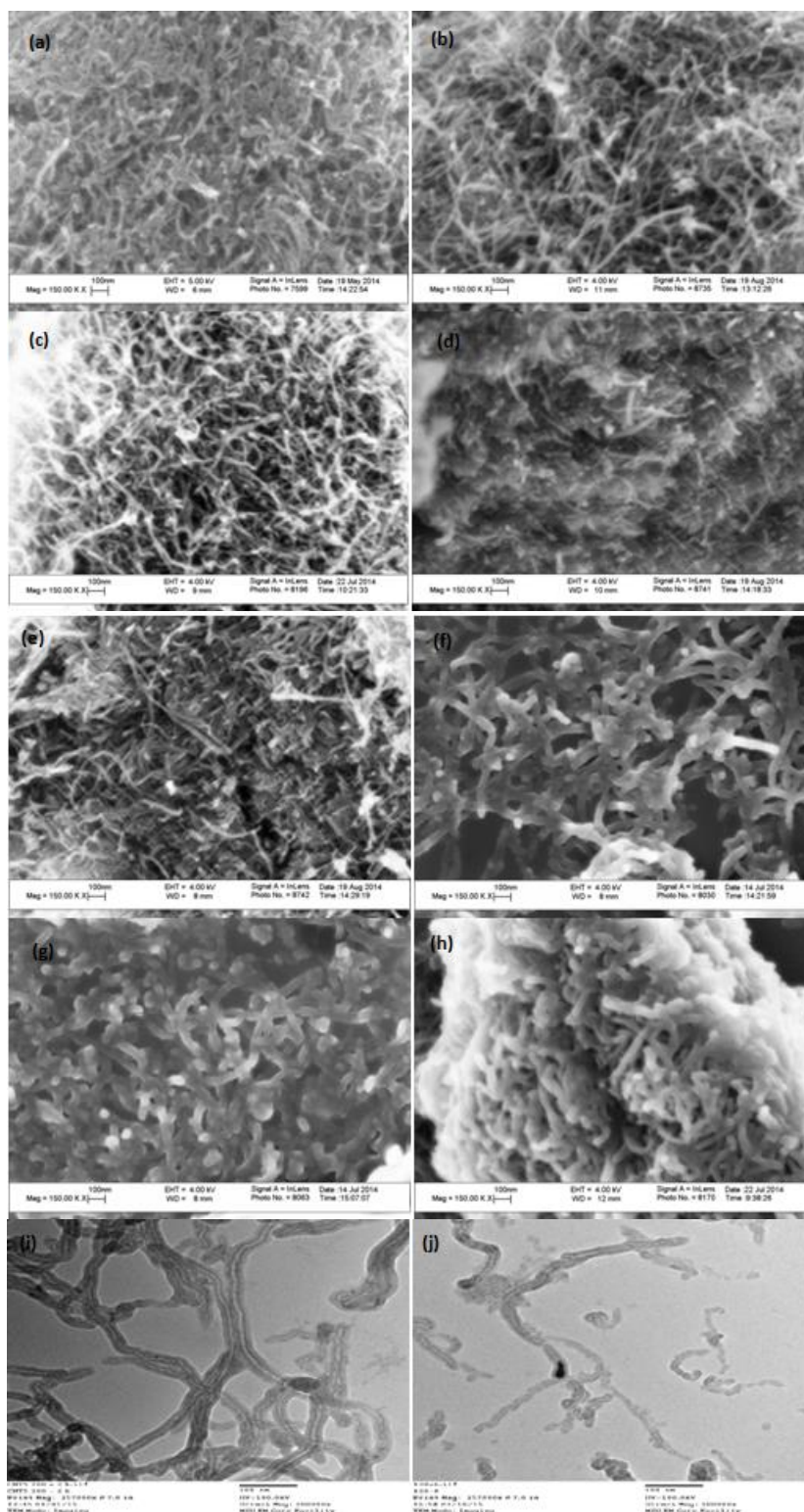


Figure 6.1 SEM images of (a) CNTs (b) f-CNT_{34.8}, (c) f-CNT_{23.8}, (d) f-CNT_{20.6}, (e) f-CNT_{16.2}, (f) f-CNT_{15.7}, (g) f-CNT_{14.9}, (h) f-CNT_{14.7}; TEM images of (i) f-CNT_{34.8} (j) f-CNT_{14.7}.

6.2.2 Electrochemical Behavior of the f-CNTs

The electrochemical properties of the different functionalized CNTs were compared with two different electrolytes. The first was 2 M Na₂SO₄ where a double layer formation was anticipated, and the second was 2 M KOH which was expected to exhibit Faradic interactions with the electrode. Figure 6.2(a) shows the cyclic voltammetry of the different f-CNTs at the scan rate of 0.01V/s in 2 M Na₂SO₄ electrolyte. The CNT and the f-CNTs showed similar voltammograms. During a CV scan, a voltage was applied onto the electrode which generated a double layer of polarized ions where electric charge was stored. The larger the layer, the charge stored increased. The defects created by carboxylation were expected to enhance the formation of electric double layer at the CNT surface. It can be seen that as the treatment time increased from 5 min to 40 min, the electrodes showed larger anodic as well as cathodic current. Once again, the current reached the maximum around 40 min of treatment. As the surface area and the number of carboxylated sites increased (Table 6.1), the ions had more active sites at the CNT-electrolyte interface, forming larger layers/Helmholtz planes and storing more charges. At higher treatment time the current appeared to drop. This was attributed to somewhat higher resistance as the tubes were damaged and shortened. One thing should be noted that the performance of raw CNTs was better than lightly treated CNTs (f-CNT_{34.8}, f-CNT_{23.8}, f-CNT_{20.6}). The areas encircled by the CV curves were also calculated and shown in Table 6.2 for the treated CNTs, current/area increased until CNT_{16.2}, after which there was no increasing trend.

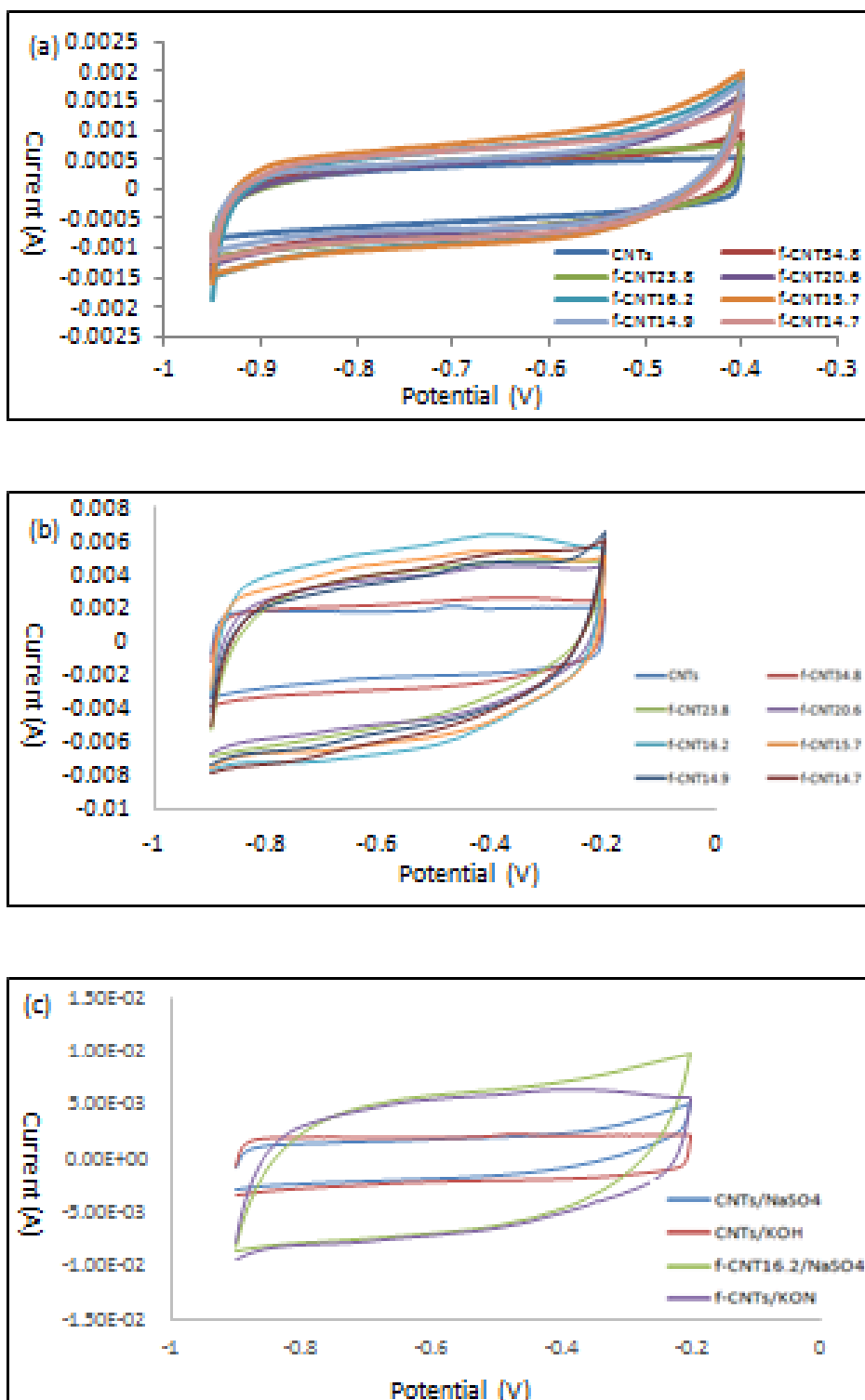
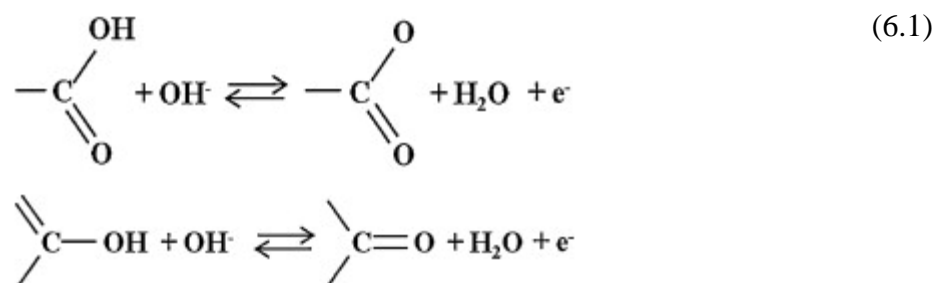


Figure 6.2 The cyclic voltammetry of different CNT samples (a) at the scan rate of 0.01V/s in 2 M Na₂SO₄ electrolyte (b) at the scan rate of 0.05V/s in 2 M KOH electrolyte (c) at the scan rate of 0.05V/s in 2 M KOH and Na₂SO₄ electrolyte.

Figure 6.2(b) shows the cyclic voltammetry in 2 M KOH. The difference between the raw CNTs and the f-CNTs was more pronounced. The CNTs showed a flat profile, and f-CNT_{34.8} was similar to the raw CNTs. The difference around -0.8 V was attributed to the reversible faradaic redox reactions on CNT surface probably caused by the metal oxide impurities in raw CNTs. This bulge shape disappeared as functionalization removed those metal/metal oxides. The peak emerged at -0.5 V also vanished in the case of f-CNTs indicating that metal/metal oxide which might cause the peak was removed. f-CNT_{34.8} onward the shape change was quite dramatic till CNT_{16.2} whose peak currents reached 6 mA. This was attributed to both the non-Faradic and Faradic effects. Due to difference in electrolytes, electrochemical process could be different. For the f-CNTs, another bulge appeared around -0.38 V, which was enhanced as the treatment time increased. This was attributed to the redox interactions of oxygen containing groups (Frackowiak, Metenier et al. 2000). It has been known that the treatment would generate oxygen containing groups, especially carboxylic groups which interact with the alkaline electrolyte via the following process (Oh, Yoo et al. 2014):



The above interaction was insignificant or even might not happen in neutral electrolyte since no peak/bulge shape was observed. Once again, high treatment times (longer than 1 hour) did not show any improvement.

CNT sample behaviors in different electrolytes were compared in Figure 6.2(c) For raw CNTs, the CV curves showed similar shapes in both electrolytes except the rise at the positive voltage end in Na₂SO₄, which can be ascribed to water decomposition and gas evolution. The electrochemical interactions between the functionalized CNT samples and electrolytes were different in neutral and basic environment: the anodic bulge at 0.4 V didn't show up in neutral Na₂SO₄ electrolyte.

For an electrode showing a capacitive behavior, specific capacitance (C_{sp}) as a resultant capacitance can be obtained using the following equation and its CV curve. The integration part in the equation is the area encircled by the CV curve and the larger the area is, the more significant the capacitive behavior is.

$$C_{sp} = \frac{1}{s \cdot m \cdot \Delta V} \int_{V_1}^{V_2} i dV \quad (6.2)$$

The areas encircled by the CV curves were also calculated and shown in Table 6.2 For the treated CNTs, current/ area increased until CNT_{16.2} and CNT_{15.7}, after which there was no increasing trend, indicating that the interactions between CNT and electrolyte (Faradic caused by carboxylic functional groups and non-Faradic caused by electric double-layer) and capacitance behavior were enhanced until certain point of treatment.

Table 6.2 The Areas Encircled by the CV Curves

	CNTs	f- CNT _{34.8}	f- CNT _{23.8}	f- CNT _{20.6}	f- CNT _{16.2}	f- CNT _{15.7}	f- CNT _{14.9}	f- CNT _{14.7}
Area in Na ₂ SO ₄ electrolyte	4.64 E-4	5.82 E-4	5.99 E-4	6.07 E-4	7.91 E-4	8.74 E-4	5.95 E-4	7.24 E-4
Area in KOH electrolyte	2.77 E-3	3.35 E-3	5.31 E-3	5.42 E-3	7.35 E-3	6.60 E-3	5.57 E-3	6.06 E-3

6.2.3 Dispersibility of the f-CNTs

The particle size of and zeta potential the f-CNTs in Milli Q water and in the presence of salts are presented in Figure 6.3 The water dispersibility of carboxylated f-CNTs is due to the negatively charged oxygen-containing groups on the surface of the tubes. In the presence of salt solutions, positively charged metal ions compressed the double layer which led to the aggregation of the tubes. Since raw CNTs and CNT_{34.8} are not dispersible in water, dispersibility study has been done for f-CNTs with treatment time longer than 5 min. In all three media, the particle size decreased as the treatment time increased from 10 min to 40 min, and did not change past 40 min. This implied that from 10 min to 40 min, the degree functionalization increased, and 40 min is long enough to maximize the number of carboxylic groups on the surface.

For all f-CNTs, the particle size in Milli Q water were smaller than those in the presence of salt, and the size in MgCl₂ were larger than those in NaCl. This observation is in line with Schulze–Hardy rule (Elimelech, Jia et al. 1998) which states that it is the valence of the counter ions that has the principal effect on the stability of the colloid. It was also observed that in the range of 10 min to 40 min, the longer treatment time led to more

negative zeta potential, beyond which it stayed unchanged. The divalent Mg salt led to a relatively larger value in the zeta potential for all the f-CNTs compared to the monovalent Na salt.

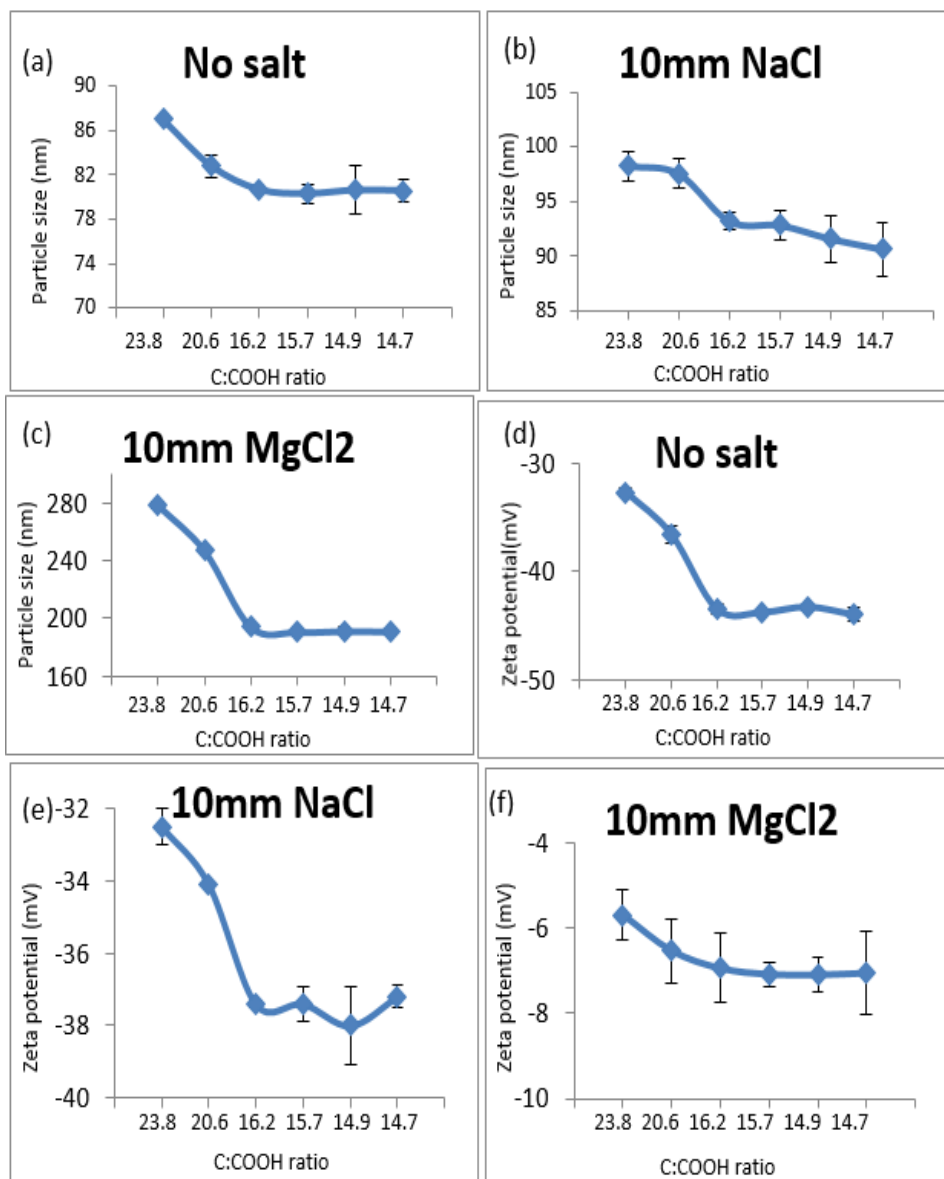


Figure 6.3 Particle size (a, b, c) and zeta potential (d, e, f) of f-CNTs in MilliQ water and in the present of NaCl and MgCl₂.

Attachment efficiency (α) was obtained from the ratio in growth of hydrodynamic size during aggregation and under the fast aggregation conditions (Elimelech, Jia et al.

1998, Ntim, Sae-Khow et al. 2012). Figure 6.4 shows attachment efficiency for the f-CNTs in the presence of NaCl and MgCl₂ respectively. At low ionic strengths, α increased with salt concentration and then reached a steady state. The critical coagulation concentration (CCC) is the point when α became independent of salt concentration. Figure 6.5 shows that the CCC value of the f-CNTs in the presence of salt. CCC values increased with the increase of treatment time from 10 min to 40 min. Beyond 40 min there was only a slight change of CCC value. This again implied that the f-CNTs prepared under longer treatment time up to 40 min were more stable in the aqueous environment. All the f-CNTs had higher CCC values in NaCl than in MgCl₂. From 10 to 120 min treatment, the CCC values increased from 142.14 to 168.69 mM with increase in treatment time in the presence of NaCl, and the corresponding increase was from 0.97 to 5.32 mM in the presence of MgCl₂.

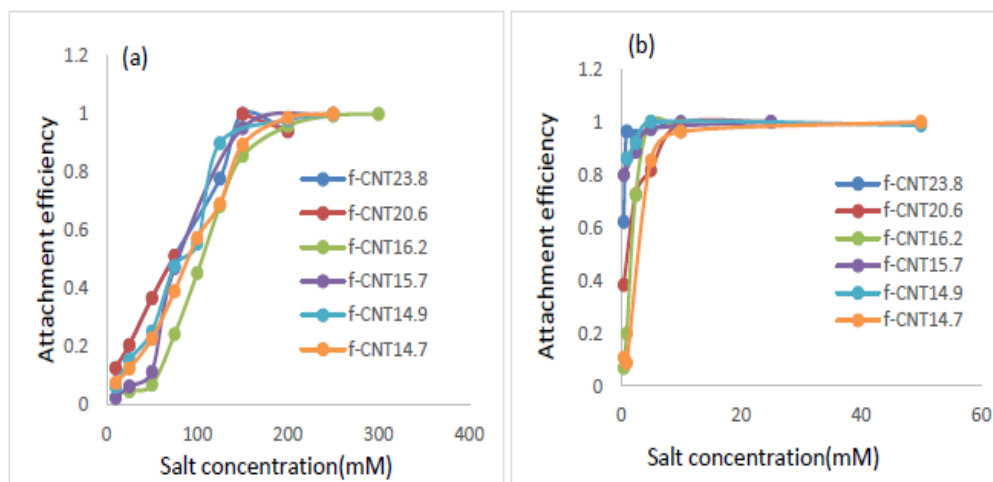


Figure 6.4 Attachment efficiency of f-CNTs in a function of (a) NaCl and (b) MgCl₂.

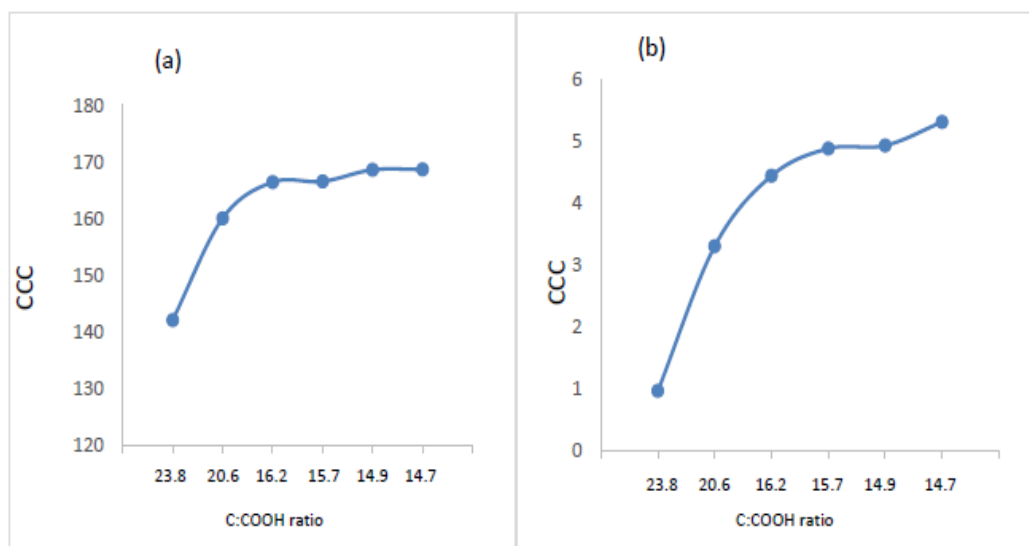


Figure 6.5 CCC value of f-CNTs in the present of (a) NaCl and (b) MgCl₂.

6.2.4 Biological Effects of f-CNTs

6.2.4.1 Effects of f-CNTs Exposure to THP-1 Cells in Vitro. The transformed human monocytic cell line THP-1 was used to assess differential f-CNT toxicity and bioactivity after a 24 hr exposure using an in vitro cell culture model. Once transformed by vitamin D₃ exposure, the THP-1 cell is phenotypically similar to an alveolar macrophage cell. There were two methods used for determination of cytotoxicity: LDH release assay and the MTS assay. Figure 6.6A shows the LDH assay results at 24 hr. Only two f-CNT (f-CNT_{15.7} and f-CNT_{14.9}) showed significant toxicity at the highest particle concentrations. Both f-CNT were two of the more functionalized CNT. In contrast, all of the CNTs showed a dose-dependent cytotoxicity compared to no particle control by MTS assay starting at the 12.5 µg/ml concentration (Figure 6.6B). The one exception was the most functionalized CNT (f-CNT_{14.7}), which showed no toxicity within this dose range. Regardless of the assay, there was no more than 20 to 25 % cell death at the highest CNTs concentration indicating that the toxicity was moderate even at the highest dose tested. The

MTS assay is considered to be a more reliable toxicity assay compared to LDH release when using functionalized carbon because the particles get caught in suspension and can affect the optical density readings in the LDH assay (Xia, Hamilton et al. 2013). This is not a problem with the MTS assay because the supernatant containing any suspended particles is completely removed for cytokine assay and replaced with fresh media containing the MTS reagent.

f-CNT bioactivity was determined in the transformed THP-1 cells by a proxy measure of NLRP3 inflammasome activation using LPS and PMA co-stimulants, which promote phagocytosis and IL-1 β release. Significant THP-1 IL-1 β release in vitro in response to particle exposure has been correlated with acute inflammatory potential for inhaled engineered nanomaterials (Hamilton, Xiang et al. 2013, Hamilton, Wu et al. 2013, Xia, Hamilton et al. 2013). Figure 6C illustrates the IL-1 β release at 24 hr post CNT exposure. Only the source CNTs (raw CNTs) exposure produced significant dose-dependent increases in IL-1 β . This result was a confirmation of previous studies showing that functionalized CNT were not inflammatory in vitro and in vivo (Hamilton, Xiang et al. 2013, Hamilton, Wu et al. 2013). The new information in Figure 6C indicated the degree of functionalization was not a factor, and even the least functionalized CNTs were completely inert with regard to NLRP3 inflammasome activation. Therefore, the amount of carboxylation on the CNT had no effect with regard to NLRP3 inflammasome activity, as the least functionalized CNT was identical to the most f-CNTs.

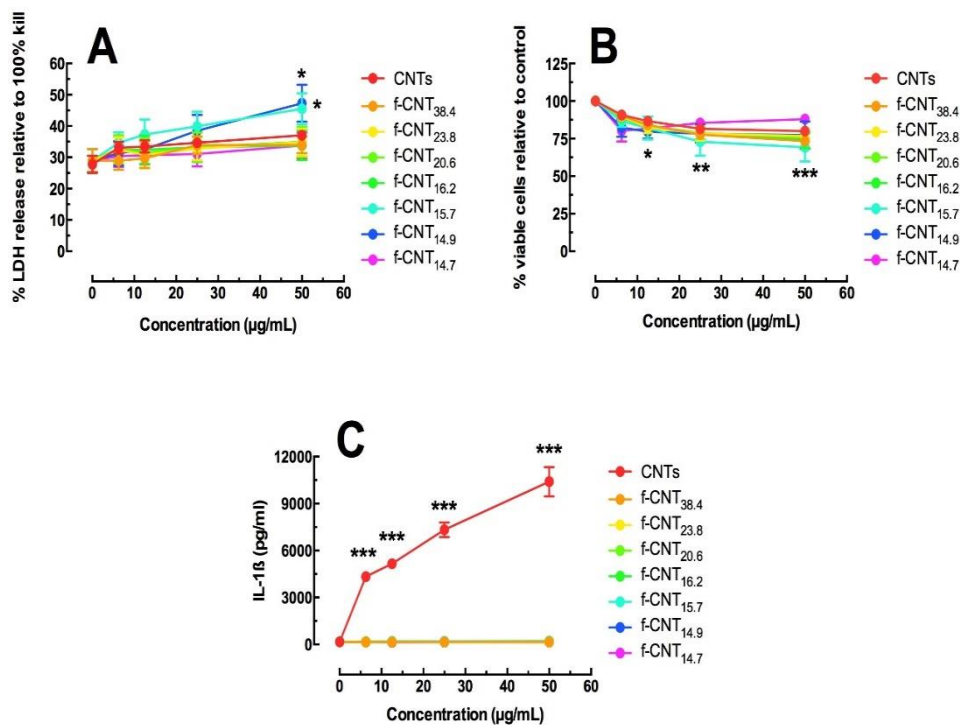


Figure 6.6 Effect of functionalized CNTs on THP-1 macrophage-like cells in an in vitro 24 hr culture. A) Cell toxicity determined by LDH activity in cell media. Data expressed as mean LDH percent \pm SEM compared to 100% cell death. B) Cell toxicity determined by MTS assay. Data expressed as mean \pm SEM viability relative to control cultures (0 μ g/ml). C) IL-1 β release expressed as mean \pm SEM pg/ml. Asterisks *** indicate $P < 0.001$, ** $P < 0.01$, or * $P < 0.05$ compared to 0 μ g/ml concentration.

6.2.4.2 Effects of Differential Functionalization on CNT Exposed to A549 Cells in

Vitro.

In addition to the macrophage, lung epithelial cells are the cells most likely to come in contact with inhaled nanomaterials. The human A549 cell line was used to determine cytotoxicity and bioactivity in response to the differentially functionalized CNTs in a 24 hr in vitro culture model. The MTS assay was used to determine cytotoxicity and three cytokines (IL-6, IL-33, and TNF- β) were used to determine potential bioactivity. The A549 cells were adherent prior to particle exposure to better mimic the exposure conditions in the lung airway lining. Figure 7A shows the relative cytotoxicity of the CNTs and the differential f-CNTs at 50 μ g/ml. Only the CNTs and the least functionalized

CNTs showed any significant toxicity compared to no-particle control cultures. All of the other f-CNTs, with the exception of f-CNT_{16,2}, showed increased MTS activity compared to the no-particle control cultures which could suggest an increase in A549 cell proliferation. Nevertheless, in all cases, the A549 response was relatively minor (10% or less compared to control) with the possible exception of the cell death caused by the CNTs (~ 25% cell loss). These results are similar to earlier reports claiming that functionalization reduced toxicity of CNT (Hamilton, Xiang et al. 2013, Hamilton, Wu et al. 2013).

Three pro-inflammatory cytokines were monitored after 24 hr in the exposed A549 culture supernatants. Figure 7B shows IL-6 release following CNT exposures. In all cases but one (f-CNT_{16,2}), the CNT-exposed A549 cells, regardless of functionalization, produced significantly less IL-6 than control cultures. This was a surprising outcome that may be a non-specific response, because it was also seen in gold nanorod-exposed A549 cells (unpublished observation). In contrast, baseline IL-33 release (Figure 6.7C) was blocked by the CNT, but returned back to normal control culture levels with increasing degree of CNT functionalization, appearing to level off after f-CNT_{16,2}. Therefore, IL-33 release showed a distinct sensitivity to the amount of functionalization on the CNTs. In contrast to the other cytokine results, TNF- α release increased compared to control cultures for the f-CNT particles only. The CNTs did not induce any significant TNF- α release. The reason for some stimulation of TNF- α release by low levels of functionalization is not clear. While there is some endotoxin contamination of the functionalized materials, which could possibly explain the difference, IL-6 production is usually a more sensitive indicator of endotoxin contamination and in that case the functionalized materials had lower levels of IL-6 release.

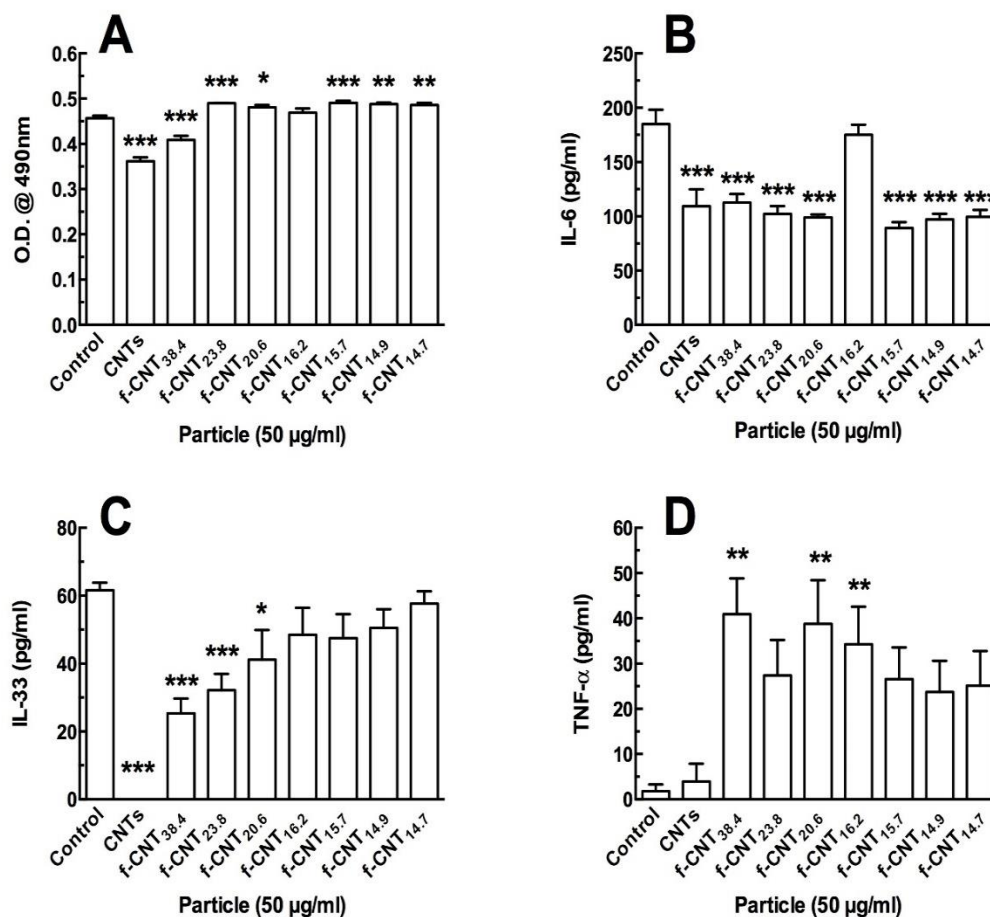


Figure 6.7 Effect of functionalized CNTs on A549 lung epithelial cells in an in vitro 24 hr culture. A) Cell toxicity determined by MTS assay. Data expressed as mean \pm SEM optical density at 490 nm. B) IL-6 release expressed as mean \pm SEM pg/ml. C) IL-33 release expressed as mean \pm SEM pg/ml. D) TNF- α release expressed as mean \pm SEM pg/ml. Asterisks *** indicate $P < 0.001$, ** $P < 0.01$, or * $P < 0.05$ compared to Control (no particle cultures).

6.3 Conclusions

CNTs were functionalized under different microwave treatment times to generate carboxylated CNTs with different levels of functionalization. Diameters, elemental composition, SSA and I_D/I_G ratio from Raman spectroscopy were used to determine the degree of functionalization. Electrochemical performance of f-CNTs increased with treatment time from 5 to 40 min beyond which it stayed constant. Based on particle sizes,

zeta potentials and CCC values in NaCl and MgCl₂, the colloidal behaviors of f-CNTs under different condition were found to be different. f-CNTs under longer treatment time (beyond 40 min) showed smaller particle sizes, more negative zeta potential values and higher CCC values. It implied that f-CNTs with higher degree of functionalization had higher colloidal stability. With regard to biological testing of the various f- CNTs, changing the degree of functionalization had very few effects in both THP-1 and A549 cell line exposure models. The biggest differences in cytotoxicity and NLRP3 inflammasome activation were always between the f-CNTs and non-functionalized CNTs, where the carboxylation reduced toxicity and inflammatory potential. This study showed that the attenuated toxicity and bioactivity produced by f-CNTs was not dependent on the degree of functionalization, but the only exception was the responses in A549 cells where there was a correlation to functionalization with IL-33 release.

REFERENCES

- Paul, A. and B. Bhattacharya (2010). "DNA functionalized carbon nanotubes for nonbiological applications." *Materials and Manufacturing Processes* 25(9): 891.
- Addo Ntim, S. and S. Mitra (2011). "Removal of trace arsenic to meet drinking water standards using iron oxide coated multiwall carbon nanotubes." *Journal of Chemical & Engineering Data* 56(5): 2077-2083.
- Ajayan, P. M., O. Stephan, C. Colliex and D. Trauth (1994). "Aligned carbon nanotube arrays formed by cutting a polymer resin—nanotube composite." *Science* 265(5176): 1212-1214.
- Anand, B., S. Addo Ntim, V. Sai Muthukumar, S. Siva Sankara Sai, R. Philip and S. Mitra (2011). "Improved optical limiting in dispersible carbon nanotubes and their metal oxide hybrids." *Carbon* 49(14): 4767-4773.
- Aqel, A., K. M. M. A. El-Nour, R. A. A. Ammar and A. Al-Warthan (2012). "Carbon nanotubes, science and technology part (I) structure, synthesis and characterisation." *Arabian Journal of Chemistry* 5(1): 1-23.
- Artyukhin, A. B., A. Shestakov, J. Harper, O. Bakajin, P. Stroeve and A. Noy (2005). "Functional one-dimensional lipid bilayers on carbon nanotube templates." *Journal of the American Chemical Society* 127(20): 7538-7542.
- Bahr, J. L., J. Yang, D. V. Kosynkin, M. J. Bronikowski, R. E. Smalley and J. M. Tour (2001). "Functionalization of carbon nanotubes by electrochemical reduction of aryl diazonium salts: a bucky paper electrode." *Journal of the American Chemical Society* 123(27): 6536-6542.
- Bandow, S., A. M. Rao, K. A. Williams, A. Thess, R. E. Smalley and P. C. Eklund (1997). "Purification of single-wall carbon nanotubes by microfiltration." *The Journal of Physical Chemistry B* 101(44): 8839-8842.
- Bianco, A., K. Kostarelos and M. Prato (2005). "Applications of carbon nanotubes in drug delivery." *Current Opinion in Chemical Biology* 9(6): 674-679.

- Birch, M. E., T. A. Ruda-Eberenz, M. Chai, R. Andrews and R. L. Hatfield (2013). "Properties that influence the specific surface areas of carbon nanotubes and nanofibers." *Annals of Occupational Hygiene* 57(9):1148-66.
- Bokobza, L. and J. Zhang (2012). "Raman spectroscopic characterization of multiwall carbon nanotubes and of composites." *Express Polymer Letters* 6(7): 601-608.
- Caddick, S. (1995). "Microwave assisted organic reactions." *Tetrahedron* 51(38): 10403-10432.
- Calvert, P. (1999). "Nanotube composites: a recipe for strength." *Nature* 399(6733): 210-211.
- Campidelli, S., C. Klumpp, A. Bianco, D. M. Guldi and M. Prato (2006). "Functionalization of CNT: synthesis and applications in photovoltaics and biology." *Journal of Physical Organic Chemistry* 19(8-9): 531-539.
- Chen, Y., Z. Iqbal and S. Mitra (2007). "Microwave-induced controlled purification of single-walled carbon nanotubes without sidewall functionalization." *Advanced Functional Materials* 17(18): 3946-3951.
- Chen, Y. and S. Mitra (2008). "Fast microwave-assisted purification, functionalization and dispersion of multi-walled carbon nanotubes." *Journal of Nanoscience and Nanotechnology* 8(11): 5770-5775.
- Cheng, H. M., F. Li, G. Su, H. Y. Pan, L. L. He, X. Sun and M. S. Dresselhaus (1998). "Large-scale and low-cost synthesis of single-walled carbon nanotubes by the catalytic pyrolysis of hydrocarbons." *Applied Physics Letters* 72(25): 3282-3284.
- Cheng, X., J. Zhong, J. Meng, M. Yang, F. Jia, Z. Xu, H. Kong and H. Xu (2011). "Characterization of multiwalled carbon nanotubes dispersing in water and association with biological effects." *Journal of Nanomaterials* 2011: 14.
- Chowdhury, D. F. and Z. F. Cui (2011). "Carbon nanotube length reduction techniques, and characterisation of oxidation state using quasi-elastic light scattering." *Carbon* 49(3): 862-868.

- Coleman, K. S., S. R. Bailey, S. Fogden and M. L. H. Green (2003). "Functionalization of single-walled carbon nanotubes via the bingel reaction." *Journal of the American Chemical Society* 125(29): 8722-8723.
- Datsyuk, V., M. Kalyva, K. Papagelis, J. Parthenios, D. Tasis, A. Siokou, I. Kallitsis and C. Galiotis (2008). "Chemical oxidation of multiwalled carbon nanotubes." *Carbon* 46(6): 833-840.
- De Heer, W. A., A. Châtelain and D. Ugarte (1995). "A carbon nanotube field-emission electron source." *Science* 270(5239): 1179-1180.
- Derjaguin, B. and L. Landau (1993). "Theory of the stability of strongly charged lyophobic sols and of the adhesion of strongly charged particles in solutions of electrolytes." *Progress in Surface Science* 43(1-4): 30-59.
- Desai, C., S. Addo Ntim and S. Mitra (2012). "Antisolvent precipitation of hydrophobic functionalized multiwall carbon nanotubes in an aqueous environment." *Journal of Colloid and Interface Science* 368(1): 115-120.
- Desai, C. and S. Mitra (2013). "Microwave induced carboxylation of nanodiamonds." *Diamond and Related Materials* 34: 65-69.
- Dieckmann, G. R., A. B. Dalton, P. A. Johnson, J. Razal, J. Chen, G. M. Giordano, E. Muñoz, I. H. Musselman, R. H. Baughman and R. K. Draper (2003). "Controlled assembly of carbon nanotubes by designed amphiphilic peptide helices." *Journal of the American Chemical Society* 125(7): 1770-1777.
- Dillon, A. C., K. M. Jones, T. A. Bekkedahl, C. H. Kiang, D. S. Bethune and M. J. Heben (1997). "Storage of hydrogen in single-walled carbon nanotubes." *Nature* 386(6623): 377-379.
- Elimelech, M., X. Jia, J. Gregory and R. Williams (1998). "Particle deposition & aggregation: measurement, modelling and simulation." Oxford, UK, Butterworth-Heinemann.
- Erlanger, B. F., B.-X. Chen, M. Zhu and L. Brus (2001). "Binding of an anti-fullerene IgG monoclonal antibody to single wall carbon nanotubes." *Nano Letters* 1(9): 465-467.

- Feng, Q.-P., X.-M. Xie, Y.-T. Liu, Y.-F. Gao, X.-H. Wang and X.-Y. Ye (2007). "Length sorting of multi-walled carbon nanotubes by high-speed centrifugation." *Carbon* 45(11): 2311-2313.
- Fenoglio, I., E. Aldieri, E. Gazzano, F. Cesano, M. Colonna, D. Scarano, G. Mazzucco, A. Attanasio, Y. Yakoub, D. Lison and B. Fubini (2012). "Thickness of multiwalled carbon nanotubes affects their lung toxicity." *Chemical Research in Toxicology* 25(1): 74-82.
- Fogden, S., R. Verdejo, B. Cottam and M. Shaffer (2008). "Purification of single walled carbon nanotubes: The problem with oxidation debris." *Chemical Physics Letters* 460(1-3): 162-167.
- Frackowiak, E., K. Metenier, V. Bertagna and F. Beguin (2000). "Supercapacitor electrodes from multiwalled carbon nanotubes." *Applied Physics Letters* 77(15): 2421-2423.
- Freiman, S., S. Hooker and K. Migler (2008). "Measurement issues in single wall carbon nanotubes." Washington, DC, National Institute of Standards and Technology.
- Fu, S.-Y., Z.-K. Chen, S. Hong and C. C. Han (2009). "The reduction of carbon nanotube (CNT) length during the manufacture of CNT/polymer composites and a method to simultaneously determine the resulting CNT and interfacial strengths." *Carbon* 47(14): 3192-3200.
- Georgakilas, V., K. Kordatos, M. Prato, D. M. Guldi, M. Holzinger and A. Hirsch (2002). "Organic functionalization of carbon nanotubes." *Journal of the American Chemical Society* 124(5): 760-761.
- Giguere, R. J., T. L. Bray, S. M. Duncan and G. Majetich (1986). "Application of commercial microwave ovens to organic synthesis." *Tetrahedron Letters* 27(41): 4945-4948.
- Goertzen, S. L., K. D. Thériault, A. M. Oickle, A. C. Tarasuk and H. A. Andreas (2010). "Standardization of the Boehm titration. Part I. CO₂ expulsion and endpoint determination." *Carbon* 48(4): 1252-1261.

- Goyanes, S., G. R. Rubiolo, A. Salazar, A. Jimeno, M. A. Corcuera and I. Mondragon (2007). "Carboxylation treatment of multiwalled carbon nanotubes monitored by infrared and ultraviolet spectroscopies and scanning probe microscopy." *Diamond and Related Materials* 16(2): 412-417.
- Hamilton Jr, R. F., M. Buford, C. Xiang, N. Wu and A. Holian (2012). "NLRP3 inflammasome activation in murine alveolar macrophages and related lung pathology is associated with MWCNT nickel contamination." *Inhalation Toxicology* 24(14): 995-1008.
- Hamilton, R. F., Jr., C. Xiang, M. Li, I. Ka, F. Yang, D. Ma, D. W. Porter, N. Wu and A. Holian (2013). "Purification and sidewall functionalization of multiwalled carbon nanotubes and resulting bioactivity in two macrophage models." *Inhalation Toxicology* 25(4): 199-210.
- Hamilton, R. F. J., Z. Wu, S. Mitra, P. K. Shaw and A. Holian (2013). "Effect of MWCNT size, carboxylation, and purification on in vitro and in vivo toxicity, inflammation and lung pathology." *Particle and Fibre Toxicology* 10(1):1.
- Hayes, B. L. (2002). "Microwave synthesis: chemistry at the speed of light." Matthews, NC, CEM Corporation.
- Heister, E., C. Lamprecht, V. Neves, C. Tîmaciu, L. Datas, E. Flahaut, B. Soula, P. Hinterdorfer, H. M. Coley, S. R. P. Silva and J. McFadden (2010). "Higher dispersion efficacy of functionalized carbon nanotubes in chemical and biological environments." *ACS Nano* 4(5): 2615-2626.
- Hetzel, R., T. Manning, D. Lovingood, G. Strouse and D. Phillips (2012). "Production of fullerenes by microwave synthesis." *Fullerenes, Nanotubes and Carbon Nanostructures* 20(2): 99-108.
- Holzinger, M., J. Abraham, P. Whelan, R. Graupner, L. Ley, F. Hennrich, M. Kappes and A. Hirsch (2003). "Functionalization of single-walled carbon nanotubes with (R-)oxycarbonyl nitrenes." *Journal of the American Chemical Society* 125(28): 8566-8580.
- Hou, P.-X., C. Liu and H.-M. Cheng (2008). "Purification of carbon nanotubes." *Carbon* 46(15): 2003-2025.

- Hu, H., A. Yu, E. Kim, B. Zhao, M. E. Itkis, E. Bekyarova and R. C. Haddon (2005). "Influence of the zeta potential on the dispersability and purification of single-walled carbon nanotubes." *The Journal of Physical Chemistry B* 109(23): 11520-11524.
- Hu, H., B. Zhao, M. A. Hamon, K. Kamaras, M. E. Itkis and R. C. Haddon (2003). "Sidewall functionalization of single-walled carbon nanotubes by addition of dichlorocarbene." *Journal of the American Chemical Society* 125(48): 14893-14900.
- Huang, W., Y. Lin, S. Taylor, J. Gaillard, A. M. Rao and Y.-P. Sun (2002). "Sonication-assisted functionalization and solubilization of carbon nanotubes." *Nano Letters* 2(3): 231-234.
- Huang, W., S. Taylor, K. Fu, Y. Lin, D. Zhang, T. W. Hanks, A. M. Rao and Y.-P. Sun (2002). "Attaching proteins to carbon nanotubes via diimide-activated amidation." *Nano Letters* 2(4): 311-314.
- Iijima, S. (1991). "Helical microtubules of graphitic carbon." *Nature* 354(6348): 56-58.
- Iijima, S. (2002). "Carbon nanotubes: past, present, and future." *Physica B: Condensed Matter* 323(1-4): 1-5.
- Iijima, S. and T. Ichihashi (1993). "Single-shell carbon nanotubes of 1-nm diameter." *Nature* 363(6430): 603-605.
- Islam, M. F., E. Rojas, D. M. Bergey, A. T. Johnson and A. G. Yodh (2003). "High weight fraction surfactant solubilization of single-wall carbon nanotubes in water." *Nano Letters* 3(2): 269-273.
- Israelachvili, J. N. (2011). "Intermolecular and surface forces: revised third edition." Cambridge, MA, Academic Press.
- Jang, B.-K. and Y. Sakka (2010). "Dispersion and shortening of multi-walled carbon nanotubes by size modification." *Materials Transactions* 51(1): 192-195.
- Jiang, L., L. Gao and J. Sun (2003). "Production of aqueous colloidal dispersions of carbon nanotubes." *Journal of Colloid and Interface Science* 260(1): 89-94.

- Jung, D.-H., Y. Koan Ko and H.-T. Jung (2004). "Aggregation behavior of chemically attached poly(ethylene glycol) to single-walled carbon nanotubes (SWNTs) ropes." *Materials Science and Engineering: C* 24(1–2): 117-121.
- Kong, J., N. R. Franklin, C. Zhou, M. G. Chapline, S. Peng, K. Cho and H. Dai (2000). "Nanotube molecular wires as chemical sensors." *Science* 287(5453): 622-625.
- Krause, B., M. Mende, P. Pötschke and G. Petzold (2010). "Dispersability and particle size distribution of CNTs in an aqueous surfactant dispersion as a function of ultrasonic treatment time." *Carbon* 48(10): 2746-2754.
- Krause, B., T. Villmow, R. Boldt, M. Mende, G. Petzold and P. Pötschke (2011). "Influence of dry grinding in a ball mill on the length of multiwalled carbon nanotubes and their dispersion and percolation behaviour in melt mixed polycarbonate composites." *Composites Science and Technology* 71(8): 1145-1153.
- Kumar, M. and Ando, Y (2011). "Carbon nanotube synthesis and growth mechanism." Rijeka, Croatia, Intech Open Access Publisher.
- Lau, X. C., Z. Wu and S. Mitra (2014). "Enhanced charge-carrier transport through shorter carbon nanotubes in organic photovoltaics." *ACS Applied Materials & Interfaces* 6(3): 1640-1645.
- Lee, C.-S., S. E. Baker, M. S. Marcus, W. Yang, M. A. Eriksson and R. J. Hamers (2004). "Electrically addressable biomolecular functionalization of carbon nanotube and carbon nanofiber electrodes." *Nano Letters* 4(9): 1713-1716.
- Lee, J., T. Jeong, J. Heo, S.-H. Park, D. Lee, J.-B. Park, H. Han, Y. Kwon, I. Kovalev, S. M. Yoon, J.-Y. Choi, Y. Jin, J. M. Kim, K. H. An, Y. H. Lee and S. Yu (2006). "Short carbon nanotubes produced by cryogenic crushing." *Carbon* 44(14): 2984-2989.
- Lin, Y., D. W. Baggett, J.-W. Kim, E. J. Siochi and J. W. Connell (2011). "Instantaneous formation of metal and metal oxide nanoparticles on carbon nanotubes and graphene via solvent-free microwave heating." *ACS Applied Materials and Interfaces* 3(5): 1652-1664.

- Lin, Y., A. M. Rao, B. Sadanadan, E. A. Kenik and Y.-P. Sun (2002). "Functionalizing multiple-walled carbon nanotubes with aminopolymers." *The Journal of Physical Chemistry B* 106(6): 1294-1298.
- Lin, Y., B. Zhou, K. Shiral Fernando, P. Liu, L. F. Allard and Y.-P. Sun (2003). "Polymeric carbon nanocomposites from carbon nanotubes functionalized with matrix polymer." *Macromolecules* 36(19): 7199-7204.
- Lu, L. Q. and Y. Wang (2011). "Sheet-like and fusiform CuO nanostructures grown on graphene by rapid microwave heating for high Li-ion storage capacities." *Journal of Materials Chemistry* 21(44): 17916-17921.
- Malvern Instruments Ltd (2004). "Zetasizer Nano Series User Manual." Worcestershire, UK, Malvern Instruments Ltd.
- Manivannan, S., I. O. Jeong, J. H. Ryu, C. S. Lee, K. S. Kim, J. Jang and K. C. Park (2009). "Dispersion of single-walled carbon nanotubes in aqueous and organic solvents through a polymer wrapping functionalization." *Journal of Material Science - Material Electronics* 20(3): 223-229.
- Martín, O., H. R. Gutierrez, A. Maroto-Valiente, M. Terrones, T. Blanco and J. Baselga (2013). "An efficient method for the carboxylation of few-wall carbon nanotubes with little damage to their sidewalls." *Materials Chemistry and Physics* 140(2-3): 499-507.
- Marulanda, J. M. (2011). "Electronic Properties of Carbon Nanotubes." Rijeka, Croatia, Intech Open Access Publisher.
- Mickelson, E. T., I. W. Chiang, J. L. Zimmerman, P. J. Boul, J. Lozano, J. Liu, R. E. Smalley, R. H. Hauge and J. L. Margrave (1999). "Solvation of fluorinated single-wall carbon nanotubes in alcohol solvents." *The Journal of Physical Chemistry B* 103(21): 4318-4322.
- Mitra, S. and Y. Chen (2009). "Microwave synthesis of metal-carbon nanotube composites." Patent, US20090304923 A1.
- Mitra, S. and Z. Iqbal (2008). "Rapid microwave process for purification of nanocarbon preparations." Patent, US20100086470 A1.

- Mitra, S. and Z. Iqbal (2010). "Microwave induced functionalization of single wall carbon nanotubes and composites prepared therefrom." Patent, US9249528 B2.
- Morales-Lara, F., M. J. Pérez-Mendoza, D. Altmajer-Vaz, M. García-Román, M. Melguizo, F. J. López-Garzón and M. Domingo-García (2013). "Functionalization of multiwall carbon nanotubes by ozone at basic pH. Comparison with oxygen plasma and ozone in gas phase." *The Journal of Physical Chemistry C* 117(22): 11647-11655.
- Naeimi, H., A. Mohajeri, L. Moradi and A. M. Rashidi (2009). "Efficient and facile one pot carboxylation of multiwalled carbon nanotubes by using oxidation with ozone under mild conditions." *Applied Surface Science* 256(3): 631-635.
- Nair, A. K., Z. Qin and M. J. Buehler (2012). "Cooperative deformation of carboxyl groups in functionalized carbon nanotubes." *International Journal of Solids and Structures* 49(18): 2418-2423.
- Nel, A., T. Xia, L. Mähler and N. Li (2006). "Toxic potential of materials at the nanolevel." *Science* 311(5761): 622-627.
- Ntim, S. A., O. Sae-Khow, C. Desai, F. A. Witzmann and S. Mitra (2012). "Size dependent aqueous dispersibility of carboxylated multiwall carbon nanotubes." *Journal of Environmental Monitoring* 14(10): 2772-2779.
- Ntim, S. A., O. Sae-Khow, F. A. Witzmann and S. Mitra (2011). "Effects of polymer wrapping and covalent functionalization on the stability of MWCNT in aqueous dispersions." *Journal of Colloid and Interface Science* 355(2): 383-388.
- Oh, Y. J., J. J. Yoo, Y. I. Kim, J. K. Yoon, H. N. Yoon, J.-H. Kim and S. B. Park (2014). "Oxygen functional groups and electrochemical capacitive behavior of incompletely reduced graphene oxides as a thin-film electrode of supercapacitor." *Electrochimica Acta* 116(0): 118-128.
- Palomäki, J., E. Väimäki, J. Sund, M. Vippola, P. A. Clausen, K. A. Jensen, K. Savolainen, S. Matikainen and H. Alenius (2011). "Long, needle-like carbon nanotubes and asbestos activate the NLRP3 inflammasome through a similar mechanism." *ACS Nano* 5(9): 6861-6870.

- Park, T.-J., S. Banerjee, T. Hemraj-Benny and S. S. Wong (2006). "Purification strategies and purity visualization techniques for single-walled carbon nanotubes." *Journal of Materials Chemistry* 16(2): 141-154.
- Pekker, S., J. P. Salvetat, E. Jakab, J. M. Bonard and L. Forró (2001). "Hydrogenation of carbon nanotubes and graphite in liquid ammonia." *The Journal of Physical Chemistry B* 105(33): 7938-7943.
- Peng, X., J. Jia, X. Gong, Z. Luan and B. Fan (2009). "Aqueous stability of oxidized carbon nanotubes and the precipitation by salts." *Journal of Hazardous Materials* 165(1-3): 1239-1242.
- Perreux, L. and A. Loupy (2001). "A tentative rationalization of microwave effects in organic synthesis according to the reaction medium, and mechanistic considerations." *Tetrahedron* 57(45): 9199-9223.
- Polshettiwar, V., M. N. Nadagouda and R. S. Varma (2009). "Microwave-assisted chemistry: a rapid and sustainable route to synthesis of organics and nanomaterials." *Australian Journal of Chemistry* 62(1): 16-26.
- Ponnusamy, V. K., V. Mani, S.-M. Chen, W.-T. Huang and J.-F. Jen (2014). "Rapid microwave assisted synthesis of graphene nanosheets/polyethyleneimine/gold nanoparticle composite and its application to the selective electrochemical determination of dopamine." *Talanta* 120: 148-157.
- Ramanathan, T., F. T. Fisher, R. S. Ruoff and L. C. Brinson (2005). "Amino-functionalized carbon nanotubes for binding to polymers and biological systems." *Chemistry of Materials* 17(6): 1290-1295.
- Ren, F., S. A. Kanaan, M. M. Majewska, G. D. Keskar, S. Azoz, H. Wang, X. Wang, G. L. Haller, Y. Chen and L. D. Pfefferle (2014). "Increase in the yield of (and selective synthesis of large-diameter) single-walled carbon nanotubes through water-assisted ethanol pyrolysis." *Journal of Catalysis* 309(0): 419-427.
- Riggs, J. E., Z. Guo, D. L. Carroll and Y.-P. Sun (2000). "Strong luminescence of solubilized carbon nanotubes." *Journal of the American Chemical Society* 122(24): 5879-5880.

- Rogel-Hernández, E., G. Alonso-Nuñez, J. P. Camarena, H. Espinoza-Gómez, G. Aguirre, F. Paraguay-Delgado and R. Somanathan (2011). "Side-wall functionalization of multi-walled carbon nanotubes with t-butyl diazoacetate." *Journal of the Mexican Chemical Society* 55(1): 7-10.
- Saleh, N. B., L. D. Pfefferle and M. Elimelech (2008). "Aggregation kinetics of multiwalled carbon nanotubes in aquatic systems: measurements and environmental implications." *Environmental Science and Technology* 42(21): 7963-7969.
- Salzmann, C. G., S. A. Llewellyn, G. Tobias, M. A. H. Ward, Y. Huh and M. L. H. Green (2007). "The Role of carboxylated carbonaceous fragments in the functionalization and spectroscopy of a single-walled carbon-nanotube material." *Advanced Materials* 19(6): 883-887.
- Sano, M., A. Kamino and S. Shinkai (2000). "Critical coagulation of langmuir monolayers: 2d Schulze-Hardy rule." *The Journal of Physical Chemistry B* 104(44): 10339-10347.
- Sano, M., J. Okamura and S. Shinkai (2001). "Colloidal nature of single-walled carbon nanotubes in electrolyte solution: The Schulze-Hardy rule." *Langmuir* 17(22): 7172-7173.
- Schudel, M., S. H. Behrens, H. Holthoff, R. Kretzschmar and M. Borkovec (1997). "Absolute aggregation rate constants of hematite particles in aqueous suspensions: a comparison of two different surface morphologies." *Journal of Colloid and Interface Science* 196(2): 241-253.
- Shelimov, K. B., R. O. Esenaliev, A. G. Rinzler, C. B. Huffman and R. E. Smalley (1998). "Purification of single-wall carbon nanotubes by ultrasonically assisted filtration." *Chemical Physics Letters* 282(5-6): 429-434.
- Si, R., K. Wang, T. Chen and Y. Chen (2011). "Chemometric determination of the length distribution of single walled carbon nanotubes through optical spectroscopy." *Analytica Chimica Acta* 708(1-2): 28-36.
- Smith, B., K. Wepasnick, K. E. Schrote, A. R. Bertele, W. P. Ball, C. O'Melia and D. H. Fairbrother (2009). "Colloidal properties of aqueous suspensions of acid-treated, multi-walled carbon nanotubes." *Environmental Science and Technology* 43(3): 819-825.

- Somani, P. R. and M. Umeno (2009). "Carbon nanotubes multifunctional materials." India, Applied Science Innovations Private Limited and Japan, Chubu University.
- Song, L., L. Ci, L. Lv, Z. Zhou, X. Yan, D. Liu, H. Yuan, Y. Gao, J. Wang and L. Liu (2004). "Direct synthesis of a macroscale single-walled carbon nanotube non-woven material." *Advanced Materials* 16(17): 1529-1534.
- Stefani, D., A. J. Paula, B. G. Vaz, R. A. Silva, N. F. Andrade, G. Z. Justo, C. V. Ferreira, A. G. S. Filho, M. N. Eberlin and O. L. Alves (2011). "Structural and proactive safety aspects of oxidation debris from multiwalled carbon nanotubes." *Journal of Hazardous Materials* 189(1-2): 391-396.
- Stercel, F., N. M. Nemes, J. E. Fischer and D. E. Luzzi (2001). "Single wall carbon nanotubes filled with metallocenes: a first example of non-fullerene peapods." *MRS Proceedings*, Cambridge, UK, Cambridge University Press.
- Stevens, J. L., A. Y. Huang, H. Peng, I. W. Chiang, V. N. Khabashesku and J. L. Margrave (2003). "Sidewall amino-functionalization of single-walled carbon nanotubes through fluorination and subsequent reactions with terminal diamines." *Nano Letters* 3(3): 331-336.
- Stobinski, L., B. Lesiak, L. Kövér, J. Tóth, S. Biniak, G. Trykowski and J. Judek (2010). "Multiwall carbon nanotubes purification and oxidation by nitric acid studied by the FTIR and electron spectroscopy methods." *Journal of Alloys and Compounds* 501(1): 77-84.
- Su, Y., Y. Zhang, H. Wei, B. Qian, Z. Yang and Y. Zhang (2012). "Length-controlled synthesis of single-walled carbon nanotubes by arc discharge with variable cathode diameters." *Physica E: Low-dimensional Systems and Nanostructures* 44(7-8): 1548-1551.
- Sun, Y.-P., K. Fu, Y. Lin and W. Huang (2002). "Functionalized carbon nanotubes: properties and applications." *Accounts of Chemical Research* 35(12): 1096-1104.
- Sun, Y.-P., W. Huang, Y. Lin, K. Fu, A. Kitaygorodskiy, L. A. Riddle, Y. J. Yu and D. L. Carroll (2001). "Soluble dendron-functionalized carbon nanotubes: preparation, characterization, and properties § , || ." *Chemistry of Materials* 13(9): 2864-2869.

- Tasis, D., N. Tagmatarchis, A. Bianco and M. Prato (2006). "Chemistry of carbon nanotubes." *Chemical Reviews-Columbus* 106(3): 1105.
- Thess, A., R. Lee, P. Nikolaev, H. Dai, P. Petit, J. Robert, C. Xu, Y. H. Lee, S. G. Kim, A. G. Rinzler, D. T. Colbert, G. E. Scuseria, D. Tománek, J. E. Fischer and R. E. Smalley (1996). "Crystalline ropes of metallic carbon nanotubes." *Science* 273(5274): 483-487.
- Thi ên-Nga, L., K. Hernadi, E. Ljubović, S. Garaj and L. Forró (2002). "Mechanical purification of single-walled carbon nanotube bundles from catalytic particles." *Nano Letters* 2(12): 1349-1352.
- Unger, E., A. Graham, F. Kreupl, M. Liebau and W. Hoenlein (2002). "Electrochemical functionalization of multi-walled carbon nanotubes for solvation and purification." *Current Applied Physics* 2(2): 107-111.
- Kumar, L., S. Addo Ntim, O. Sae-Khow, C. Janardhana, V. Lakshminarayanan and S. Mitra (2012). "Electro-catalytic activity of multiwall carbon nanotube-metal (Pt or Pd) nanohybrid materials synthesized using microwave-induced reactions and their possible use in fuel cells." *Electrochimica Acta* 83(0): 40-46.
- Verdejo, R., S. Lamoriniere, B. Cottam, A. Bismarck and M. Shaffer (2007). "Removal of oxidation debris from multi-walled carbon nanotubes." *Chemical Communications* 0(5): 513-515.
- Verwey, E. J. W. and J. T. G. Overbeek (1999). "Theory of the Stability of Lyophobic Colloids", Mineola, NY, Dover Publications.
- Wang, X., T. Xia, S. A. Ntim, Z. Ji, S. George, H. Meng, H. Zhang, V. Castranova, S. Mitra and A. E. Nel (2010). "Quantitative techniques for assessing and controlling the dispersion and biological effects of multiwalled carbon nanotubes in mammalian tissue culture cells." *ACS Nano* 4(12): 7241-7252.
- Wang, Y., Z. Iqbal and S. Mitra (2006). "Rapidly functionalized, water-dispersed carbon nanotubes at high concentration." *Journal of the American Chemical Society* 128(1): 95-99.
- Wang, Z., M. D. Shirley, S. T. Meikle, R. L. D. Whitby and S. V. Mikhalovsky (2009). "The surface acidity of acid oxidised multi-walled carbon nanotubes and the

influence of in-situ generated fulvic acids on their stability in aqueous dispersions." *Carbon* 47(1): 73-79.

Wang, Z., Z. Wu, G. Di Benedetto, J. L. Zunino and S. Mitra (2015). "Microwave synthesis of highly oxidized and defective carbon nanotubes for enhancing the performance of supercapacitors." *Carbon* 91: 103-113.

Watts, P. C. P., W. K. Hsu, G. Z. Chen, D. J. Fray, H. W. Kroto and D. R. M. Walton (2001). "A low resistance boron-doped carbon nanotube-polystyrene composite." *Journal of Materials Chemistry* 11(10): 2482-2488.

Weiser, H. B. and J. W. a. Sons (1949). "A textbook of colloidal chemistry." *Journal of the American Pharmaceutical Association* 38(11): 621-621.

Wiesner, M. R., G. V. Lowry, P. Alvarez, D. Dionysiou and P. Biswas (2006). "Assessing the risks of manufactured nanomaterials." *Environmental science and technology* 40(14): 4336-4345.

Wu, Z., R. F. Hamilton Jr, Z. Wang, A. Holian and S. Mitra (2014). "Oxidation debris in microwave functionalized carbon nanotubes: Chemical and biological effects." *Carbon* 68(0): 678-686.

Wu, Z. and S. Mitra (2014). "Length reduction of multi-walled carbon nanotubes via high energy ultrasonication and its effect on their dispersibility." *Journal of Nanoparticle Research* 16(8): 1-7.

Xia, T., R. F. Hamilton, J. C. Bonner, E. D. Crandall, A. Elder, F. Fazlollahi, T. A. Girtsman, K. Kim, S. Mitra and S. A. Ntim (2013). "Interlaboratory evaluation of in vitro cytotoxicity and inflammatory responses to engineered nanomaterials: the NIEHS nano GO consortium." *Environmental Health Perspectives* 121(6): 683-690.

Yu, A., E. Bekyarova, M. E. Itkis, D. Fakhruddinov, R. Webster and R. C. Haddon (2006). "Application of centrifugation to the large-scale purification of electric arc-Produced single-walled carbon nanotubes." *Journal of the American Chemical Society* 128(30): 9902-9908.

Yudasaka, M., M. Zhang, C. Jabs and S. Iijima (2000). "Effect of an organic polymer in purification and cutting of single-wall carbon nanotubes." *Applied Physics A: Materials Science & Processing* 71(4): 449-451.

Yun, Y., V. Shanov, Y. Tu, M. J. Schulz, S. Yarmolenko, S. Neralla, J. Sankar and S. Subramaniam (2006). "A multi-wall carbon nanotube tower electrochemical actuator." *Nano Letters* 6(4): 689-693.

Zhang, L., V. U. Kiny, H. Peng, J. Zhu, R. F. M. Lobo, J. L. Margrave and V. N. Khabashesku (2004). "Sidewall functionalization of single-walled carbon nanotubes with hydroxyl group-terminated moieties." *Chemistry of Materials* 16(11): 2055-2061.

Zhang, W., J. Crittenden, K. Li and Y. Chen (2012). "Attachment efficiency of nanoparticle aggregation in aqueous dispersions: modeling and experimental validation." *Environmental Science and Technology* 46(13): 7054-7062.

Zou, Y., J. Kan and Y. Wang (2011). "Fe₂O₃-graphene rice-on-sheet nanocomposite for high and fast lithium ion storage." *The Journal of Physical Chemistry C* 115(42): 20747-20753.